Technische Universität München

Fakultät für Chemie

Lehrstuhl für Biotechnologie

The regulation of Hsp90 by its essential co-chaperone Cns1

Florian Helmut Schopf

Vollständiger Abdruck der von der Fakultät für Chemie der Technischen Universität München zur Erlangung des akademischen Grades eines Doktors der Naturwissenschaften genehmigten Dissertation.

Vorsitzende(r)	Prof. Dr. Ville R. I. Kaila
Prüfer der Dissertation:	
	1. Prof. Dr. Johannes Buchner
	2. Prof. Dr. Matthias J. Feige
	3. Prof. Brian C. Freeman, Ph.D.

Die Dissertation wurde am 25.08.2016 bei der Technischen Universität München eingereicht und durch die Fakultät für Chemie am 16.11.2016 angenommen.

to Anna

Contents

1 Introduction

1.1 Protein folding

Proteins are the major components of every living cell. To fulfill their function, they have to acquire a precise three-dimensional conformation - the native state (Hartl et al., 2011). The process in which a polypeptide chain gains its native structure is termed *protein folding*.

In the 1960s Christian B. Anfinsen showed that the sequence of amino acids contains all the information needed for the three-dimensional structure of a protein (Anfinsen, 1973). Subsequent *in vitro* experiments have confirmed for many proteins that they fold into the biological active state without assistance (cf. Jaenicke 1987). Nevertheless, the ground-breaking work by Anfinsen left the question, how a protein folds into its native state, unanswered. Assuming that a protein, after being fully synthesized by the ribosome, would randomly screen all possible conformations until it reaches the native state and also taking temporal restrictions into account, C. Levinthal reasoned that the time required for protein folding based on a random search would exceed the lifetime of the universe (Levinthal, 1968).

Although some newly synthesized proteins are able to acquire their native state *in vivo* without any further help, many proteins are prone to misfolding (Kim et al., 2013). Whereas unassisted folding might be true for small proteins, folding of larger proteins is often inefficient (Brockwell and Radford, 2007). This is further exacerbated by excluded volume effects in the highly crowded cytosol of living cells (approx. 400 g/L proteins and other macromolecules in *E. coli*) termed *molecular crowding* (Ellis, 2001; Hartl and Hayer-Hartl, 2002), which leads to exposure of hydrophobic surfaces and subsequently to challenges such as protein misfolding and aggregation (Taipale et al., 2010). Moreover, due to the large number of possible conformations ($>100^{30}$ for a 100 amino acid protein) a protein can adopt, protein folding is inherently error prone (Balchin et al., 2016).

Due to this large number of possible conformations, protein folding is highly complex

and heterogenous and relies on the cooperation of many weak, noncovalent interactions. Especially, hydrophobic forces are driving chain collapse and the packing of non-polar and hydrophobic amino acids within the interior of a folding protein (Kim et al., 2013).

It is thought that polypeptide chains sample various conformations in a funnel-shaped folding energy landscape rather than following a single pathway (Figure 1).

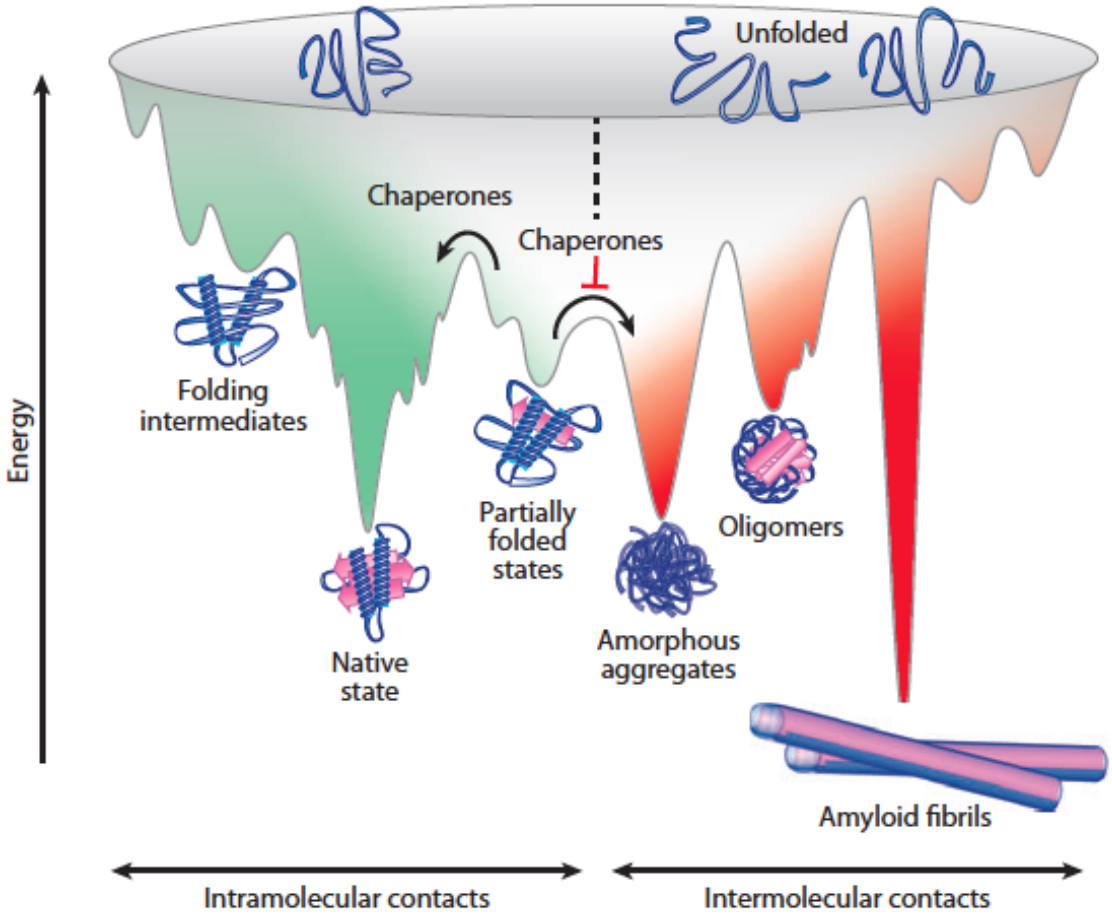

Figure 1: Energy landscape of protein folding and aggregation. Proteins travel on a free energy landscape toward the thermodynamically favorable native state; molecular chaperones lower the free energy barriers for kinetically trapped intermediates and prevent aberrant intramolecular protein interactions and protein aggregation (figure from Kim et al. 2013, Annual Review of Biochemistry)

This energy landscape is thought to be rugged (Brockwell and Radford, 2007) for many proteins and, on the route to the native state, proteins may end up in kinetically trapped

folding intermediates or misfolded states. Thus, proteins have to cross these kinetic barriers. Intermediates can accumulate for example at slow folding steps, e.g. prolyl-isomerization and disulfide bond formation, which can be overcome by prolyl isomerases and protein disulfide isomerases (Braakman and Hebert, 2013; Schmidpeter and Schmid, 2015). Additionally, exposure of hydrophobic patches and unstructured regions in partially folded proteins can lead to accumulation of folding intermediates and aggregation. Although, most aggregates are amorphous, some of them are able to form amyloid fibrils, consisting of perpendicular running β-sheets (Balchin et al., 2016). Interestingly, 15-30% of the mammalian proteome is thought to be at least partially unstructured and some proteins form toxic aggregates associated with diseases like Alzheimer's or Parkinson's (Dunker et al., 2008; Balchin et al., 2016).

In the cell, protein misfolding and aggregation is prevented by a remarkable class of proteins - the molecular chaperones - which are found in all branches of life. They bind, stabilize and help unfolded proteins to acquire their native state, but they are not part of the final structure (Hartl and Hayer-Hartl, 2009).
The first hints for chaperone-assisted protein folding resulted from the Hsp60 dependence of an imported mitochondrial protein to reach its native state (Cheng et al., 1989; Ostermann et al., 1989; Horwich et al., 1990) and since then many other molecular chaperones have been discovered. As many of them were found under heat stress conditions, they were termed *heat shock proteins (Hsp)* (Georgopoulos and Welch, 1993; Richter et al., 2010), despite the fact that many of them are also constitutively expressed under normal conditions.

As mentioned above, since abnormal protein folding and aggregation is a major threat to every cell, all organisms have developed a substantial set of control mechanisms to ensure protein homeostasis. Molecular chaperones are at the core of this repertoire (Taipale et al., 2010). Not only do they help newly synthesized proteins in folding (Hartl and Hayer-Hartl, 2009; Finka et al., 2016), but also assemble and disassemble macromolecular complexes (Ellis, 2007) and help in refolding of aberrant proteins as well as breaking up protein aggregates (Doyle et al., 2007). Additionally, they cooperate with the ubiquitin-proteasome system (McClellan et al., 2005) and autophagy (Balchin et al., 2016) to clear misfolded proteins by degradation.

1.2 Chaperone networks and chaperone cooperation

In vivo protein folding starts already during vectorial translation at the ribosome from the N- to the C-terminus of a protein. The earliest contribution to protein folding is already made in the ribosomal exit tunnel and by the ribosome surface itself (Wilson and Beckmann, 2011; Kosolapov and Deutsch, 2009; O'Brien et al., 2011; Nilsson et al., 2015; Holtkamp et al., 2015; Kaiser et al., 2011).

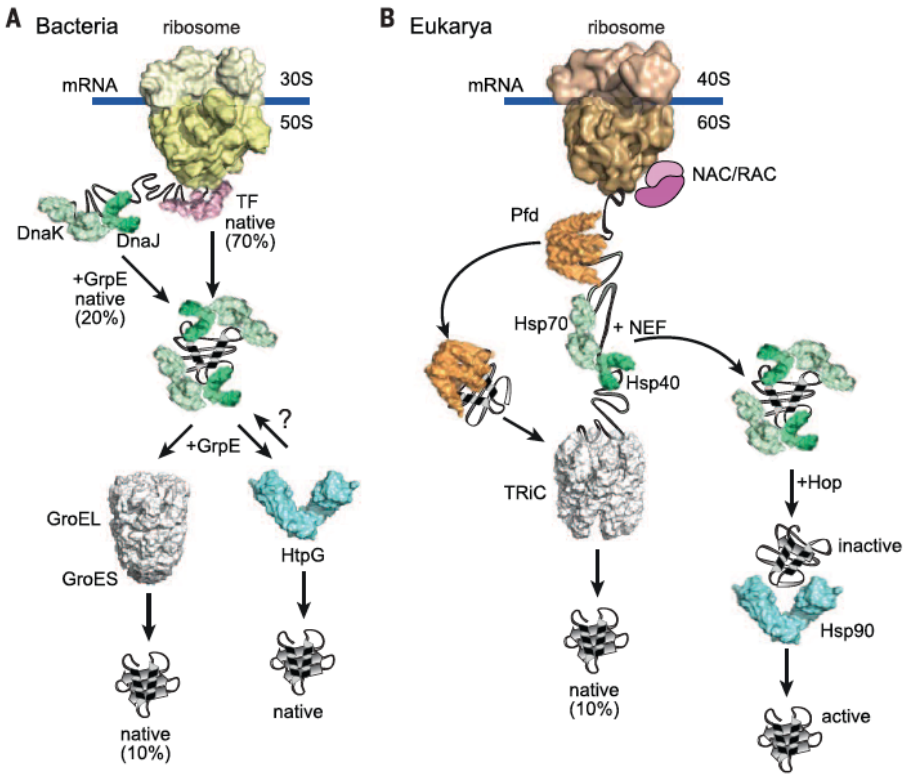

Figure 2: Chaperone network in the bacterial and the eukaryotic cytosol. A) Cytosolic chaperone network in bacteria; B) Cytosolic chaperone network in eukarya (figure from Balchin et al. 2016; Science, used with permission from The American Association for the Advancement of Science)

In bacteria, the first chaperone to interact with a nascent chain is the ribosome interacting chaperone trigger factor (TF, Figure 2A) (Kramer et al., 2002; Ferbitz et al., 2004; Merz et al., 2008). The release of the protein from TF is ATP(adenosine triphosphate)-independent and leads to protein folding or transfer to the bacterial Hsp70 DnaK (Kim

et al., 2013). In eukaryotes, ribosome-associated complex (RAC)and nascent chain associated complex (NAC) have a role similar to TF (Figure 2B), although they are structurally different. RAC, in yeast, consists of the Hsp70 Ssz1 and the Hsp40 co-chaperone zuotin (Zuo1) (Kim et al., 2013; Gautschi et al., 2002, 2001; Peisker et al., 2008) and cooperates with the ribosome-Hsp70 Ssb1/Ssb2 (Rakwalska and Rospert, 2004; Koplin et al., 2010).
NAC is a heterodimer consisting of α and β subunits (Egd1 and Egd2 in yeast) and associates with the ribosome (Preissler and Deuerling, 2012; Wegrzyn et al., 2006; Pech et al., 2010). Its function is at least to some extent redundant with Ssb and, moreover, RAC/Ssb/NAC may be involved in ribosome biogenesis (Koplin et al., 2010).
The classical cytosolic Hsp70 chaperone system is a central protein folding hub in both bacteria and eukaryotes and contributes to protein folding downstream of protein synthesis by the ribosome and the ribosome-associated chaperones (Figure 2A&B). Hsp70s (DnaK in bacteria, Ssa1-4 in yeast and Hsc70 in metazoans and mammalian cells) act on nascent chains as well as newly synthesized proteins, but they do not directly interact with the ribosome (Hartl et al., 2011; Calloni et al., 2012). They are regulated by co-chaperones from the Hsp40 family (also J proteins; e.g. DnaJ in bacteria, various J proteins in yeast an mammals) and nucleotide exchange factors (NEFs) (Kampinga and Craig, 2010).
In addition to ATP-dependent folding and refolding, the Hsp70-Hsp40 system also contributes to transfer to downstream chaperone systems (see Figure 2 A and B), namely the chaperonins (GroEL in bacteria and TRiC/CCT in eukaryotes, respectively), and the Hsp90 system (Hsp90 in eukaryotes and HtpG in bacteria, respectively).

1.3 Chaperone classes and mechanisms

Molecular chaperones are classified based on sequence homology and molecular weight into five classes: (1) Hsp70s, (2) chaperonins (Hsp60s), (3) small heat shock proteins (sHsps), (4) Hsp100s and (5) Hsp90s (Walter and Buchner, 2002).
Hsp70s, Hsp90s, Hsp100s and chaperonins promote protein folding in an ATP-dependent manner and functionally cooperate with ATP-independent chaperones, so called holdases, like the sHsps (Hartl et al., 2011; Haslbeck et al., 2005a). The general ATP-dependent mechanism for chaperone function of Hsp70 is depicted in Figure 3 and is also referred to as *kinetic partitioning*. Here, ATP-dependent cycles of substrate binding and release

promote folding and rebinding of not fully folded proteins prevents aggregation (Balchin et al., 2016; Hartl et al., 2011).

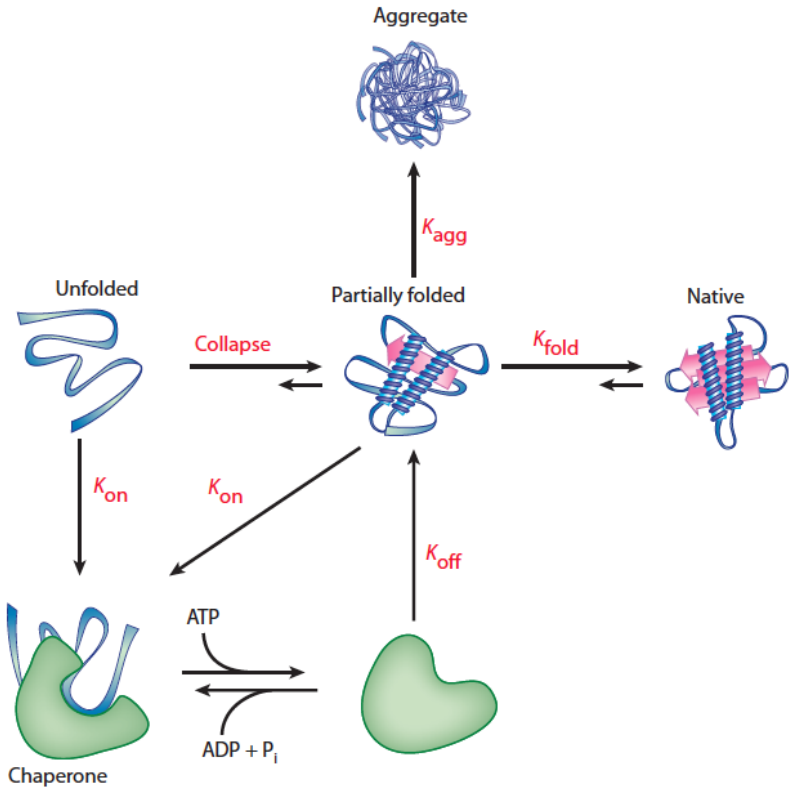

Figure 3: Chaperone action by kinetic partitioning. ATP-dependent chaperones switch from an high affinity to a low affinity state depending on the nucleotide bound to them; (figure from Balchin et al., 2016 Science, used with permission from The American Association for the Advancement of Science)

1.3.1 Hsp70: structure, reaction cycle and regulation

Hsp70 is one of the most highly conserved chaperones. The prokaryotic DnaK shares about 60% sequence identity with eukaryotic Hsp70 proteins. Under physiological conditions, Hsp70s are involved in *de novo* protein folding and under stress conditions they prevent aggregation and unfolding of proteins (Richter et al., 2010). Moreover, they can even refold aggregated proteins (Mayer and Bukau, 2005; Finka et al., 2016).
Hsp70 chaperones consist of a N-terminal nucleotide binding domain (NBD) and a C-terminal substrate binding domain (SBD) which are connected by a hydrophobic linker. The NBD shows an actin-like fold and consists of two lobes which again consist of two subdomains. The nucleotide binding site lies between the two lobes (Bukau and Horwich, 1998; Zuiderweg et al., 2013). The SBD consists of a β-sandwich-fold domain and a α-helical lid domain (Figure 4a, left). The SBD recognizes 5-7 hydrophobic residues flanked by charged amino acids (Bukau and Horwich, 1998). ATP binding leads to conformational changes in the NBD which are allosterically coupled to the SBD and lead to the binding of the lid and the linker to the NBD (Figure 4a, right) (Kityk et al., 2012; Zhuravleva and Gierasch, 2011, 2015). Upon ATP hydrolysis the lid gets freed from the NBD which leads to closing of the SBD (Bertelsen et al., 2009). The ATP-bound state shows high on and off rates for substrates, in contrast to the ADP (adenosine diphosphate)-bound closed state in which on and off rates are low (Bukau and Horwich, 1998; Mayer, 2010).
In addition to Hsp70 regulation by ATP hydrolysis and substrate binding, Hsp70 function is also modulated by co-chaperones. In particular, Hsp40s and nucleotide exchange factors regulate the Hsp70 reaction cycle (Mayer, 2010; Hartl and Hayer-Hartl, 2009).
Hsp40 proteins contain a J domain that binds the NBD and the linker region and stimulate ATP hydrolysis, thereby promoting stable Hsp70-substrate complexes (Mayer, 2010; Hartl and Hayer-Hartl, 2009). Nucleotide exchange factors (NEFs) exchange ADP to ATP and thereby promote substrate release (Figure 3 and 4b).

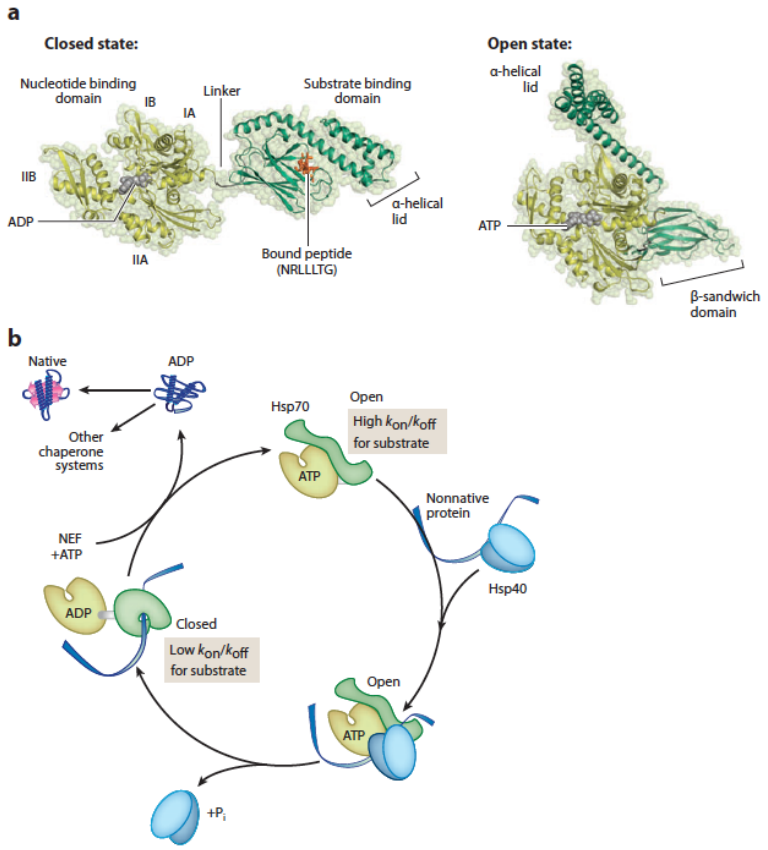

Figure 4: Structure and reaction cycle of Hsp70. a) Closed ADP-bound high substrate affinity state (left) and ATP-bound low substrate affinity state of Hsp70 (right); b) Chaperone cycle of Hsp70: Substrates are bound by Hsp40 and transferred to Hsp70; ATP hydrolysis leads to the closed high affinity Hsp70-substrate complex and release of Hsp40. NEFs exchange ADP to ATP which causes substrate release and Hsp70 is ready to fold the next substrate. (figure from Kim et al. 2013, Annual Review of Biochemistry)

1.3.2 Chaperonins

Chaperonins (Hsp60) are ring-shaped chaperones (Richter et al., 2010; Balchin et al., 2016). They form multisubunit cylindrical complexes that enclose nonnative proteins in a central cavity for protein folding. Chaperonins are divided into group I and group II chaperonins. Group I chaperonins are found in bacteria (GroEL), mitochondria (Hsp60) and chloroplasts (Cpn60), whereas group II chaperonins are found in archea (thermosome) and eukaryotes (CCT/TRiC) (Horwich et al., 2006; Balchin et al., 2016; Hayer-Hartl et al., 2016; Richter et al., 2010; Grallert and Buchner, 2001).

Both classes consist of 7-9 subunits of around 60 kDa each, that form ring structure

complexes of about 1 MDa (Balchin et al., 2016).
The GroEL-GroES system from *Escherichia coli* is the best studied group I chaperonin (Hartl and Hayer-Hartl, 2009; Horwich and Fenton, 2009; Hartl et al., 2011). GroES (Hsp10 in mitochondria) is a 10 kDa protein that functions as a co-factor for GroEL. GroEL forms a cylinder of two heptameric rings (Richter et al., 2010). Each subunit comprises of an equatorial ATPase domain, a hinge domain and a apical domain (Saibil et al., 2013).The apical domain forms the entrance to the central cavity and is required for substrate binding. Two heptameric rings of GroEL (14 subunits total) form two sequentially acting folding chambers, regulated allosterically by ATP binding (Clare et al., 2012; Gruber and Horovitz, 2016). ATP and GroES bind to the substrate bound ring (Figure 5). This leads to encapsulating of the nonnative protein in the GroEL cavity. GroES forms the cap structure of this nanocage which can contain proteins of a size up to 60 kDa for the time it takes GroEL to hydrolyze ATP to ADP (Gupta et al., 2014; Balchin et al., 2016). ATP binding to the opposite ring leads to ADP dissociation, and the release of GroES and the folded protein. For incompletely folded or misfolded proteins rebinding and unfolding followed by another cycle of encapsuling and folding is possible (Lin et al., 2008; Sharma et al., 2008).
Whether the chaperone mechanism of chaperonins is strictly sequential or sometimes parallel, with both folding cavities capped by GroES simultaneously, is still under debate (Sparrer et al., 1997; Taguchi, 2015; Gruber and Horovitz, 2016; Hayer-Hartl et al., 2016).
Encapsulating of the substrate has the advantage that disruption of protein folding by upstream chaperones or by aggregation can be avoided (Balchin et al., 2016). In addition to passive prevention of aggregation (Horwich and Fenton, 2009; Brinker et al., 2001), GroEL-GroES can also contribute to folding acceleration (Sparrer et al., 1997; Beissinger et al., 1999; Brinker et al., 2001; Tang et al., 2006; Chakraborty et al., 2010).

Group II chaperonins (CCT/TRiC in eukaryotes) consist of 8 paralogous subunits per ring (Frydman, 2001; Muñoz et al., 2011; Douglas et al., 2011). They differ from group I chaperonins especially in their apical domains. Group II chaperonins contain finger-like protrusions that form an iris-like, built-in lid that replaces GroES (Hartl et al., 2011). Thus, they can cycle between an open and closed conformation without the requirement of a co-factor. Interestingly, the iris-like lid does not seal completely which allows domain-wise folding of proteins (Rüßmann et al., 2012). Moreover, their subunits

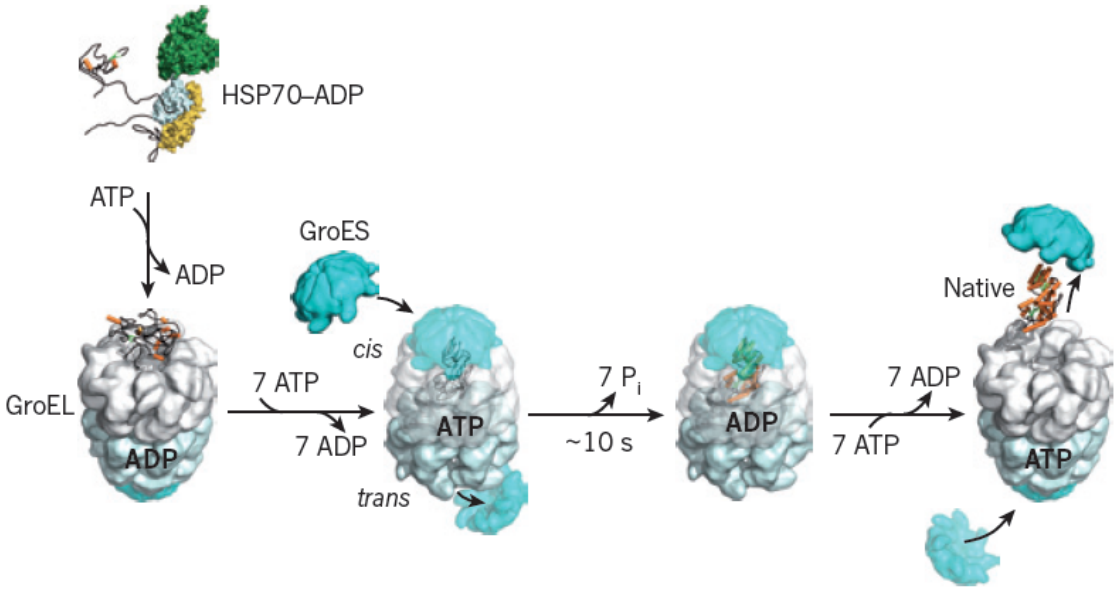

Figure 5: Chaperonin-dependent protein folding. Partially folded substrates get transfered (often from Hsp70) to GroEL. ATP and GroES bind and a nanocage for protein folding is formed. ATP hydrolysis and subsequent ATP binding to the opposite GroEL ring leads to ADP and GroES dissociation and the release of the folded substrate. (figure from Hartl et al. 2011, Nature, used with permission from Nature Publishing Group)

differ in ATP affinity suggesting conformational changes to be sequential (Reissmann et al., 2012; Rivenzon-Segal et al., 2005).

1.3.3 Small Heat Shock Proteins

sHsps are the most widespread and most poorly conserved family of molecular chaperones (Richter et al., 2010). Their major role is to prevent and control protein aggregation (Horwitz, 1992; Jakob and Buchner, 1994). They show a high degree of heterogeneity in sequence and size (Haslbeck et al., 2005a), yet, all of them have a conserved α-crystallin domain as a common feature. Often they form large oligomers of 24 subunits and more (Van Montfort et al., 2001).

In contrast to many other cytosolic chaperones, sHsps are ATP-independent chaperones, also referred to as holdases. Notably, also in contrast to other chaperones, sHsps are able to bind several substrate molecules at a time (Haslbeck et al., 1999; Lee et al., 1997). Moreover, stable substrate binding to sHsps is believed to keep misfolded proteins in a refolding-competent state (Ehrnsperger et al., 1997; Kampinga et al., 1994; Lee et al.,

1997; McHaourab et al., 2009).

sHsps are activated by various triggers like temperature (Franzmann et al., 2008; Haslbeck et al., 1999; Lee et al., 1995), redox state (Kumsta and Jakob, 2009), post translational modifications (Aquilina et al., 2004; Peschek et al., 2013; Rogalla et al., 1999) and pH (Fleckenstein et al., 2015). These triggers control the equilibrium distribution of oligomers which, in turn, correlates with chaperone activity (Fleckenstein et al., 2015). Moreover, they are believed to serve as storage place for unfolded proteins (Richter et al., 2010), but are also part of aggregates and cooperate with Hsp70 and Hsp100 in refolding of aggregated and misfolded proteins (Haslbeck et al., 2005b; Cashikar et al., 2005; Liberek et al., 2008). The proposed chaperone action of sHsps is summarized in Figure 6.

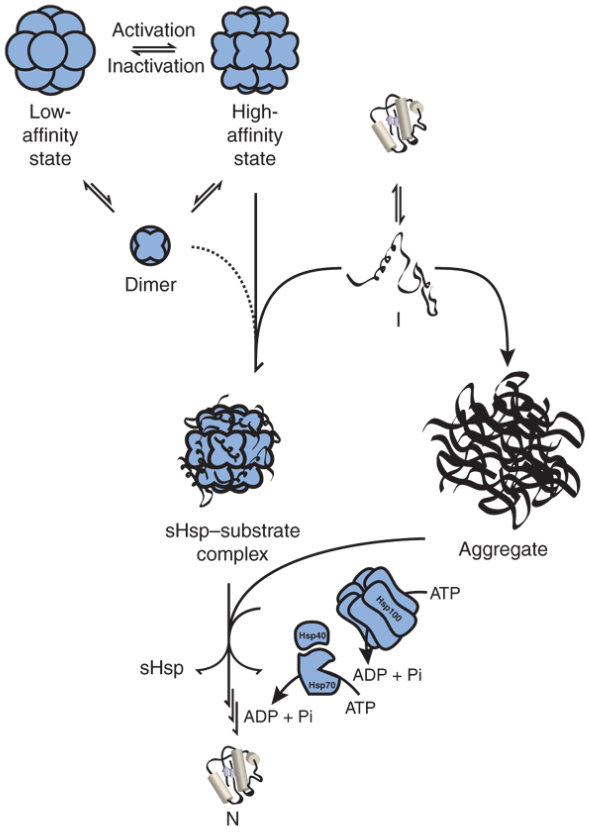

Figure 6: sHsp prevent protein aggregation. An external trigger leads to sHsp activation. Binding of unfolded proteins to sHsps prevents aggregate formation and protein refolding can be achieved by the help of ATP-dependent chaperones. (figure from Haslbeck et al. 2005a, Nature Structural and Molecular Biology, used with permission from Nature Publishing Group)

1.3.4 Hsp100

Hsp100 chaperones belong to a conserved family of AAA+-ATPases (Beyer, 1997; Neuwald et al., 1999). Hsp100s form a hexameric ring and also function as unfolding component of certain proteases (Jeng et al., 2015; Sauer and Baker, 2011; Alexopoulos et al., 2012). The discovery that yeast Hsp104 functions in protein disaggregation (Parsell et al., 1994), in contrast to protein degradation, established the Hsp100s as a new family of ATP-dependent molecular chaperones (Jeng et al., 2015; Richter et al., 2010). Other members of the family were soon discoverd in bacteria (ClpB) and plants (Hsp101) (Jeng et al., 2015). In general, Hsp100s are thought to pull misfolded or aggregated proteins through their central pore in an unfolded state, so that they get the ability to refold. Depending on their number of AAA+ domains per monomer, Hsp100s are divided into two groups: Class 1 contains two AAA+ domains per monomer, class 2 Hsp100s have one AAA+ domain (Richter et al., 2010).

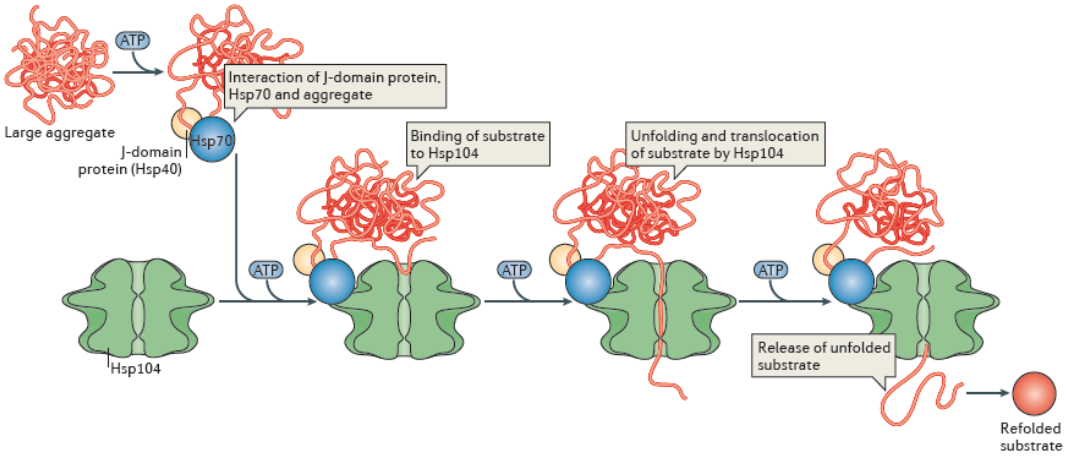

Figure 7: Hsp100s contribute to refolding of aggregated proteins. Hsp104 is recruited to protein aggregates by Hs70-Hsp40. The substrate gets unfolded and pulled through the central pore of Hsp104 in an ATP-dependent manner. Unfolded substrates can refold afterwards. (figure from Doyle et al. 2013, Nature Reviews Molecular Cell Biology, used with permission from Nature Publishing Group)

The functionally active species of yeast Hsp104 is the homohexamer (Lee et al., 2003, 2007, 2010; Carroni et al., 2014). To recover functional proteins from aggregates, yeast Hsp104 needs the help of Hsp70 and Hsp40 (Glover and Lindquist, 1998), whereas bacterial ClpB requires the assistance of DnaK, DnaJ and GrpE (Motohashi et al., 1999; Goloubinoff et al., 1999; Zolkiewski, 1999)(Figure 7). Hsp70 targets Hsp104 to both,

amorphous and ordered aggregates (Doyle et al., 2013; Tipton et al., 2008; Winkler et al., 2012) and Hsp104 then uses an ATP-driven power stroke to extract proteins from aggregates and unfolds misfolded proteins by threading them through its cental pore (Figure 7) (Jeng et al., 2015; Lum et al., 2004). The unfolded proteins are then believed to fold spontaneously or to be substrates for other chaperones (Doyle et al., 2013).

It is noteworthy, that some higher eukaryotes like nematods, arthropodes and mammals lack cytosolic Hsp100 class 1 porteins. In contrast to TRiC/CCT that seems to act mechanistically similar to GroEL-GroES, these organisms don't seem to have a related protein complex with disaggregation acitivity (Richter et al., 2010), but for the human and nematode Hsp70 system it was reported that they can fullfil a similar function in concert with J proteins (Nillegoda et al., 2015).

1.4 The molecular chaperone Hsp90

The molecular chaperone Hsp90 is - already under unstressed conditions - one of the most abundant proteins in a cell, comprising 1-2% of a cell's protein content (Welch and Feramisco, 1982; Lai et al., 1984). Hsp90 is evolutionary conserved and is responsible for the folding, activation and assembly of Hsp90-dependent proteins, termed clients (Pearl et al., 2008; Pratt et al., 2008). In the yeast *Saccharomyces cerevisiae*, high-throughput studies suggest that a vast number of the proteome is Hsp90-dependent (Hartson and Matts, 2012). The growing list of client proteins
(http://www.picard.ch/downloads/Hsp90interactors.pdf) is quite diverse and contains many different protein classes like kinases, transcription factors, signalling molecules and many other protein classes involved in a broad range of biological processes (Zhao et al., 2005; McClellan et al., 2007).
Hsp90 is found in eukaryotes and eubacteria, but only in eukaryotes it is essential under normal conditions (Borkovich et al., 1989; Pratt and Toft, 2003). Whereas prokaryotes carry only a non-essential form of Hsp90 (HtpG), eukaryotes contain multiple forms of Hsp90 including two cytosolic variants (Hsp90α and Hsp90β in mammals and Hsp82 and Hsc82 in yeast, respectively) (Sreedhar et al., 2004).
Moreover, there are different Hp90 isoforms expressed in different cellular compartments: Grp94 in the endoplasmic reticulum (ER), TRAP1 in mitochondria and Hsp90C in plastids (Johnson, 2012; Stankiewicz and Mayer, 2012; Taipale et al., 2010; Mayer and

Le Breton, 2015).

1.4.1 Structure of Hsp90

Hsp90 forms homodimers and the dimerization is essential *in vivo* (Mayer and Le Breton, 2015; Wayne and Bolon, 2007). Each protomer consists of three highly conserved domains: The N-terminal ATP-binding domain, the middle domain and the C-terminal dimerization domain (Prodromou et al., 1997a). The N-terminal domain (NTD, N-domain) and the middle domain (MD, M-domain) are connected by an unstructured, charged linker important for the *in vivo* function of Hsp90. The C-terminal domain (CTD, C-domain) contains an MEEVD-motif important for the binding of *tetratricopeat* (TPR)-containing co-chaperones (Wandinger et al., 2008; Hainzl et al., 2009; Tsutsumi et al., 2009, 2012). Hsp90 dimerization is promoted by the C-terminal domain leading to a V-shaped (open) conformation (Shiau et al., 2006). During folding of its client proteins, Hsp90 undergoes various ATP-driven conformational changes. ATP binding induces a shift from the open to the closed conformation (Figure 8) in which the N-terminal domains dimerize and the middle domains are reorientated to support efficient ATP-hydrolysis (Ali et al., 2006). Several intermediates of the Hsp90 and HptG chaperone cycle have been identified and some Hsp90 co-chaperones target these intermediate states (Graf et al., 2009; Mayer et al., 2009; Mickler et al., 2009; Hessling et al., 2009; Krukenberg et al., 2008; Dollins et al., 2007).

Although crystal structures from bacterial, yeast and mammalian Hsp90s in apo, ADP and AMP-PNP (adenylyl imidotriphosphat) bound state, despite being in different conformational states, seem to be symmetric (Ali et al., 2006; Dollins et al., 2007; Shiau et al., 2006), also asymmetric states may be important for Hsp90 function (Mayer and Le Breton, 2015). For example, the structure of TRAP1 from *Danio rerio* in complex with ATP analoga shows asymmetry in the closed state (Lavery et al., 2014). Since the only other crystal structure of Hsp90 in the closed state contained also two molecules of Sba1/p23 per Hsp90 dimer (Ali et al., 2006), which influence the conformation of the MD and the CTD (Graf et al., 2014; Karagöz et al., 2011), asymmetric states might be a more general feature of Hsp90 than thought previously (Mayer and Le Breton, 2015).

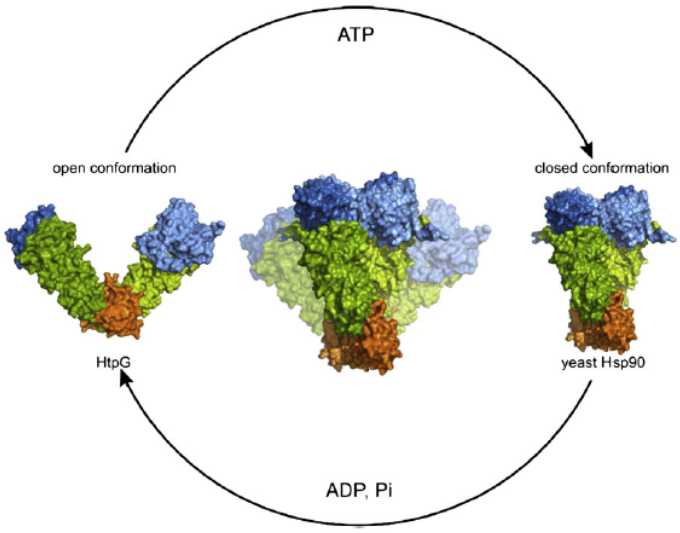

Figure 8: Hsp90 shifts from an open to a closed conformation (and back). ATP binding leads to N-domain dimerization and structural rearrangements to shift Hsp90 from an V-shaped open conformation to a closed conformation. ATP hydrolysis leads to N-domain dissociation and Hsp90 switches back to the open conformation (figure from Li et al. 2012, Biochimica et Biophysica Acta (BBA) - Molecular Cell Research, used with permission from Elsevier)

1.4.2 ATP-binding and hydrolysis

Hsp90 belongs to the GHKL (gyrase, HSP90, histidine kinase and MutL) superfamily of ATPases (Taipale et al., 2010; Pearl and Prodromou, 2006).

The nucleotide binding site is located in the NTD of Hsp90 and shows an α- and β-sandwich motif (Figure 9). Hsp90 has a quite low ATP affinity ($K_D \sim 400$ µM) and shows intrinsically low (yeast Hsp90 one ATP molecule per 1-2 min, human Hsp90 ten-fold slower) ATPase activity (Prodromou et al., 1997a; Stebbins et al., 1997; Prodromou et al., 1997b; Panaretou et al., 1998; Scheibel et al., 1997; Weikl et al., 2000; Young and Hartl, 2000; McLaughlin et al., 2002; Wayne and Bolon, 2007; Richter et al., 2008).

In the apo state, Hsp90 adopts an open V-shaped conformation. Binding of ATP, in order to acquire the catalytically active state, triggers Hsp90's ATP lid, consisting of several conserved amino acid residues in the NTD, to close over the ATP-bound, but not ADP-bound, nucleotide binding pocket, leading to the first intermediate (I1) state. Concomitant structural rearragements induce a closed state, where the N-domains dimerize and associate with the middle domains (I2). In this state, ATP hydrolysis takes place. Moreover, a catalytic loop from the middle domain containing a catalytic Arg residue

is involved in ATP hydrolysis. After hydrolysis, the N-domains dissociate, ADP and P_i (orthophosphate) is released and Hsp90 returns to the open conformation. (Li et al., 2012; Taipale et al., 2010; Meyer et al., 2003; Prodromou et al., 2000; Richter et al., 2002; Hessling et al., 2009; Prodromou, 2012).

Figure 9: N-terminal domain of Hsp90 The N-terminal domain of Hsp90 (orange) binds and hydrolyses ATP (red). pdb-code: 2CG9

The ATPase activity of Hsp90 has been reported to be essential *in vivo* (Obermann et al., 1998; Panaretou et al., 1998; Mishra and Bolon, 2014), but our recent results have challenged this observation suggesting that the ability to bind ATP is sufficient for *in vivo* function (Zierer, Tippel, Schopf, Buchner; unpublished).

1.4.3 Regulation by co-chaperones

During the Hsp90 chaperone cycle, various helper proteins – named co-chaperones – interact with Hsp90. They regulate its ATPase activity, conformational state and are recruited to specific subsets of Hsp90 clients (Chen and Smith, 1998; Prodromou et al., 1999; Panaretou et al., 2002; Richter et al., 2004; Roe et al., 2004). Some of them contain TPR domains that recognize the C-terminal MEEVD pentapeptide in Hsp90 via a conserved clamp domain (Figure 10). TPR domains consist of 34 amino acid

repeats which form two anti-parallel α-helices separated by a turn. Three helix-turn-helix motifs stack on each other, forming a superhelical groove, which interacts with the very C-terminus of Hsp90 (Li et al., 2012; Das et al., 1998; Scheufler et al., 2000).

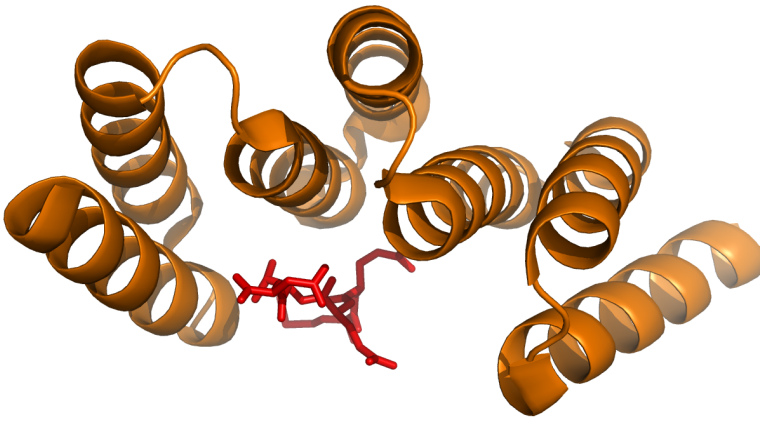

Figure 10: Structure of TPR2A from HOP. Crystal structure of the TPR2A domain of HOP (orange) in complex with the Hsp90 peptide MEEVD (red). pdb-code: 1ELR

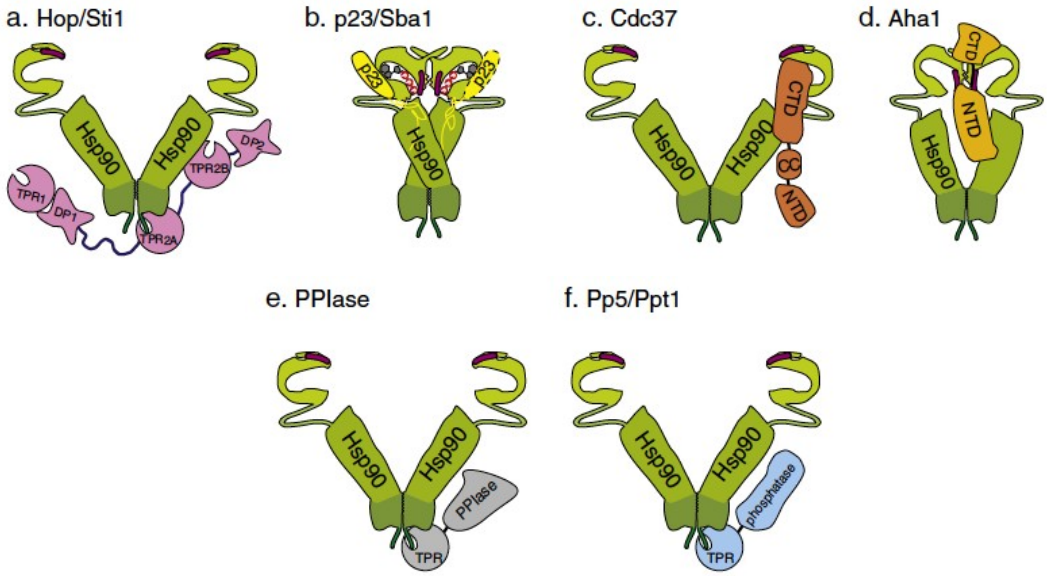

Figure 11: Association of Hsp90 with various co-chaperones. a) Hop/Sti1, b)p23/Sba1, c) Cdc37, d)Aha1, e)PPIase, f)Pp5/Ppt1 (figure modified from Li et al. 2012, Biochimica et Biophysica Acta (BBA) - Molecular Cell Research, used with permission from Elsevier)

In the following, a selection of well characterized Hsp90 co-chaperones is described in more detail. Note, that Cns1, the major topic of this thesis, is described in an extra

section at the end of the introduction.

Sti1/Hop

Sti1/Hop binds Hsp90 in the open conformation (Figure 11a) and inhibits the ATPase activity (Prodromou et al., 1999; Johnson et al., 1998; Richter et al., 2003; Li et al., 2011). It contains three TPR domains and two DP domains which allow simultanous binding and modulation of Hsp90 and Hsp70 which facilitates client protein transfer (Chen and Smith, 1998; Wegele et al., 2003, 2006; Schmid et al., 2012).
Sti1/Hop is a monomeric protein and binding of one Sti1 molecule per Hsp90 dimer is sufficient to inhibit Hsp90's ATPase activity (Yi et al., 2010; Li et al., 2011). Sti1/Hop is also regulated by posttranslational modifications, e.g. S-nitrosylation is involved in maturation of cystic fibrosis transmembrane conductance regulator (CFTR) (Marozkina et al., 2010) and, moreover, Sti1 is subject to regulation by phosphorylation (Röhl et al., 2015).

Sba1/p23

Sba1/p23 binds specifically to the closed conformation (Figure 11b) of Hsp90 (Chadli et al., 2000; Grenert et al., 1999). The binding site is predominantly at the N-terminal domain (Ali et al., 2006; Prodromou et al., 2000). Sba1 partially inhibits the ATPase activity of Hsp90 (Richter et al., 2004; McLaughlin et al., 2006) and was found in steroid hormone receptor complexes with Hsp90 (Johnson and Toft, 1994). Additionally, p23/Sba1 has an unstructured C-terminal tail, which is important for its intrinsic chaperone activity (Weikl et al., 1999; Weaver et al., 2000).

Cdc37

Another co-chaperone that inhibits the ATPase activity of Hsp90 is Cdc37. This is achieved by preventing lid closure and the association of the Hsp90-N domains (Figure 11c) (Gaiser et al., 2010; Siligardi et al., 2002). Early studies on the oncoprotein v-Src (viral Src kinase) identified Cdc37 as part of the Hsp90-kinase complex (Dey et al., 1996; Brugge, 1986). Later, it was shown to specifically facilitate the maturation of kinases (MacLean and Picard, 2003; Mandal et al., 2007; Taipale et al., 2014, 2013, 2012; Boczek et al., 2015; Verba et al., 2016).

In *S. cerevisiae* deletion of *CDC37* is lethal, highlighting its importance as an Hsp90 co-chaperone (Breter et al., 1983).

Aha1 and Hch1

Aha1 (Figure 11d) was shown to be a potent accelerator of Hsp90's ATP turnover (Panaretou et al., 2002; Meyer et al., 2004). Although the double deletion of *AHA1* and its homologue *HCH1* are not lethal in yeast (Mayer et al., 2002), maturation of clients like v-Src or hormone receptors is severely affected in double knock-out cells (Lotz et al., 2003).
Aha1 binds both, the Hsp90 M- and N-domain and accelerates the ATPase cycle by supporting closing of the N-domains in an asymmetric manner (Lotz et al., 2003; Retzlaff et al., 2010; Hessling et al., 2009). Aha1 seems to bypass the I1 state of Hsp90, moving directly to I2 (Hessling et al., 2009). Moreover, Aha1 is required for the controlled exit of Sti1 from the Hsp90 chaperone cycle (Li et al., 2013). Human Aha1 furthermore seems to be regulated by phosphorylation (Dunn et al., 2015).
Interestingly, like Hop (see above), Aha1 is also involved in maturation of CFTR, making it a theurapeutic target for cystic fibrosis (Wang et al., 2006).

PPIases

Work on steroid hormone receptors identified peptidyl-prolyl-isomerases (PPIases) as TPR-containing co-chaperones of Hsp90. Examples for mammalian proteins are Fkbp52, Fkbp51 and Cyp40 (Johnson and Toft, 1994; Pirkl and Buchner, 2001; Peattie et al., 1992; Ratajczak et al., 2009). In addition to their TPR domain(s) for Hsp90 interaction (Figure 11e), they contain a PPIase domain which catalyzes the cis/trans isomerization of peptide bonds prior to proline residues (Fanghänel and Fischer, 2004).
In *S. cerevisiae*, Cpr6 and Cpr7 are the two known members of TPR-containing peptidyl-prolyl-isomerases that are Hsp90 co-chaperones (Duina et al. 1996a; Duina et al. 1996b). They bind Hsp90 via a TPR motif (Figure 11e) and additionally harbour intrinsic chaperone activity (Bose et al., 1996; Freeman et al., 1996; Mayr et al., 2000). Although, Cpr6 was shown to form mixed complexes with Hsp90 and Sti1 (Li et al., 2011), the specific role of PPIases in client maturation is not understood. Due to the overlapping function of Cpr7 with Cns1, the major topic of this thesis, more details on this PPIase are presented below (section 1.4.7).

Ppt1/PP5

The protein phosphatase Ppt1 also binds Hsp90 via its N-terminal TPR domain (Figure 11f). The phosphatase activity is intrinsically inhibited and becomes active after binding to Hsp90 (Kang et al., 2001). Ppt1 specifically catalyzes the dephosphorylation of Hsp90 and Cdc37 (Wandinger et al., 2006; Vaughan et al., 2008) and the Hsp90 phosphorylation status was shown to be important for client maturation and Hsp90 conformational switching (Wandinger et al., 2006; Soroka et al., 2012).

1.4.4 Hsp90 regulation by post-translational modification

In addition to the regulation of Hsp90 by co-chaperones, post-translational modifications (PTMs) add a further layer to the complexity of the Hsp90 chaperone cycle. In the following, a short overview of Hsp90's PTMs and some selected examples are given.

Phosphorylation

The most frequent PTM of Hsp90 is phosphorylation (Li et al., 2012). Serines, threonines as well as tyrosines were reported to be phosphorylated (Scroggins and Neckers, 2007a). Hyperphosphorylation of Hsp90 in the absence of Ppt1 leads to decreased client activation in yeast and affects conformational switching (Wandinger et al., 2006; Soroka et al., 2012). Neckers and co-workers showed that Wee1/Swe1 phosphorylates a specific tyrosine residue in the N-domain of Hsp90 in a cell cycle dependent manner and that this phosphorylation affects geldanamycin binding and the sensitivity of cancer cells to Hsp90-inhibitor-induced apoptosis (Mollapour et al., 2010).
Furthermore, CKII dependent phosphorylation of threonine 22 in Hsp90's N-domain was reported to modulate ATPase activity, client activation and co-chaperone interactions and this modification was shown to alter drug sensitivity (Mollapour et al. 2011a, Mollapour et al. 2011b).

Acetylation

Hsp90 is also subject to acetylation. p300 was reported to acetylate Hsp90, whereas HDAC6 appears to be an Hsp90 deacetylase (Yang et al., 2008; Kovacs et al., 2005). Blocking HDAC6 activity was shown to compromise interaction with clients and acety-

lation seems to be a key regulator in yeast and man, influencing co-chaperone binding and client maturation (Kovacs et al., 2005; Bali et al., 2005 Scroggins et al., 2007b; de Zoeten et al., 2011).

SUMOylation

One of the most recent discovered Hsp90 PTMs is SUMOylation (Mollapour et al., 2014). In general, protein SUMOylation modifies the activity of the target protein by altering its conformation, localization, or interaction with co-factors (Flotho and Melchior, 2013; Mayer and Le Breton, 2015).
In yeast Hsp90, K178 is SUMOylated in an asymmetric manner and supports the recruitment of the ATPase activator Aha1 and, interestingly, the binding of Hsp90 inhibitors (Mollapour et al., 2014).

Other PTMs and complexity of PTMs

In addition to the above mentioned PTMs, also S-nitrosylation and methylation of Hsp90 were reported (reviewed in Li et al. 2012). The complexity of all posttranslational modifications currently known exceeds the capacities for analysis. For example $3x10^{42}$ and $7x10^{41}$ different variants of Hsp90α and Hsp90β, respectively, are possible, which is more than the number of Hsp90 molecules in the human body (ca. 10^{21})(Mayer and Le Breton, 2015). This suggests, that not all possible modifications and their combinations have relevance *in vivo*.

1.4.5 The Hsp90 chaperone cycle

During the maturation of client proteins, Hsp90 functions in concert with a vast number of co-chaperones which are crucial to drive the chaperone cycle of Hsp90 client protein interactions (Li et al., 2012). Maturation of several client proteins involves cooperation of the Hsp90 system with Hsp70. Sti1 serves as an adaptor and connects Hsp90 with Hsp70 (Johnson et al., 1998; Wegele et al., 2006; Schmid et al., 2012).
Research on the assembly of Hsp90 with steroid hormone receptors has shown that several distinct Hsp90-co-chaperone complexes are formed during the maturation processes (Pratt and Toft, 1997; Smith, 1993; Johnson and Toft, 1994; Smith et al., 1992). A new model for the Hsp90 chaperone cycle emerges from recent studies (Li et al., 2011, 2013). One Sti1 binds to Hsp90 and blocks the ATPase reaction. The client protein is first

bound to Hsp70/Hsp40 and then transfered to Hsp90. Sti1 serves as an adaptor in this process. The second TPR acceptor site of Hsp90 is occupied by a PPIase forming an asymmetric complex. Binding of ATP and Sba1/p23 releases Sti1/Hop and Hsp70 and the late complex is formed. Then ATP is hydrolyzed and the PPIase, Sba1/p23 and the mature client are released (Figure 12).

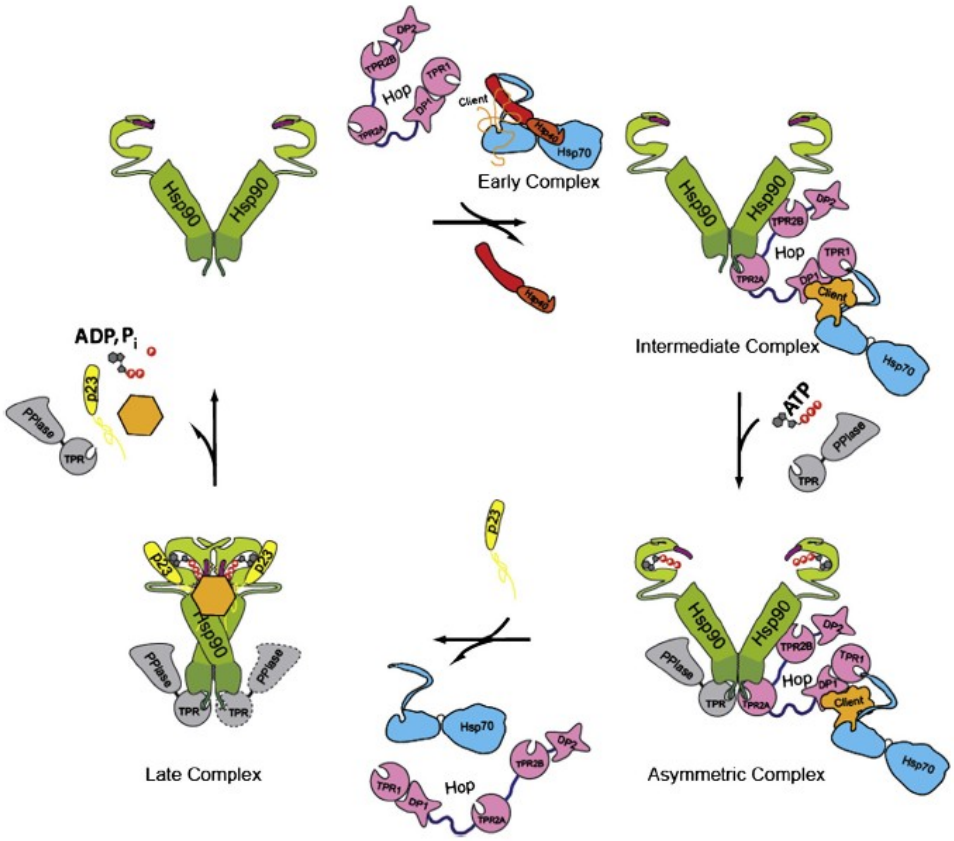

Figure 12: Model of the Hsp90 chaperone cycle. Hop/Sti1 acts as an adaptor between the Hsp70-Hsp40-substrate-complex and Hsp90, leading to the formation of an asymmetric complex. After substrate transfer Hsp70 and Hop/Sti1 get released and the closed complex is formed. After ATP hydrolysis the folded substrate and the remaining co-chaperones get released (figure from Li et al. 2012, Biochimica et Biophysica Acta (BBA) - Molecular Cell Research, used with permission from Elsevier)

1.4.6 Hsp90 client proteins

In order to be classified as a Hsp90 client, a protein has to fulfill two critera. First, it must physically interact with Hsp90 and, second, inhibition of Hsp90 must lower the client's activity (Taipale et al., 2010).

In contrast to Hsp70, Hsp90 clients don't seem to share structural features or sequence

motifs and their intrinsic thermodynamic (in)stability seems rather to be the important criterion. Therefore, interaction half-life increases with increased unfolding propensity (Taipale et al., 2012). Thus, Hsp90 is thought to act at late stages in protein folding (Mayer and Le Breton, 2015).
In yeast, approx. 20% of the proteome (BIOGRID database) seems to be influenced by Hsp90 (Taipale et al., 2010; Oughtred et al., 2016). This is in contrast with the view that Hsp90 has a limitied client spectrum, but given the fact, that Hsp90 clients often are at central regulatory nodes, genetic interactions often capture an entire biological process rather that a specific genetic interaction. Moreover, physical interaction partners do not only contain co-chaperones and *bona fide* clients, but also proteins that don't need Hsp90 for their function (Taipale et al., 2010), for example due to unspecific interactions.

Glucocorticoid receptor (GR)

GR was one of the earliest characterized Hsp90 clients (Joab et al., 1984; Schuh et al., 1985; Sanchez et al., 1985). It requires Hsp40, Hsp70, HOP, Hsp90 and p23 as the minimal chaperone machine (Morishima et al., 2000). Two studies used the ligand binding domain (LBD) of GR for detailed investigations on client chaperoning by Hsp90 (Lorenz et al., 2014; Kirschke et al., 2014). Due to the intrinsic instability of GR-LBD (Seitz et al., 2010; Bledsoe et al., 2002), the researchers had to introduce either stabilizing mutations or fuse it to maltose binding protein. Interestingly, the GR-LBD slowed down the transition of yeast Hsp90 from the open to the closed state, decreasing the ATPase activity. This adds another layer of complexity to the Hsp90 chaperone cycle, suggesting that not only co-chaperones, but also clients themselves modulate Hsp90. (Lorenz et al., 2014). One interesting aspect of GR regulation by chaperones is that incubation of GR with Hsp70, Hsp40 and ATP seems to lead to a loss of hormone binding capacity, which is restored by the addition of Hsp90, HOP and p23 (Kirschke et al., 2014).
Interestingly, GR stays with Hsp90 even after activation and travels with it to the nucleus (Pratt et al., 1999; Harrell et al., 2004).

Kinases

The largest coherent group of Hsp90 clients is kinases (Taipale et al., 2012). Indeed, Hsp90 was first found in complex with viral Src kinase (Brugge et al., 1981; Schuh et al.,

1985; Brugge, 1986), which is now known to be one of the most stringent Hsp90 clients, but also other kinases like Cdk4, BRAF or ERBB2 are Hsp90 clients (Taipale et al., 2010).
During the last few years, it was shown that kinase maturation by Hsp90 is strongly dependent on the co-chaperone Cdc37 (MacLean and Picard, 2003; Mandal et al., 2007; Taipale et al., 2014, 2013, 2012; Boczek et al., 2015; Verba et al., 2016).

Other clients

In addition to the two well characterized client groups kinases and steroid hormone receptors (see above), many other client proteins were reported (see Figure 13 for an overview). These include for example mitochondrial proteins, myosin, viral proteins, eNOS, TERT, HSF1, but also the intrinsically disordered protein Tau (reviewed in Taipale et al. 2010; Mayer and Le Breton 2015), as well as E3 ligases (Taipale et al., 2012).

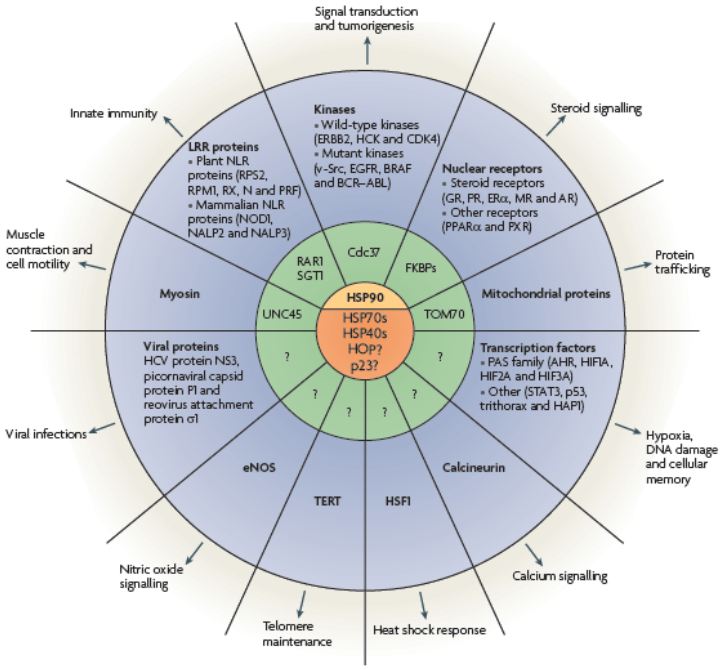

Figure 13: Overview of Hsp90 clients (figure from Taipale et al. 2010, Nature Reviews Molecular Cell Biology, used with permission from Nature Publishing Group)

1.4.7 The co-chaperones Cns1/TTC4 and Cpr7

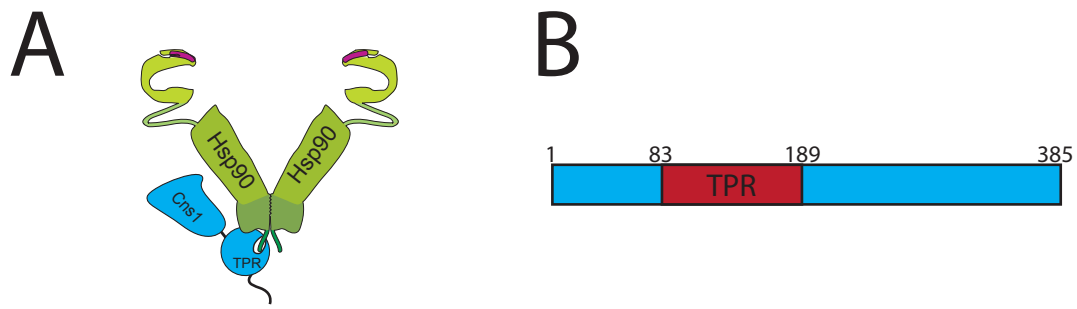

Figure 14: The interaction of Cns1 with Hsp90. A) Cns1 interacts with Hsp90 via its C-terminal domain. B) Domain architecture of Cns1.

In yeast, only three Hsp90 co-chaperones are essential. Cdc37, Sgt1 and the TPR containing co-chaperone Cns1, the major topic of this thesis (Figure 14A). It is known, that Cdc37 functions in kinase maturation (see above) and Sgt1 was shown to facilitate kinetochor assemby by linking Hsp90 to Skp1 (Kitagawa et al., 1999; Catlett and Kaplan, 2006) as well as being involved in regulation of adenylat cyclase (Dubacq et al., 2002; Flom et al., 2012), wheras the essential function of Cns1 remains unclear.
Cns1 consists of an N-terminal uncharacterized domain, a central TPR domain and a C-terminal domain with unknown function (Figure 14B). It was found to be an allel-specific suppressor of Hsp90 mutations in yeast (Nathan et al., 1999). The lethality of a *CNS1* deletion can not be suppressed by overexpression of other TPR containing co-chaperones (Dolinski et al., 1998), but overexpression of *CNS1* can cure the growth defect of a *cpr7* deletion mutant. Therefore, it is thought, that Cns1 and Cpr7 have a similar function *in vivo* (Marsh et al., 1998; Tesic et al., 2003). In addition, Cns1 overexpression can restore nucleotide-dependent binding of Cpr6 to Hsp90 in a *cpr7* deletion strain (Zuehlke and Johnson, 2012). Moreover, Cns1 and Cpr7 were reported to be involved in prion propagation (Kumar et al., 2015; Moosavi et al., 2010; Lancaster et al., 2013) as well as being interactors of the intact ribosome (Tenge et al., 2015).
Furthermore, it was shown that a thermo-sensitive *cns1* mutant shows a specific growth defect in a double mutant with a form of Hsp90 lacking the C-terminal MEEVD motif. Additionally, it was reported that the viability of yeast cells is not affected by deletion of Cns1's C-terminal domain (Tesic et al., 2003). Besides binding to Hsp90, Cns1 also binds to Hsp70/Ssa1 and stimulates its ATPase activity, whereas the ATPase activity of Hsp90 is not affected (Hainzl et al., 2004).

In higher eukaryotes, homologues of Cns1 were found, e.g. the Drosophila protein Dpit47 was shown to be a nuclear Hsp90 co-chaperone that interacts with DNA polymerase α (Crevel et al., 2001). The human orthologue TTC4 was identified through its localisation to a genomic region associated with breast cancer (Su et al., 1999). It was shown to localize to the cytoplasm and the nucleus and that its nuclear transport depends on the cell cycle (Dmitriev et al., 2007, 2009). Furthermore, it is known that TTC4 interacts with CDC6 which might link Hsp90 to DNA replication (Crevel et al., 2008).
Except for the above-mentioned bits and pieces, the precise function(s) of Cns1/TTC4 and whether its essential function is Hsp90- or Hsp70-dependent remain(s) still enigmatic.

2 Objective and Significance

This PhD thesis focuses on the characterization of the essential co-chaperone Cns1, both *in vivo* and *in vitro*.
In the first part, plasmid shuffling will be used to determine the *in vivo* function of the single Cns1 domains. Moreover, this method will help to identify a minimal construct required for cell viability as well as whether Cns1's essential function is dependent on Hsp90 or Hsp70. Based on these results, several constructs will be selected for further *in vitro* analyses.
After purification, binding of Cns1 and mutant constructs thereof will be tested for Hsp90 interaction using analytical ultracentrifugation. In addition, these constructs will be investigated on their effect on the Hsp90 ATPase activity using a regenerative system based ATPase assay.
Moreover, the structure of Cns1 will be characterized in more detail. This part of the project will implicate CD spectroscopy, protein crystallography, small angle X-ray scattering and NMR spectroscopy.
Furthermore, multi-copy-suppressor and synthetic genetic array screens will help to identify genetic interactors of *cns1* mutants and will contribute to a broader understanding of the *in vivo* function of Cns1. These assays will be combined with *in vivo* pull-down assays to identify Cns1-interacting proteins in the cell. Findings from these experiments will then be investigated in more detail on their *in vivo* relevance.
In addition to Cns1, its human orthologue TTC4 will be characterized. This will be achieved by using 5'-FOA shuffling to determine a possible functional replacement of Cns1 by TTC4 in yeast cells and *in vitro* analysis using aUC, ATPase assays and CD spectroscopy as well as protein crystallography.

In summary, the results of this work will not only contribute to a better understanding of the co-chaperone Cns1 in general, but will also provide significant insights into the biochemistry and biology of the Hsp90 chaperone machine.

3 Materials and Methods

3.1 Materials

3.1.1 Chemicals

Table 1: Chemicals used in this study

2-propanol	Roth, Karlsruhe, Germany
$^{15}NH_4Cl$	Cortecnet, Voisins-Le-Bretonneux, France
5'-fluoroorotic acid (5'-FOA)	Thermo Fisher, Walham, USA
β-mercaptoethanol	Sigma, St. Louis, USA
Acetic acid	Roth, Karlsruhe, Germany
Acrylamid/Bis solution 38:2 (40% w/v)	Serva, Heidelberg, Germany
Adenine	Sigma, St. Louis, USA
Adenosin-5'-diphosphate (ADP) disodium salt	Roche, Mannheim, Germany
Adenosin-5'-triphosphate (ATP) disodium salt	Roche, Mannheim, Germany
Adenylyl Imidodiphosphat (AMP-PNP)	Roche, Mannheim, Germany
Agar Agar	Serva, Heidelberg, Germany

Chemicals used in this study (continued)

Agarose	Serva, Heidelberg, Germany
Alanine	Sigma, St. Louis, USA
Ammonium persulfate (APS)	Roth, Karlsruhe, Germany
Ammonium suflate 14-18 hydrate	Sigma, St. Louis, USA
Ampicilin sodium salt	Roth, Karlsruhe, Germany
Arginine	Sigma, St. Louis, USA
Asparagine	Sigma, St. Louis, USA
Aspartic acid	Sigma, St. Louis, USA
Bacto-pepton	BD Biosciences, Franklin Lakes, USA
Bacto-trypton	BD Biosciences, Franklin Lakes, USA
Biotin	Sigma, St. Louis, Germany
$CaCl_2$	Sigma, St. Louis, USA
$CoCl_2$	Sigma, St. Louis, USA
Coomassie Brilliant Blue G-250	Serva, Heidelberg, Germany
Coomassie Brilliant Blue R-250	Serva, Heidelberg, Germany
$CuCl_2$	Sigma, St. Louis, USA
Desoxynucleotide triphosphates (dNTPs)	Roche, Mannheim, Germany
Deoxyribonucleic acid, single stranded from salmon testes (ssDNA)	Sigma, St. Louis, USA
Dimethyl sulfoxide (DMSO)	Sigma, St. Louis, USA
Dithiothreitol (DTT)	Roth, Karlsruhe, Germany
Doxycycline	Sigma, St. Louis, USA
Ethanol	Sigma, St. Louis, USA
Ethylenediaminetetraactetic acid (EDTA)	Merck, Darmstadt, Germany

Chemicals used in this study (continued)

$FeCl_3$	Merck, Darmstadt, Germany
Galactose	Merck, Darmstadt, Germany
Geneticin (G418)	Sigma, St. Louis, USA
Glucose	Merck, Darmstadt, Germany
Glutamic acid	Sigma, St. Louis, USA
Glutamine	Sigma, St. Louis, USA
Glycerol	Roth, Karlsruhe, Germany
Glycine	Sigma, St. Louis, USA
H_3BO_3	Sigma, St. Louis, USA
Histidine	Sigma, St. Louis, USA
Hygromycin B (HygB)	Sigma, St. Louis, USA
Imidazole	Sigma, St. Louis, USA
Isoleucine	Sigma, St. Louis, USA
Isopropyl β-D-1-thiogalaktopyranoside (IPTG)	Serva, Heidelberg, Germany
$K_2HPO_43.H_2O$	Merck, Darmstadt, Germany
KH_2PO_4	Merck, Darmstadt, Germany
Kanamycin sulfate	Roth, Karlsruhe, Germany
LB medium	Serva, Heidelberg, Germany
Leucine	Sigma, St. Louis, USA
Lithium acetate	Roth, Karlsruhe, Germany
Lysin	Sigma, St. Louis, USA
Methionine	Sigma, St. Louis, USA
$MgCl_27.H_2O$	Merck, Darmstadt, Germany

Chemicals used in this study (continued)

$MgSO_4.7H_2O$	Merck, Darmstadt, Germany
Milk powder	Roth, Karlsruhe, Germany
$MnCl_2$	Sigma, St. Louis, USA
Molybdic acid	Sigma, St. Louis, USA
N-(2-Hydroxyethyl)-piperazine-N´-2-ethanesulfonic acid (HEPES)	Roth, Karlsruhe, Germany
$Na_2HPO_4.2H_2O$	Merck, Darmstadt, Germany
$NaH_2PO_4.2H_2O$	Merck, Darmstadt, Germany
NH_4Cl	Merck, Darmstadt, Germany
Niacinamide	MP Biomedicals, Santa Ana, USA
Nicotine amide dinucleotide (NADH)	Roche, Mannheim, Germany
$NiSO_4$	Sigma, St.Louis, USA
Nourseothricin (clonNAT)	Jena Bioscience, Jena, Germany
NP-40	Sigma, St. Louis, USA
Ortho-phorphoric acid	Roth, Karlsruhe, Germany
Peptone	BD Biosciences, Franklin Lakes, USA
Phenylalanine	Sigma, St. Louis, USA
Phenylmethylsulfonyl fluoride (PMSF)	Sigma, St. Louis, USA
Phosphoenolpyruvate (PEP)	Sigma, St. Louis, USA
Polyethylene glycol (PEG) 3350	Sigma, St. Louis, USA
Potassium chloride	Roth, Karlsruhe, Germany
Proline	Sigma, St. Louis, USA

Chemicals used in this study (continued)

Protease inhibitor Mix FY, G, HP, M	Serva, Heidelberg, Germany
Pyridoxin	Merck, Darmstadt, Germany
Riboflavin	Merck, Darmstadt, Germany
Selenomethionine	Carbosynth, Compton, UK
Serine	Sigma, St. Louis, USA
Sodium chloride	Merck, Darmstadt, Germany
Sodium dodecylsulfate (SDS)	Serva, Heidelberg, Germany
Thiamine	Merck, Darmstadt, Germany
Tetramethylethylenediamine (TEMED)	Roth, Karsruhe, Germany
Threonine	Sigma, St. Louis, USA
Tris-(2-carboxyethyl)phosphine (TCEP)	Roth, Karlsruhe, Germany
Tris-(hydroxymethyl)-aminomethane (TRIS)	Roth, Karlsruhe, Germany
Tryptophane	Sigma, St. Louis, USA
Uracil	Sigma, St. Louis, USA
Valine	Sigma, St. Louis, USA
Yeast Extract (Servabacter)	Serva, Heidelberg, Germany
Yeast Nitrogen Base (YNB) -amino acids	BD Biosciences, Franklin Lakes, USA
YNB - amino acids -ammonium sulfate	BD Biosciences, Franklin Lakes, USA
$ZnCl_2$	Merck, Darmstadt, Germany

3.1.2 Enzymes, standards and kits

Table 2: Enzymes, standards and kits used in this study

1 kb DNA ladder	Peqlab, Erlangen, Germany
ATTO488	Atto tec, Siegen, Germany
Dnase I	AppliChem PanReac, Darmstadt, Germany
Go-Taq DNA Polymerase	NEB, Ipswich, USA
Immersol 518F	Zeiss, Jena, Germany
MEEVD peptide	Biomatik corporation, Cambridge, Ontario Canada
Lactate dehydrogenase (LDH)	Roche, Mannheim, Germany
peqGOLD Protein Marker IV	Peqlab, Erlangen, Germany
Pyruvate kinase (PK)	Roche, Mannheim, Germany
Q5 High-Fidelity DNA Polymerase	NEB, Ipswich, USA
Restriction enzymes & buffers	NEB, Ipswich, USA
T4 DNA Polymerase	NEB, Ipswich, USA
Vent Polymerase	NEB, Ipswich, USA
Wizard Miniprep kit	Promega, Madison, USA
Wizard PCR product purification and gel extraction kit	Promega, Madison, USA
Stain G	Serva, Heidelberg, Germany
Zymolyase 100T	AMS Biotechnology, Abingdon, UK

3.1.3 Chromatography columns

All chromatography columns used for protein purification are listed in Table 3.

Table 3: Chromatography columns used in this study

HiPrep 26/10 Desalting column	GE Healthcare, Freiburg, Germany
HisTrap FF 5 mL	GE Healthcare, Freiburg, Germany
Hydroxy apatite column	Biorad, München, Germany
Resource-Q; Source 15 (6 mL)	GE Healthcare, Freiburg, Germany
Superdex 75 Prep Grade	GE Healthcare, Freiburg, Germany
Superdex 200 Prep Grade	GE Healthcare, Freiburg, Germany

3.1.4 Consumables

Table 4: Consumables used in this study

Amicon Ultra Centrifugal filter units	Merck Millipore, Darmstadt, Germany
Glass beads	Roth, Karlsruhe, Germany
GFP-Trap agarose beads	Chromotek, Martinsried, Germany
PD-10 columns	GE Healthcare, Freiburg, Germany
PE tubes (50/15 ml)	Greiner & Sohne, Nurtingen, Germany
TG PRIME gradient gels	Serva, Heidelberg, Germany

3.1.5 Equipment

Table 5: Equipment used in this study

Centrifuges	
Avanti J25	Beckman Coulter, Brea, USA

Avanti J26 XP	Beckman Coulter, Brea, USA
Centrifuge 5418	Eppendorf, Hamburg, Germany
JA10 rotor	Beckman Coulter, Brea, USA
JA25.50 rotor	Beckman Coulter, Brea, USA
Universal 320R	Hettich Lab, Tuttlingen, Germany
XL-1	Beckman Coulter, Brea, USA
Equipment for protein purification	
Äkta FPLC system	Amersham, Uppsala, Sweden
Super loop, 150 ml	Amersham, Uppsala, Sweden
Microscopy	
Zeiss Axiovert 200	Zeiss, Jena, Germany
Zeiss Plan- NEOFLUAR 63x.1.25 oil 440461 objective	Zeiss, Jena, Germany
Zeiss FluoArc	Zeiss, Jena, Germany
Hamamatsu 4792-95 Digital Camera	Hamamatsu, Herrsching am Ammersee, Germany
Spectrophotometer	
Cary 50	Varian, Palo Alto, USA
Cary 100	Varian, Palo Alto, USA
Huber Compatible Control	Peter Huber Kältemaschinenbau GmbH, Offenburg, Germany
Jascro 715	JASCO, Easton, USA
Jasco PTC-384WI	JASCO, Easton, USA)

Equipment used in this study	
Peqlab ND-1000	Peqlab, Erlangen, Germany
Ultrospec 1100pro	Amersham Biosciences, Uppsala, Sweden
further equipment	
AVIV fluorescence detector	Aviv biomedical Inc., Lakewood, USA
Basic Z cell disruptor	Constant Systems, Warwick, UK
Tube rotator	VWR, Darmstadt, Germany
T100 Termal cycler	Biorad, Hercules, USA
Thermomixer comfort	Eppendorf, Hamburg, Germany

3.1.6 Software

Table 6: Software used in this study

Adobe Creative Suite 4	Adobe Inc., San Jose, USA
Microsoft Office	Microsoft, Redmond, USA
mCoffee	http://tcoffee.crg.cat/
NEBuilder	http://nebuilder.neb.com/
Origin 9.0	http://www.originlab.de/
ProtParam	web.expasy.org/protparam/
Pymol	https://www.pymol.org/
SedView	(Hayes and Stafford, 2010)
Serial Cloner 2.6	http://serial-cloner.de.softonic.com
Simple PCI 5.3	Compix Inc., Cranberry Township, USA
Spell Database	http://spell.yeastgenome.org/

3.2 Bacteria and cloning techniques

3.2.1 Bacterial strains

Bacterial strains used for cloning (XL-1), plasmid amplification (Mach1) and protein expression (BL21) are listed in Table 7.

Table 7: Bacterial strains used in this study

***E. coli* strain**	**genotype**	**source**
BL21 (DE3) Codon Plus	F^- ompT $hsdS_B$ (r_B^- m_B^-) gal endA argU ileY leuW Cam^R	Stratagene, LaJolla, USA
Mach-1	F^- φ80(lacZ)ΔM15 ΔlacX74 hsdR(r_K^- m_K^+) ΔrecA1398 endA1 tonA	Invitrogen, Groningen, Netherlands
XL-1 Blue	endA1 gyrA96(nal^R) thi-1 recA1 relA1 lac glnV44 F'[::Tn10 proAB+ $lacI^q$ Δ(lacZ)M15] hsdR17(r_K^- m_K^+)	Stratagene, LaJolla, USA

3.2.2 Media for growing bacteria

Table 8: Media and antibiotics used for growing bacteria

LB_0	20 g LB powder per 1 L
2xYT (1 L)	10 g NaCl
	10 g Yeast extract
	16 g Peptone
Agar	20 g agar per 1 L (for plates)
Antibiotics	
Kanamycin	50 µg/mL
Ampicillin	100 µg/mL

3.2.3 Plasmid preparation from *E. coli*

Plasmids from *E. coli* were isolated from 5 mL overnight cultures in LB medium containing the required antibiotics. The preparation was performed using the WIZARD Plus SV mini-prep kit following the manufacturer's protocol.

3.2.4 Restriction digest of plasmids

Plasmids were digested using restriction enzymes and buffers from NEB (Ipswich, USA). Typically, 1 µg plasmid DNA was digested over night at 37°C in CutSmart buffer following the manufacturers instructions. When available, HF variants of restriction enzymes were used. Digested plasmids were then purified using the Wizard PCR product purification and gel extraction kit (Promega, Madison, USA).

3.2.5 Agarose gel electrophoresis

DNA was separated on 1%(w/v) agarose gels in 1xTAE buffer (40 mM TRIS acetate, 1 mM EDTA, pH 8.0) containing 1 µL/100 mL Stain G (Serva, Heidelberg, Germany). Electrophoresis was carried out in 1xTAE as running buffer at a constant current of 120 V using a Electrophoresis Power Supply EPS-601 (Amersham Pharmacia Biotech, Uppsala, Sweden). Bands were detected under UV light (BioDoc II, Biometra, Göttingen, Germany).
1 kb DNA ladder (Peqlab) was used as a standard.

3.2.6 SLIC cloning

Sequence and Ligation Independent Cloning (SLIC) is a simple and time-saving method for cloning (Jeong et al., 2012). Basically, the sequence of interest is amplified with primers containing 15-20 base pairs (bp) homology up- and down-stream to the insertion site on the cut target vector. In the absence of nucleotides T4 DNA Polymerase acts as a 3'-5' exonuclease and is here used to produce sticky ends on the vector and the insert to be cloned. The resulting constructs can then be directly transformed into *E. coli* cells which carry out the ligation between the insert and the vector.
The method used here was modified from (Jeong et al., 2012). All primers were designed by using the NEBuilder Assembly tool (http://nebuilder.neb.com/). PCRs were

carried-out using Q5 DNA Polymerase (NEB, Ipswich, USA). Tables 9 and 10 show the PCR reaction mix and the general PCR cycling settings, respectively.
PCR products were run on 1% agarose gels and purified using the Wizard PCR product purification and gel extraction kit (Promega, Madison, USA).
SLIC was also used to generate fusion proteins (chimera, GFP-tagged proteins) using a strategy where each insert overlaps on the one end with one end of the vector sequence and at the other end with the other insert.

Table 9: PCR reaction mix for SLIC cloning using Q5 DNA Polymerase

32.6 µL	H_2O
1 µL	template (100 ng/µL)
10 µL	5X Q5 Reaction Buffer
1 µL	dNTPs (10 mM)
2.5 µL	primer 1 (10 µM)
2.5 µL	primer 2 (10 µM)
0.4 µL	Q5 DNA Polymerase

Table 10: Temperature programm for SLIC cloning using Q5 DNA Polymerase

step	**temperature [°C]**	**time**
initial denaturation	98	30 sec
35 Cycles	98	10 sec
	50-72	20 sec
	72	20-30 sec/kb
final extention	72	2 min
hold	4	

Table 11 shows the reaction setup of a typical SLIC reaction. T4 DNA Polymerase was added last and the mix was incubated for exactly 2.5 min at room temperature followed by stopping the reaction by chilling the samples 10 min on ice. Between 2 and 5 µL were

then directly used for *E. coli* transformation. Single colonies were then grown in liquid culture, plasmids were preped as described in 3.2.3 and positive clones were confirmed by sequencing.

Table 11: SLIC reaction setup

x µL (100 ng)	vector DNA
1 µL	NEB buffer 2.1
2-fold molar excess	insert DNA
to total of 10 µL	H_2O
0.4 µL	T4 DNA Polymerase

3.2.7 Transformation of *E. coli*

E. coli strains described in Section 3.2.1 were made competent as described in Hanahan (1983) and transformed using a simplified method from the mentioned reference. In brief, 1 µL plasmid DNA for re-transformations or 2-5 µL of cloning reactions where mixed with 100 µL competent cells and incubated for 15 min on ice. Then the cells were heat shocked at 42°C for 1 min, again cooled on ice for 2 minutes and recovered at 37°C in 1 ml pre-warmed LB_0 medium for 1 h. Finally, the cells were plated on LB agar plates containing the proper antibiotic for plasmid selection. For re-transformations 100 µL of the cell suspension was plated, for cloning cells were spun down briefly, the pellet was resuspended in 100 µL LB_0 and all cells were plated onto selective plates. Plates were incubated at 37°C for 1-2 days.

3.2.8 Plasmid sequencing

All obtained plasmids were confirmed by sequencing at GATC Biotech (Konstanz, Germany) using appropriate primers.

3.2.9 Protein expression

Proteins where expressed from plasmids (see Table 12) in *E. coli BL21 (DE3) Codon Plus*.
Cns1, its variants as well as TTC4 were expressed as follows: 50 mL over-night cultures

in LB + 50 µg/ml kanamycin were used to inoculate 2 L of LB + 50 µg/ml kanamycin and were grown to OD_{600}=0.8 at 37°C. Cell cultures were shifted to 25°C and protein expression was induced using 1 mM IPTG. Cells were harvested 4 h after induction and proteins were purified as described in section 3.4.7.

For expression of Hsp90, 50 mL over-night culture in LB + 50 µg/ml kanamycin were used to inoculate 2 L of 2xYT + 50 µg/ml kanamycin and cells were grown to OD_{600}=0.8 at 37°C. Expression was induced by adding 1 mM IPTG (final concentration) and cells were kept at 37°C for 4 h. Finally, cells were harvested by centrifugation and proteins were purified as described in 3.4.8.

Typically, 8 L expression culture was grown for Hsp90 expression and 4 L for Cns1 expression, respectively.

Table 12: Plasmid used for protein expression

plasmid	source
pET28-yHsp90	K. Richter
pET28-SUMO-CNS1^{wt}	this study
pET28-SUMO-CNS1$^{51\text{-}385}$	this study
pET28-SUMO-CNS1$^{36\text{-}385}$	this study
pET28-SUMO-CNS1$^{1\text{-}190}$	this study
pET28-SUMO-CNS1$^{1\text{-}82}$	this study
pET28-SUMO-CNS1$^{169\text{-}385}$	this study
pET28-SUMO-CNS1$^{36\text{-}205}$	this study
pET28-SUMO-CNS1$^{70\text{-}220}$	this study
pET28-SUMO-CNS1$^{221\text{-}385}$	this study
pET28-SUMO-CNS1$^{1\text{-}220}$	this study
pET28-SUMO-CNS1$^{36\text{-}220}$	this study
pET28-SUMO-CNS1$^{1\text{-}82\text{-}L\text{-}221\text{-}385}$	this study
pET28-SUMO-TTC4	this study
pET28-SUMO-CNS1N/TTC4	this study
pET28-SUMO-TTC4$^{217\text{-}387}$	this study

3.2.10 Selenomethionine (SeMet) labeling for protein crystallization

For protein crystallization experiments, proteins were selenomethionine-labeled using a modified protocol published previously (Van Duyne et al., 1993).
The exact media components used for SeMet labeling are described in Table 13.
5 ml pre-culture LB + 50 µg/mL kanamycine were inoculated in the morning. 100 mL pre-culture in minimal medium were then inoculated with 1 mL of the LB starting culture and grown over night at 37°C. 50 mL of this preculture were used to inoculate 2 L of minimal medium and the cells were grown to and OD_{600}=0.8. Then, 0.5 g/L feed-back inhibition mix was added, cultures were shifted to 25°C and after 15 min expression was induced with 1 mM IPTG (final concentration). Cells were harvested 4 h after induction and proteins purified as described below.

Table 13: Media components for SeMet labeling

M9 medium per 1 L	6 g	Na_2HPO_4
pH=7.3	3 g	KH_2PO_4
autoclaved	0.5 g	NaCl
add (sterile filtered)	10 ml	0.1 g/L NH_4Cl
	2 mL	1 M $MgSO_4$
	20 mL	20% glucose
	1 mL	1000x vitamins
	10 mL	100x trace elements
1 L 100x trace elements	5 g	EDTA
pH=7.0	0.8 g	$FeCl_3$
sterile filtered	0.05 g	$ZnCl_2$
	0.01 g	$CuCl_2$
	0.01 g	$CoCl_2$
	0.01 g	H_3BO_3
	1.6 g	$MnCl_2$
	some	Ni_2SO_4
	some	molybdic acid

Media components for SeMet labeling

500 ml 1000x vitamins	0.5 g	riboflavin
sterile filtered	0.5 g	niacinamide
	0.5 g	pyridoxine monohydrate
	0.5 g	thiamine
feedback inhibition mix	1 g	lysine
	1 g	threonine
	1 g	phenylalanine
	0.5 g	leucine
	0.5 g	isoleucine
	0.5 g	L(+)-selenomethionine

3.2.11 Labeling of proteins for NMR (nuclear magnetic resonance) spectroscopy

For ^{15}N-labeling of proteins, *E.coli* expression strains were inoculated in the morning in 5 mL LB + 50µg/ml kanamycin. 100 mL ^{15}N-containing M9 medium + 50 µg/ml kanamycin was then inoculated with 1 mL of the starting culture in the evening and cells were grown over night at 37°C. 50 mL were then used to inoculate 1 L ^{15}N-containing M9 medium + 50µg/ml kanamycin. Cells were grown to OD_{600}=0.8, shifted to 25°C and protein expression was induced with 1 mM IPTG. Cells were harvested 4 h after induction and proteins purified as described below.

Table 14: Media components for ^{15}N-labeling

M9 medium per 1 L	6 g	Na_2PO_4
pH=7.3	3 g	KH_2PO_4
autoclaved	0.5 g	NaCl
add (sterile filtered)	10 mL	20% glucose
	10 mL	0.1 g/ml $^{15}NH_4Cl$

Media components for ^{15}N-labeling		
	1 mL	1 M $MgSO_4$
	0.3 mL	$CaCl_2$
	1 mL	1 mg/mL ThiamineHCl
	10 mL	trace elements (100x)
	1 ml	1 mg/ml biotin
1 L 100x trace elements	5 g	EDTA
pH=7.5	0.8 g	$FeCl_3$
sterile filtered	0.084 g	$ZnCl_2$
	0.01 g	$CuCl_2$
	0.01 g	$CoCl_2$
	0.01 g	H_3BO_3
	1.6 g	$MnCl_2$

3.2.12 Cell disruption for protein purification from *E.coli*

For subsequent protein purification, *E. coli* cells were lysed using a cell disruptor. Pellets were resuspended in Buffer A (approx. 5 mL/g cells) from the first chromatography step and protease inhibitors and DNAse I were added. Cells were lysed using a Basic Z model cell disruption system at 1.8 kbar at 8°C.

3.3 Yeast methods

3.3.1 Yeast gene and protein nomenclature

Wild-type genes are written in uppercase, italic letters (e.g. *YFG1, your favorite gene 1*). Mutant genes are written in lowercase, italic letters (e.g. *yfg1*, your favorite gene 1 mutant). *yfg1*Δ indicates, that the entire open reading frame of a gene of interest was deleted (deletion mutant). Yfg1 is used for proteins.

3.3.2 Yeast strains

All yeast strains used in this study are listed in Table 15.

Table 15: Yeast strains used in this study

strain	**genotype**	**source**
BY4741	MAT**a** *his3Δ*1 *leu2Δ*0 *met15Δ*0 *ura3Δ*0	EUROSCARF, Frankfurt, Germany
R1158	MAT**a** *URA3::CMV-tTA his3Δ*1 *leu2Δ*0 *met15Δ*0	Dharmacon, Lafayette, USA
tet07-*CNS1*	MAT**a** *pCNS1::kanR-tet07-TATA URA3::CMV-tTA his3Δ*1 *leu2Δ*0 *met15Δ*0	Dharmacon, Lafayette, USA
Y8205	MATα *can1Δ::STE2pr-Sp-his5 lyp1Δ::STE3pr-Sp-LEU2 his3Δ*1 *leu2Δ*0 *ura3Δ*0	C. Boone
Y8205 *cpr7Δ* (bait)	MATα *can1Δ::STE2pr-Sp-his5 lyp1Δ::STE3pr-Sp-LEU2 his3Δ*1 *leu2Δ*0 *ura3Δ*0 *cpr7Δ::natMX*	this study
Y8205 tet07-*CNS1* (bait)	MATα *pCNS1::natR-tet07-TATA URA3::CMV-tTA can1Δ::STE2pr-Sp-his5 lyp1Δ::STE3pr-Sp-LEU2 his3Δ*1 *leu2Δ*0	this study
sti1Δ	BY4741 *sti1Δ::kanMX*	EUROSCARF, Frankfurt, Germany
aha1Δ	BY4741 *aha1Δ::kanMX*	EUROSCARF, Frankfurt, Germany
hch1Δ	BY4741 *hch1Δ::kanMX*	EUROSCARF, Frankfurt, Germany
cpr6Δ	BY4741 *cpr6Δ::kanMX*	EUROSCARF, Frankfurt, Germany
cpr7Δ	BY4741 *cpr7Δ::kanMX*	EUROSCARF, Frankfurt, Germany
tah1Δ	BY4741 *tah1Δ::kanMX*	EUROSCARF, Frankfurt, Germany

Yeast strains used in this study

*pih1*Δ	BY4741 *pih1*Δ*::kanMX*	EUROSCARF, Frankfurt, Germany
cdc37-DAmP	BY4741 *cdc37-DAmP::kanMX*	Dharmacon, Lafayette, USA
*ppt1*Δ	BY4741 *ppt1*Δ*::kanMX*	EUROSCARF, Frankfurt, Germany
*sba1*Δ	BY4741 *sba1*Δ*::kanMX*	EUROSCARF, Frankfurt, Germany
*cns1*Δ [*CNS1*] (Cns1 shuffling)	MATα *his3Δ*1 *leu2Δ*0 *met15Δ*0 *ura3Δ*0 [p426-GPD-CNS1^{wt}]	L. Mitschke
*hsp82*Δ *hsc82*Δ [*HSP82*] (Hsp90 shuffling)	MATα *his3Δ*1 *leu2Δ*0 *ura3Δ*0 *lys2Δ*0 *arg4*Δ*::kanMX hsc82*Δ*::kanMX hsp82*Δ*::natMX* [pKAT-HSC82-URA3]	this study
cns1-1	BY4741 *cns1-1::kanMX*	C. Boone

3.3.3 Yeast cell cultivation and media

Yeast cells were grown in culture sizes ranging from 5 mL to 1 L depending on the experiment. Growth was monitored by measuring OD_{600} on a Ammersham Biosciences Ultrospec 1100pro (GE healthcare, Freiburg, Germany). The media and inhibitors used are listed in Table 16 and 17, respectively.

Table 16: Yeast media

YPD	Yeast extract	10 g/L
	Pepton	20 g/L
	Glucose	20 g/L
SD	YNB -AA	6.7 g/L
	amino acid drop-out mix	1g/L
	Glucose	20g/L

Table 17: Yeast antibiotics and inhibitors

5'- FOA	1 g/L
G418	200 mg/L
clonNAT	200 mg/L
Doxycycline	10 mg/L
Hygromycin B	300 mg/L

Table 18 lists the general composition of the amino acid mix used in this study. In drop-out mixes, one or multiple components were left out depending on the auxotrophic selection properties required.

Table 18: Amino acid drop-out mix

adenine	0.5 g	leucine	10 g
alanine	2 g	lysine	2 g
arginine	2 g	methionine	2 g

Amino acid drop-out mix			
asparagine	2 g	phenylalanine	2 g
aspartic acid	2 g	proline	2 g
glutamic acid	2 g	serine	2 g
glutamine	2 g	threonine	2 g
glycine	2 g	tryptophane	2 g
histidine	2 g	uracil	2 g
isoleucine	2 g	valine	2 g

Plates additionally contained 20 g/L agar.
The media used in the SGA screens are described in Tong and Boone (2006).

3.3.4 Yeast plasmids

Table 19: Yeast plasmids used in this study

plasmid	**source**
p425-GPD	Addgene, Cambridge, USA
p425-GPD-CNS1^{wt}	this study
p425-GPD-CNS1$^{1\text{-}200}$	this study
p425-GPD-CNS1$^{1\text{-}190}$	this study
p425-GPD-CNS1$^{1\text{-}185}$	this study
p425-GPD-CNS1$^{169\text{-}385}$	this study
p425-GPD-CNS1$^{36\text{-}385}$	this study
p425-GPD-CNS1$^{41\text{-}385}$	this study
p425-GPD-CNS1$^{46\text{-}385}$	this study
p425-GPD-CNS1$^{51\text{-}385}$	this study
p425-GPD-CNS1$^{36\text{-}205}$	this study
p425-GPD-CNS1$^{36\text{-}200}$	this study
p425-GPD-CNS1$^{36\text{-}195}$	this study
p425-GPD-CNS1$^{1\text{-}82}$	this study
p425-GPD-CNS1$^{1\text{-}220}$	this study
p425-GPD-CNS1$^{191\text{-}385}$	this study

Yeast plasmids used in this study

p425-GPD-CNS1$^{1\text{-}82\text{-}L\text{-}169\text{-}385}$	this study
p425-GPD-CNS1$^{1\text{-}82\text{-}L}$	this study
p425-GPD-CNS1$^{1\text{-}82\text{-}L\text{-}191\text{-}385}$	this study
p425-GPD-CNS1$^{1\text{-}82\text{-}L\text{-}191\text{-}220}$	this study
p425-GPD-CNS1$^{221\text{-}385}$	this study
p425-GPD-CNS1$^{1\text{-}82\text{-}L\text{-}221\text{-}385}$	this study
p425-GPD-TTC4	this study
p425-GPD-Cns1N-/TTC4	this study
p425-GPD-HSC82	this study
p425-GPD-HSC82-1-82	this study
p425-GPD-1-82-HSC82	this study
p425-GPD-SSA1	this study
p425-GPD-SSA1-1-82	this study
YSC5103 genome tiling library	Dharmacon, Lafayette, USA
pGP564	Dharmacon, Lafayette, USA
pRS315-RPS2-yeGFP	this study
pAJ907 (RPL25-eGFP)	(Hedges et al., 2005)
p425-GPD-STI1	(Schmid et al., 2012)
p425-GPD-STI1$^{\text{TPR1}}$	(Schmid et al., 2012)
p425-GPD-STI1$^{\text{TPR2A}}$	(Schmid et al., 2012)
p425-GPD-STI1$^{\text{TPR2B}}$	(Schmid et al., 2012)
p425-GPD-CNS1$^{1\text{-}82\text{-}TPR1}$	this study
p425-GPD-CNS1$^{1\text{-}82\text{-}TPR2A}$	this study
p425-GPD-CNS1$^{1\text{-}82\text{-}TPR2B}$	this study
p425-GPD-CNS1$^{\text{wt-GFP}}$	this study
p425-GPD-CNS1$^{1\text{-}190\text{-}GFP}$	this study
p425-GPD-CNS1$^{1\text{-}82\text{-}GFP}$	this study
p425-GPD-CNS1$^{51\text{-}385\text{-}GFP}$	this study
p425-GPD-CNS1$^{169\text{-}385\text{-}GFP}$	this study
p425-GPD-CNS1$^{\text{GFP}}$	this study

3.3.5 Yeast transformation

Yeast transformation was carried out following a modified protocol described previously (Gietz and Woods, 2002). In brief, cells were grown over night in 5 ml YPD medium and reinoculated into 50 ml YPD to a starting OD_{600}=0.15. After two cell divisions (approx. 4.5 h) cells were harvested by centrifugation at 500 g, washed with 25 mL sterile H_2O, washed again with 1 ml 0.1 M lithium acetate (LiAc) and finally resuspended in 0.5 mL 0.1 M LiAc. For one single transformation reaction 50 µL of the cell suspension were spun down briefly at 500 g, the supernatant was discarded and the transformation mix described in Table 20 was added.

Table 20: Yeast transformation mix

volume	**component**
240 µL	50% PEG3350 (w/v)
36 µL	1 M LiAc
10 µL	ssDNA (10 mg/mL)
x µL	plasmid DNA or PCR reaction product
74-x µL	H_2O

For plasmid transformations 1-5 ng plasmid DNA and for PCR-derived linear DNA constructs for chromosomal integration 50 µL of a PCR reaction were used. The transformation mixes were then vortexed thoroughly and incubated at 30°C for 30 min followed by another 30 min of heat shock at 42°C. Plasmid transformations were spun down for 30 s at 500 g, the supernatant was discarded, 1 mL sterile water was added and, after resuspension of the cells, 200 µL were plated onto selective plates.
For chromosomal integration and selection of antibiotic resistances, transformed cells were spun down, resuspended in 1 mL YPD and recovered at 30°C for 2-6 h. Finally, cells were harvested at 500 g, resuspended in 200 µL YPD and plated onto selective plates.
Plates were then incubated for 2-4 days at 30°C or as indicated.

3.3.6 Plasmid preparation from *S. cerevisiae*

Plasmids from *S. cerevisiae* were isolated from cell grown over night in 5 mL liquid cultures under selective conditions. Cells were harvested by centrifugation and resuspended in cell resuspension solution from the WIZARD Plus SV mini-prep kit. After resuspension 100 U/mL zymolyase was added followed by an incubation step at 37°C for 1-2 h. All subsequent steps were carried out as described in the WIZARD Plus SV mini-prep kit manual.
Since plasmid preparation from *S. cerevisiae* leads to very low yields, the obtained plasmids were retransformed into *E. coli Mach1* for amplification.

3.3.7 Multi-copy-suppressor screening

Multi-copy-suppressor screening was carried out using the yeast strain containing the *cns1-1* temperature-sensitive mutation and a commercially available plasmid library (YSC5103, Yeast Genomic Tiling Collection Assay Ready DNA, Dharmacon, Lafayette, USA). The strain was transformed with 3 ng of the library and plated onto selective plates. Plates were incubated over night at 25°C to allow the cells to recover and shifted to the non-permissive temperature (37°C) after 24 h. The transformants were then grown for another 3 days. 2 plates were kept at 25°C to determine the total number of transformants. Colonies that grew faster than the background at 37°C were then re-streaked to a fresh plate and grown again for 48 h at 37°C to confirm the phenotype. Finally, plasmids were isolated and sequenced.

3.3.8 Synthetic genetic array screening

Synthetic genetic array analysis was carried out as described previously (Tong and Boone, 2006, 2007). Y8205 was used as a starting strain.
For the *cpr7Δ* screen, *CPR7* was knocked out in Y8205 using a natMX resistance cassette. The genotype of the resulting strain was confirmed by colony PCR and used for the SGA screen.
For the *tet07-CNS1* screen, a strain bearing the *CNS1* gene under the control of the tet07 promoter (Mnaimneh et al., 2004) was crossed with Y8205. The kanMX resistance cassette was replaced by natMX using the swapping method (Tong and Boone, 2007). The resulting strain was sporulated and finally selected on -Arg -Lys -Leu +Can +Thia

+Lys +clonNAT to select the haploid MATα *tet07-CNS1* starting strain.
SGA screening was carried out at the Max-Planck-Institut für Biochemie in the lab of Stefan Jentsch by Jochen Rech. The scoring of the *cpr7* screen was done by comparing the single mutant selection step (-His-Arg-Lys+Can+Thia+G418) with the double mutant selection step (-His-Arg-Lys+Can+Thia+G418+clonNAT). The double mutants were considered synthetic lethal when no growth was observed, or synthetic sick when the growth rate was reduced.
The *tet07-CNS1* screen was scored by comparing the growth of the double mutants (selected on -His-Arg-Lys+Can+Thia+G418+clonNAT) with growth on 10 µg/mL doxycycline containing YPD plates to repress *CNS1* expression.
Both screens were carried out as technical duplicates and genetic interaction was only scored as true when the phenotype was observed twice.

3.3.9 Microscopy

Yeast microscopy experiments were performed on a Zeiss Axiovert 200 with a Zeiss Plan-NEOFLUAR 63x.1.25 oil 440461 objective and a FluoArc system (Zeiss, Jena, Germany) using either DIC or GFP filters. Images were recorded using a Hamamatsu 4792-95 Digital Camera (Hamamatsu, Herrsching am Ammersee, Germany) and the program Simple PCI 5.3 (Compix Inc., Cranberry Township, USA).
Immersion oil (Immersol 518F) was purchased from Zeiss (Jena, Germany).

3.3.10 Ribosome fractionation

Ribosome fraction was carried out at the Max-Planck-Institut für Biochemie (Martinsried, Germany) with the help of Timm Hassemer in the lab of Ulrich Hartl. The method described below was modified from Choe et al. (2016).
Yeast cultures were grown to OD_{600}=0.8-1 and 160 OD_{600} units were harvested by centrifugation. Whole cell lysates were prepared in 10 mM Tris-HCl pH 7.5, 100 mM NaCl, 30 mM $MgCl_2$, 1 mM DTT and protease inhibitor-cocktail (Roche) with glass beads using a FastPrep-24 homogenizer (MP Biomedicals).
30 OD_{254} units of lysate were layered on a continuous 7-47% sucrose gradient prepared in 40 mM Tris-Acetate pH 7.0, 50 mM NH_4Cl, 12 mM $MgCl_2$, 1 mM DTT. Gradients were centrifuged for two hours at 40,000 rpm and 4°C using a SW41 rotor (Beckman) and

fractionated using a piston gradient fractionator coupled to an A_{254nm} spectrophotometer (Biocomp) for recording ribosome profiles.

3.3.11 GFP-Trap

Yeast cells carrying GFP-tagged variants of Cns1 on a plasmid (p425-GPD) were grown in 50 mL SD medium to an OD_{600}=0.8 and 40 OD_{600} units were harvested by centrifugation. Cells were lysed in 0.5 mL lysis buffer (50 mM TRIS 100 mM NaCl 1.5 mM $MgCl_2$ 0.15% NP-40 containing protease inhibitor HP and PMSF) by glass bead disruption and the lysate was cleared by centrifugation at 15,000 g for 2 min. For Immunoprecipitation 25 µL GFP-Trap beads (ChromoTek, Martinsried, Germany) were equilibrated by washing them three times with lysis buffer. Next, the cell lysate was added to the beads, followed by a 1 h incubation step at 4°C on an overhead shaker. The beads were washed three times with lysis buffer to get rid of unspecific interactions, the proteins were eluted by boiling in 30 µL Laemmli buffer, finally separated by SDS-PAGE and visualized by colloidal coomassie staining.

3.3.12 Yeast spot assays

Cells were grown over-night at 30°C in 5 mL YPD medium. Then, 10 OD_{600} units were harvested by centrifugation, washed once with sterile water and resuspended in 1 mL sterile water to yield a OD_{600}=10 cell suspension. The cell suspension was then diluted in 96 well plates to a starting OD_{600}=1 and several 10-fold dilutions were prepared (e.g. OD_{600}=1; OD_{600}=0.1; OD_{600}=0.01; ...). Finally, 5 µL of the diluted cell suspensions were spotted onto plates as indicated.

3.4 Protein purification

3.4.1 Immobilized metal ion affinity chromatography

Immobilized metal ion affinity chromatography is a widely used chromatographic method in protein purification. It is based on the specific and reversible interaction of a tagged protein with a matrix bound partner. Ni^{2+} ions can be immobilized using nitrile triacetic acid (NTA) as an anchor to attach it to the column material. NiNTA columns show high specificity toward the His_6-tag, which can be fused to the protein of interest. Elution

is achieved by competition with high levels of free imidazole (the functional group of histidine), which is added to the elution buffer and is competing with the His side chains of the His_6-tag.
NiNTA purification was performed using HisTrap FF column (GE Healthcare, Freiburg, Germany).

3.4.2 Ion exchange chromatography

Ion exchange chromatography is based on the interaction between differently charged molecules. Proteins carry due to their charged side chains positive and negative charges. This makes binding to a column material with opposite charge possible. The overall charge of a protein is dependent on the amino acid composition, which determines its isoelectric point (pI), and the pH in the buffer. Thus, the column material and the pH of the buffer are selected depending on the amino acid composition of the protein.
Elution is normally performed by gradually increasing the salt concentration in the buffer.
Ion exchange chromatography purification was performed using Resource Q 6ml columns (GE Healthcare, Freiburg, Germany).

3.4.3 Size exclusion chromatography

Size exclusion chromatography (SEC) is used to separate proteins based on their hydrodynamic radius. The column matrix consists of micro-granules with defined particle and pore sizes. Proteins, which have a bigger radius than the pore size, are not able to diffuse into the particles and therefore elute first. Smaller proteins, however, are able to enter the particles and it takes them longer to get across the column. The smaller the hydrodynamic radius of a protein is, the longer it takes to get through the column. Furthermore, SEC can be used to separate different oligomeric states of a protein, to get a protein in its monodisperse form.
SEC was performed using Superdex 75 Prep Grade and Superdex 200 Prep Grade columns (GE Healthcare, Freiburg, Germany).

3.4.4 Buffer exchange using a desalting column

Desalting columns can be used for quick buffer exchange. The method is similar to SEC, although the pore size of the column material is so small that proteins can not enter the particles whereas buffer components of the original buffer can and therefore elute separated from the protein. HiPrep 26/10 Desalting columns (GE Healthcare, Freiburg, Germany) were used in this study.

3.4.5 Buffers used for protein purification from *E. coli*

Table 21 lists the buffers used for protein purification form *E. coli*. For Hsp90 purification there was additionally 1 mM EDTA in the IEC buffers. All buffers used for Cns1 purification additionally contained 1 mM DTT.

Table 21: Buffers used for protein purification

NiNTA	Buffer A	40 mM K_2HPO_4/KH_2PO_4 pH 8.0
		300 mM KCl
		20 mM imidazole
	Buffer B	40 mM K_2HPO_4/KH_2PO_4 pH 8.0
		300 mM KCl
		500 mM imidazole
IEC	Buffer A	40 mM K_2HPO_4/KH_2PO_4 pH 8.0
		10 mM KCl
	Buffer B	40 mM k_2HPO_4/KH_2PO_4 pH 8.0
		1 M KCl
HAT	Buffer A	40 mM K_2HPO_4/KH_2PO_4 pH 8.0
	Buffer B	500 mM K_2HPO_4/KH_2PO_4 pH 8.0
SEC	Buffer	40 mM HEPES/KOH, pH 7.5
		150 mM KCl
		5 mM $MgCl_2$

3.4.6 Protein concentration

In order to concentrate protein solutions, ultrafiltration across a membrane with defined molecular weight cut-off was used. With this method the volume of a protein solution can be reduced and the proteins are concentrated above the membrane. Depending on the volume, Amicon Ultra-15, Ultra-4 or Ultra-0.5 Filter Units were used with various molecular weight cut-offs (3 kD, 10 kD and 30 kD) depending on the molecular weight of the protein.

3.4.7 Purification of SUMO-tagged proteins from *E. coli*

All protein purification steps were carried out at 4°C.
SUMO-tagged Cns1 and TTC4 were expressed as described in 3.2.9. Pellets were then dissolved in NiNTA Buffer A and DNAse I, Protease inhibitor HP and PMSF (2 mM final concentration) were added. Cells were disrupted as described in 3.2.12 and lysates were cleared by centrifugation at 40,000 g at 4°C in a JA25.50 rotor. Then, lysates were loaded on a His-Trap FF column and subsequently washed with 10 column volumes buffer A, followed by washing with 10 column volumns 3% NiNTA buffer B and eluted with 100% NiNTA buffer B. Protease inhibitor G (Serva) was immediately added to the elution fractions to prevent protein degradation by metalloproteases. Fractions were run over a HiPrep 26/10 Desalting column equilibrated with SEC buffer and the SUMO-tag was cleaved off over night by adding His-tagged SUMO protease (in house preparation). The His-SUMO tag and the protease were then removed by running the sample again over the His-Trap FF column. The collected flow-through was concentrated and run on a gel filtration column equilibrated in SEC buffer. Purity was finally checked by SDS-PAGE.
For the TTC4 constructs, additional ion exchange chromatography was necessary. After the first Ni-column, the elution fractions were run over a HiPrep 26/10 Desalting column equilibrated in IEC buffer A and the fractions containing the target protein were loaded on a Resource Q column. After washing with 10 column volumes IEC buffer A, bound proteins were eluted over a gradient from 0-50% IEC buffer B over 200 mL. Fractions were again run over a HiPrep 26/10 Desalting column equilibrated with SEC buffer and the SUMO-tag was cleaved as described above. All subsequent steps were carried out as described for Cns1.

3.4.8 Purification of yeast Hsp90 from *E. coli*

All protein purification steps were carried out at 4°C.
His-tagged yHsp90 was expressed as described in 3.2.9. Pellets were then resuspended in NiNTA Buffer A and DNAse I, Protease inhibitor HP and PMSF (2 mM final concentration) were added. Cells were disrupted as described in 3.2.12 and lysates were cleared by centrifugation at 40,000 g at 4°C in a JA25.50 rotor. Then, lysates were loaded on a His-Trap FF column and subsequently washed with 10 column volumes buffer A, followed by washing with 10 column volumns 3% NiNTA buffer B and eluted with 100% NiNTA buffer B.
Elution fractions were filled up to 150 mL with IEC Buffer A and run-over a Resource Q column. After washing with 20 column volums IEC Buffer A, bound proteins were eluted over a gradient from 0-50% IEC buffer B over 200 mL. The fractions containing full length Hsp90 were then filled up to 150 mL HAT Buffer A, loaded onto a HAT column, washed with 10 column volumes HAT buffer A and eluted over a gradient from 0-100% HAT buffer B over 200 mL. Hsp90 containing fractions were concentrated and run over a SEC column equilibrated with SEC buffer. Purity was checked by SDS-PAGE.

3.5 Protein analytics, activity assays and structural characterization

3.5.1 SDS-PAGE

Sodium duodecylsulfate polyacrylamide gel electrophoresis (SDS-PAGE) was performed to analyze protein purifications and co-immunoprecipitations. Proteins were either separated on self-made gels (7 x 9 x 0.075 cm, stacking gel:<3% acrylamide, 125 mM TRIS-HCl pH 8.6, 0.2% SDS; resolving gel: 10-15% acrylamide, 375 mM TRIS-HCl pH 8.8, 0.2% SDS) or commercially available 8-16% gradient gels (Serva TG Prime, Heidelberg, Germany).
Samples were mixed with Laemmli loading buffer, heated at 95°C for 5 minutes and loaded onto the gels. peqGOLD Protein-Marker IV (Peqlab, Erlangen, Germany) was used as a marker.
Proteins were separated using a constant current of 30 mA per gel (self-made gels) or

according to the manufacturers protocol (pre-cast gels) using a Electrophoresis Power Supply EPS-601 (Amersham Pharmacia Biotech, Uppsala, Sweden).

3.5.2 Coomassie staining of SDS-PAGE gels

After SDS-PAGE gels were stained using two different methods.

Fairbanks staining

Protein purification gels were stained with a simplified version of a method described before (Fairbanks et al., 1971). In brief, gels were stained with Fairbanks A solution (25% (v/v) Isopropanol, 10% (v/v) acetic acid, 0.05% Coomassie Blue R) and destained with Fairbanks D solution (10% (v/v) acetic acid). Solutions were heated up in a microwave to reduce incubation times.

Colloidal coomassie staining

Colloidal coomassie staining shows higher sensitivity than the method described above. Therefore, a method that is able detect even small amounts of proteins (Dyballa and Metzger, 2009) was used in immunoprecipitation experiments.

In brief, gels were washed three times with deionized water, stained overnight with solution A (0.02% (w/v) CBB G-250, 5% (w/v) aluminum sulfate-(14-18)-hydrate, 10% (v/v) ethanol, 2% (v/v) orthophosphoric acid) and destained with solution B (10% (v/v) ethanol, 2% (v/v) orthophosphoric acid) for 1 h.

3.5.3 Fluorescence labeling of proteins

Cns1 was randomly labeled using ATTO488 (ATTO-TEC, Siegen, Germany) on lysine residues as recommended by the manufacturer. The reaction was carried out in 40 mM HEPES/KOH pH 7.5, 50 mM KCl, 5 mM $MgCl_2$. 5 mg/ml protein were labeled with a 1:1 stoichiometry protein:label for 2 h on ice.

The reaction was quenched with a molar excess of TRIS (1 M pH 8.0). Excess label was removed by running the protein over a PD-10 Desalting Column (GE Healthcare, Freiburg, Germany) equilibrated in 40 mM HEPES/KOH pH 7.5, 150 mM KCl, 5 mM $MgCl_2$ and 1 mM DTT. The degree of labeling was finally calculated following the manufacturer's protocol.

3.5.4 Analytical ultracentrifugation

Analytical ultracentrifugation (aUC) measurements were performed by Daniel Rutz (Lehrstuhl für Biotechnologie, Technische Universität München).
For Hsp90 interaction studies, 500 nM randomly labeled Cns1 (*Cns1) was used. Experiments were conducted with a ProteomLab Beckman XL-A centrifuge (Beckman Coulter, Brea, California) equipped with an AVIV fluorescence detection system (Aviv biomedical Inc., Lakewood, USA). Hsp90, Cns1 variants, co-chaperones and nucleotides were added as indicated in the Results Section. 40 mM HEPES/KOH pH 7.5, 50 mM KCl, 5 mM $MgCl_2$ was used as a measurement buffer.
Data were analyzed using SedView (Hayes and Stafford, 2010) and manual data analysis was performed using Origin 9.0.

3.5.5 ATPase assays using an ATP-regenerating system

The ATPase assay used in this study is based on a regenerative, coupled enzymatic test (Nørby, 1988; Ali et al., 1993), in which ATP after hydrolysis to ADP and orthophosphate is regenerated by consumption of NADH. ATP is synthesized by pyruvate kinase (PK) which uses phosphoenol pyruvate (PEP) as substrate. The resulting pyruvate is reduced by lactate dehydrogenase (LDH) to lactate. NADH is used as a co-substrate in this reaction and consumption of NADH to NAD+ can be monitored spectroscopically at a wavelength of 340 nm.
Reactions were performed in 50 mM HEPES/KOH pH=7.5, 5 mM $MgCl_2$, 2 mM PEP, 0.2 mM NADH, 0.4 U PK and 2 U LDH. 150 µL of this mix were filled up to 200 µL with 50 µL of buffer containing the ATPase (and other proteins as indicated).
Assays were performed on a Cary 50 Bio UV/Vis spectrometer (Varian, Palo Alto, USA) at 30°C. Using Origin 9.0 the slope of the decrease of the progression curve was used to calculate the hydrolysis rates.

3.5.6 UV/VIS spectroscopy

Absorption of electromagnetic radiation is dependent on transfer of π-electrons to an excited, high-energy state.
Proteins absorb between 180 to 300 nm. Disulfide bonds are responsible for absorption at 250 nm, peptide bonds for absorption at around 190 nm and the aromatic amino

acids absorb between 250 and 300 nm (Table 22) .

Table 22: Absorbants in UV/VIS spectroscopy

amino acid	λ_{max} **in nm**	ε_{max} **in** $M^{-1}cm^{-1}$
tryptophane	280	5600
tyrosine	274	1400
phenylalanine	257	200
disulide bridge	250	300
peptide bond	190	$\sim$ 7000

Protein concentrations were determined by UV/VIS spectroscopy. ProtParam was used to calculate molar extinction coefficients and concentrations were calculated using the Lambert-Beer-equation:

$$A = \epsilon * c * d$$

A... absorption at 280 nm
ε... molar extiction coefficient
d... thickness of the cuvette
c... concentration in mol/L

3.5.7 CD spectroscopy

Circular dichroism (CD) is the characteristic of optically active molecules to absorb left or right circularly-polarized light of the same wavelength with different intensity. The optical activity of proteins is dependent on asymmetric carbon atoms and/or aromatic amino acids. Proteins show circular dichroism, because they consist of a large number of optically active amino acids and additionally form asymmetric secondary structures. The ellipticity Θ (in degrees) is the quantitive measure for circular dichroism. The molar ellipticity is the correlation of the ellipticity, the molecular weight and the amino acid composition of a given protein.

$$\Theta_{\mathrm{MRW}} = \frac{\Theta * 100 * M}{c * d * N_{\mathrm{AS}}}$$

Θ_{MRW} ... molar ellipticity
Θ... measured ellipticity in [mdeg]
M ... molecular weight in [kD]
c ... protein concentration [mg/ml]
d ... path lengths of the cuvette
N ... number of amino acids

Proteins display characteristic CD signals in the far-UV region (170-250 nm).
Two adjacent minima (208 and 222 nm) result form α-helices, a minimum at 218 nm is characteristic for the presence of β-sheets. Disordered proteins show very low ellipticity above 210 nm and a minimum at around 195 nm. Therefore, CD spectroscopy is a well suited method to characterize the general folding status of a given protein.
CD spectra were recorded on a JASCO J-715 CD spectrometer in combination with a JASCO PTC-384WI peltier element (JASCO, Easton, USA) and a Huber Compatible Control water bath (Peter Huber Kältemaschinenbau GmbH, Offenburg, Germany). Measurement settings are shown in Table 23. 25 mM NaH_2PO_4, 100 mM NaCl, 1 mM TCEP pH 7.5 was used as measurement buffer.

Table 23: CD spectroscopy settings

parameter	**setting**
starting wavelength	260 nm
end wavelength	200 nm
resolution	0.1 nm
accumulations	10
scanning speed	50 nm/min
cuvette thickness	0.1 cm
temperature	20°C

3.5.8 Protein crystallization

Protein crystallization experiments were performed in cooperation with Dr. Eva Huber, Astrid König and Prof. Dr. Michael Groll (Lehrstuhl für Biochemie, Technische Universität München).
TPR constructs were prepared in 10 mM TRIS/HCl pH7.5, 10 mM TCEP and a 1.3-fold excess of MEEVD (15 mM stock in 100 mM TRIS pH 7.5) was added (modified from Schmid et al. (2012)).

Crystallization of Cns1 domains

TPR construct (36-220)

Sitting drop vapour diffusion experiments were performed with protein (60 mg/mL) supplemented with 1.3-fold excess of MEEVD peptide. Equal volumes of protein and reservoir solutions were mixed and stored at 20 °C. After a few days one single crystal grown in the presence of 0.2 M ammonium sulfate, 0.1 M Tris pH 8.5, 25% (v/v) PEG3350 was identified. It was soaked with a 1:1 (v/v) mixture of reservoir and 50% (v/v) PEG400 and super-cooled in liquid nitrogen. Albeit its small size, the crystal diffracted to a resolution of about 3.2 Å. However, indexing and space group determination by XDS (Kabsch, 2010) as well as reproduction of the crystal failed so far.

TPR construct (70-220)

The TPR-domain of CNS1 was crystallized by the sitting and hanging drop vapour diffusion method by mixing equal volumes of protein (100 mg/mL, supplemented with MEEVD peptide) and reservoir solution (0.2 M $MgCl_2$, 0.1 M Bis-Tris pH 5.5-6.1, 22-25% (v/v) PEG3350). Crystals were cryoprotected by the addition of PEG400 (final concentration of 25% (v/v)) and diffraction data were collected to a resolution of 2.0 Å. X-ray intensities were evaluated with XDS (Kabsch, 2010). The unit cell axes together with the crystal symmetry indicate that the asymmetric unit contains 6-7 molecules. For phasing, crystals were soaked with $PtCl_4$ (Hampton heavy atom screen) and anomalous diffraction data were collected at λ= 1.07122 Åto 3.5 Å, which could be indexed in space group P622 but with a smaller unit cell compared to the non-derivatized crystal. According to the Matthew's coefficient, the asymmetric unit contains only one molecule of the TPR-domain. However, experimental phasing did not yield interpretable electron density maps so far.

C-terminal domain (221-385)

Selenomethionine-labelled protein was concentrated to 15 mg/mL and mixed with equal volume of reservoir solutions in sitting drop vapour diffusion crystal plates. Crystals grew from buffer conditions containing 0.1 M Hepes PH 7.5, 10% (v/v) isopropanol and 20% (v/v) PEG4000 and were cryoprotected by the addition of PEG400 to a final concentration of 25% (v/v). Anomalous data were recorded at the peak wavelength of Se (λ= 0.9794 Å) and evaluated with the program package XDS (Kabsch, 2010). SHELXD (Schneider and Sheldrick, 2002) identifies 10 Se sites, which were further refined by SHARP (de La Fortelle and Bricogne, 1997) . Solvent flattening with SOLOMON (Cowtan and Main, 1996) resulted in an interpretable electron density map, which was traced with COOT (Emsley et al., 2010). The model was completed by cyclic refinement and model building steps followed by final TLS refinement with REFMAC5 (Vagin et al., 2004).

Crystallization of TTC4

C-terminal domain (217-387)

Crystals of TTC4 were grown at 20°C using the sitting drop vapor diffusion method. Drops contained equal volumes of protein (15 mg/mL) and reservoir solutions (1.4 M Na/K phosphate pH 8.2). Crystals were cryoprotected by the addition of a 1:1 (v/v) mixture of mother liquor and 60% (v/v) glycerol. Diffraction datasets were recorded at the beamline ID30B, European Synchrotron Radiation Facility (ESRF), Grenoble, France. X-ray intensities were analyzed with the program package XDS (Kabsch, 2010) and structure determination was performed by Patterson search calculations with PHASER (McCoy et al., 2007) using the coordinates of the CNS1-C-domain as a search model. Cyclic refinement and model building steps were performed with REFMAC5 (Vagin et al., 2004) and COOT (Emsley et al., 2010). TLS refinements finally yielded excellent values for R_{crys}, R_{free}, r.m.s.d. bond and angle values as well as good stereochemistry from the Ramachandran Plot (see Table 25 in Results Section).

3.5.9 Small angle X-ray scattering (SAXS)

SAXS experiments were performed in cooperation with Assoz. Prof. Mag. Dr.rer.nat. Tobias Madl (Technische Universität München). SAXS data for solutions of full-length Cns1, Cns1 1-220, Cns1 Δ69, Cns1 70-220, Cns1 36-220, Cns1 221-384, Hsp90 and Cns1-

Hsp90 complexes were recorded on an in-house SAXS instrument (SAXSess mc^2, Anton Paar, Graz, Austria) equipped with a Kratky camera, a sealed X-ray tube source and a two-dimensional Princeton Instruments PI•SCX:4300 (Roper Scientific) CCD detector. The scattering patterns were measured with 90-minutes exposure times (540 frames, each 10 seconds) for several solute concentrations in the range from 1.3 to 5.0 mg/ml. Radiation damage was excluded based on a comparison of individual frames of the 90-minute exposures, where no changes were detected. A range of momentum transfer of $0.012 < s < 0.63$ Å-1 was covered ($s = 4\pi\sin(\vartheta)/\lambda$, where $2\vartheta$is the scattering angle and $\lambda = 1.542$ Åis the X-ray wavelength).

All SAXS data were analyzed with the package ATSAS (version 2.5). The data were processed with the SAXSQuant software (version 3.9), and desmeared using the programs GNOM and GIFT (Svergun, 1992). The forward scattering, I(0), the radius of gyration, R_g, the maximum dimension, D_{MAX}, and the inter-atomic distance distribution functions, (P(R)), were computed with the program GNOM. The masses of the solutes were evaluated by comparison of the forward scattering intensity with that of a human serum albumin reference solution (molecular mass 69 kDa) and using Porod's law. To generate ab initio shape models, a total number of 50 models were calculated using the program DAMMIF (Franke and Svergun, 2009) and aligned, and averaged using the program DAMCLUST. The structures of Cns1 were modelled using the program CORAL (Petoukhov et al., 2012). Input was the crystal structure of the C-terminal Cns1 domain, a homology model of the TPR domain (swissmodel, template: 4j8f). The N-terminal 54 residues and 5 residues connecting the TPR and the C-terminal domain were kept flexible. A total of 50 structures were calculated, and the best structures based on the fit to the experimental data selected to prepare the figures. The ab initio shape models were aligned with the SAXS-based rigid body model using the program SUPCOMB (Kozin and Svergun, 2001).

3.5.10 NMR

NMR experiments and data analysis was carried out by Dr. Lee Freiburger in the lab of Prof. Dr. Michael Sattler and Materials and Methods were kindly provided by Dr. Abraham Lopez (Lehrstuhl für Biomolekulare NMR-Spektroskopie, Technische Universität München, Germany).

Two and three-dimensional NMR experiments were performed at 303 °K in Bruker 600

and 900 MHz spectrometers equipped with a TCI cryoprobe. Experiments were recorded using uniformly ^{15}N-labeled samples of Cns1 constructs at a concentration of 1 mM in PBS buffer (4 mM KH_2PO_4, 16 mM Na_2H2PO_4,115 mM NaCl, pH=7.4, 1 mM TCEP) containing 10% D_2O. ^{1}H-^{15}N HSQC experiments comprised 256 and 1024 complex points (F1, F2), with 16 scans per increment. Water suppression was achieved by watergate flip-back scheme. ^{15}N-edited NOESY experiments comprised 260, 88, 1024 complex points (F1, F2, F3), with 16 scans per increment. Spectra were processed with Topspin software (Bruker Corp., Karlsruhe, Germany) and analyzed with CcpNmr Analysis software (Vranken et al., 2005).

4 Results

4.1 Identification of the essential Cns1 domains using 5'-FOA shuffling

Hsp90 is regulated by a cohort of co-chaperones. Most of them are dispensable in yeast under normal growth conditions, but three of them (Sgt1, Cdc37 and Cns1) are essential (see introduction). Sgt1 is known to be involved in kinetochor assembly (Kitagawa et al., 1999; Catlett and Kaplan, 2006) and Cdc37 is crucial for kinase maturation (see introduction), but the essential role of Cns1 *in vivo* remains enigmatic.

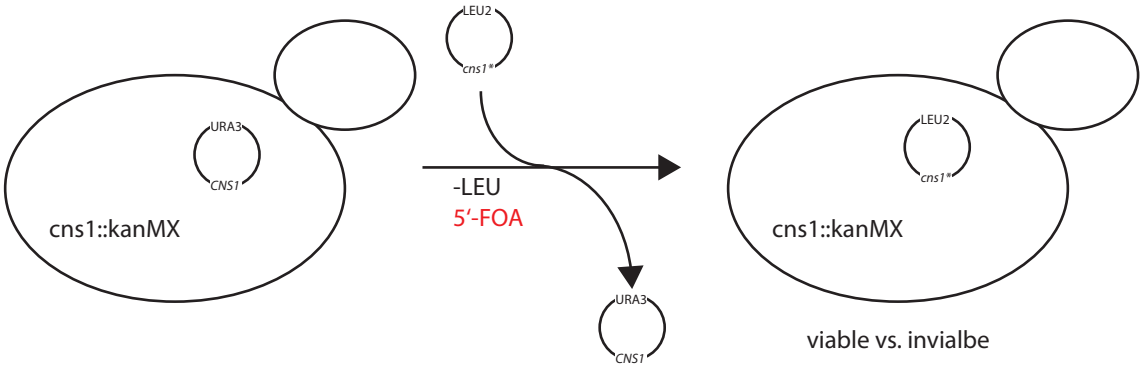

Figure 15: 5'-FOA shuffling to test *cns1* mutants in vivo (experimental setup overview). The genomic copy of *CNS1* is replaced by a kanMX cassette. To maintain viability, wildtype *CNS1* is provided from a plasmid containing a *URA3* marker. *cns1* variants can be introduced on a second plasmid. Restreaking to plates containing 5'-FOA leads to the loss of the *URA3* plasmid and functionality of the *cns1* mutants can be scored by monitoring growth.

In order to gain a better understanding of the single Cns1 domains *in vivo*, a Cns1-shuffling mutant (*cns1*Δ [*CNS1-URA3*]) strain was constructed in the lab previously (Mitschke, 2012, PhD thesis). This mutant contains a genomic disruption of the *CNS1* gene. In addition, the wildtype coding sequence of *CNS1* is provided on a plasmid con-

taining also a *URA3* marker. Now, a second plasmid containing a *cns1* mutant can be introduced by plasmid transformation and selected using a second auxotrophy marker (e.g. *LEU2*). The *URA3* gene product catalyzes the reaction from 5'-FOA to 5'-FU, which is toxic for yeast cells. Thus, the cells need to loose the *URA3* and *CNS1* wildtype containing plasmid after restreaking onto plates containing 5'-FOA. If the second plasmid contains a *cns1* mutant that is able to provide the essential function, the cells are viable, although they might already show a growth defect, when the essential function is not fully provided. If the second plasmid contains an inviable mutant, no growth is observed (Figure 15).

4.1.1 The C-terminal domain of Cns1 is dispensable for cell viability

It was already known, that the amino acids C-terminal of the TPR domain are dispensable for growth (Tesic et al., 2003). Data from previous work in the lab suggested that also the largest part of the amino acids N-terminal of the TPR domain can be deleted (Mitschke, 2012, PhD thesis; Hainzl, 2008; PhD thesis), but these results were not reproducible (data not shown). Therefore, several truncation mutants lacking the C-terminal segment of Cns1 as well as a plasmid expressing only amino acids 169-385 under control of the strong GPD promoter were cloned (Figure 16A). Plasmids containing these variants did not affect cell growth on -Ura-Leu plates (Figure 16B), but when restreaked onto 5'-FOA plates , as expected, only $Cns1^{wt}$, $Cns1^{1\text{-}200}$, $Cns1^{1\text{-}190}$, $Cns1^{1\text{-}185}$ supported growth, whereas the empty vector negative control and the C-terminal construct ($Cns1^{169\text{-}385}$) did not, even when the cells were incubated for six days (Figure 16C and D).

Tesic et al. (2003) had shown that the amino acids 1-212 of Cns1 are sufficient to support growth. The viability of the $Cns1^{1\text{-}185}$ mutant now provides evidence, that even a further truncation is possible (Figure 16B and C) and that the last few residues of the TPR (amino acids 186-189) domain are not necessary to support growth at 30°C.

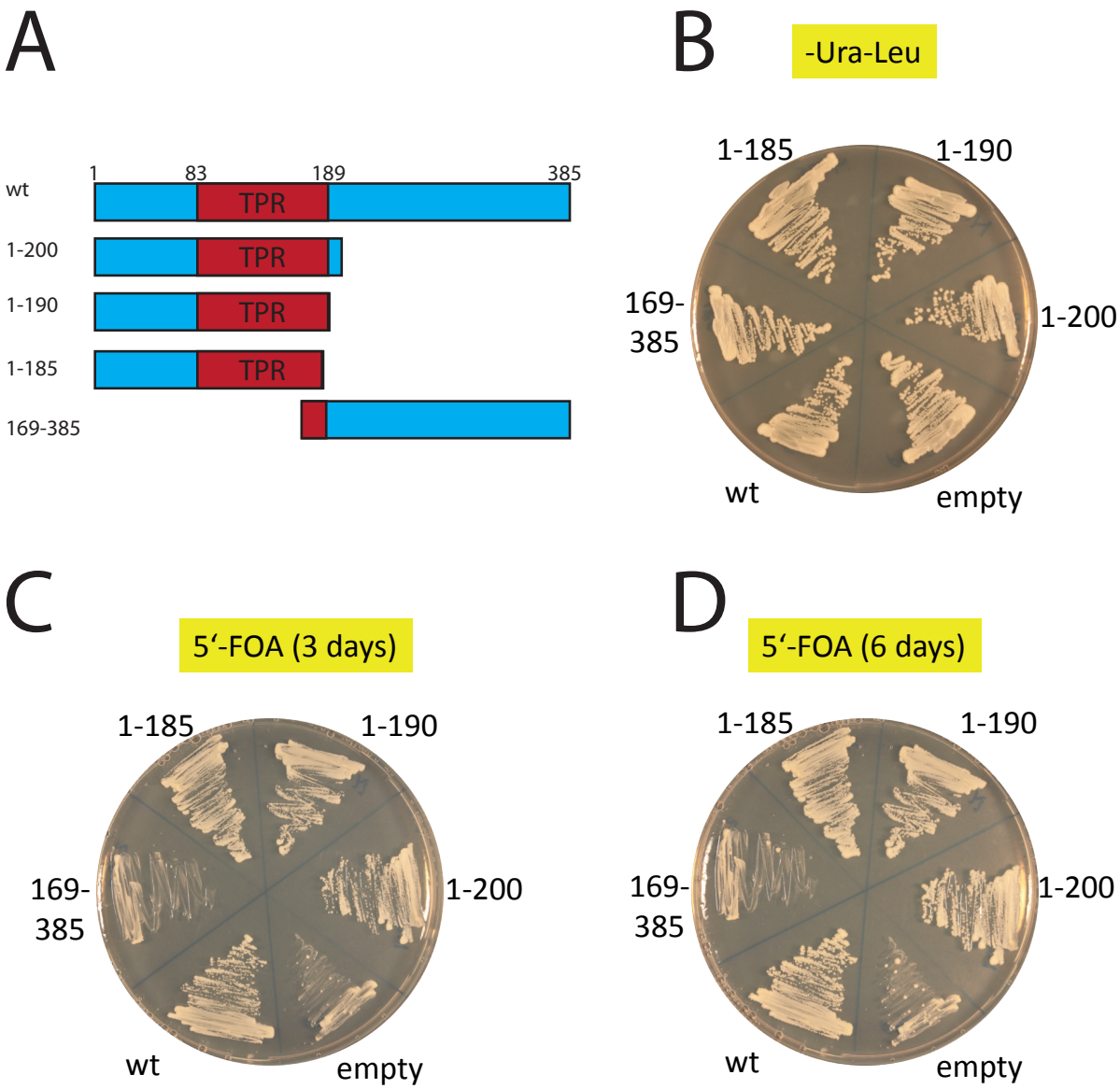

Figure 16: The C-terminal domain of Cns1 is dispensable *in vivo* A) Schematic overview of truncation mutants of Cns1 lacking the C-terminal domain. B) *cns1*Δ [*CNS1*-URA3] strain expressing variants from A) on a p425-GPD vector grown on -Ura-Leu plates. Cells were grown at 30°C for three days. C and D) strains from B were restreaked onto plates containing 5'-FOA and incubated at 30°C for 3 days and 6 days, respectively. $Cns1^{wt}$ and empty vector were used as positive and negative controls, respectively.

4.1.2 Deletion of the first 35 amino acids does not affect *in vivo* function of Cns1

Next, in order to get a better understanding of the *in vivo* function of the Cns1 N-terminal segment, several N-terminal truncation mutants were cloned (Figure 17A) and tested using the 5'-FOA shuffling assay. Again, none of the overexpressed mutants affected cell growth on -Ura-Leu plates (Figure 17B).
Surprisingly, the deletion of the first 35 amino acids ($Cns1^{36\text{-}385}$), did not have any noticeable effect on Cns1 function *in vivo*, but a further truncation of five amino acids ($Cns1^{41\text{-}385}$) dramatically reduced the growth of yeast cells on plates containing 5'-FOA. Moreover, $Cns1^{46\text{-}385}$ and $Cns1^{51\text{-}385}$ expressing cells did not show any growth even after six days of incubation (Figure 17C and D).

To investigate the requirement of the first 35 amino acids in the absence of the C-terminal domain, a number of constructs containing Cns1 variants truncated form both, the N- and the C-terminus were tested (Figure 18A). Interestingly, $Cns1^{36\text{-}205}$, $Cns1^{36\text{-}200}$ and $Cns1^{36\text{-}195}$ expressing strains showed only poor growth on plates containing 5'-FOA after three days (Figure 18C) compared to the mutant lacking only the first 35 amino acids (Figure 17C), but the cells were still viable after six days (Figure 18D). Therefore, one can conclude, that the C-terminal domain is important for full *in vivo* function of Cns1 when the first 35 amino acids are missing.

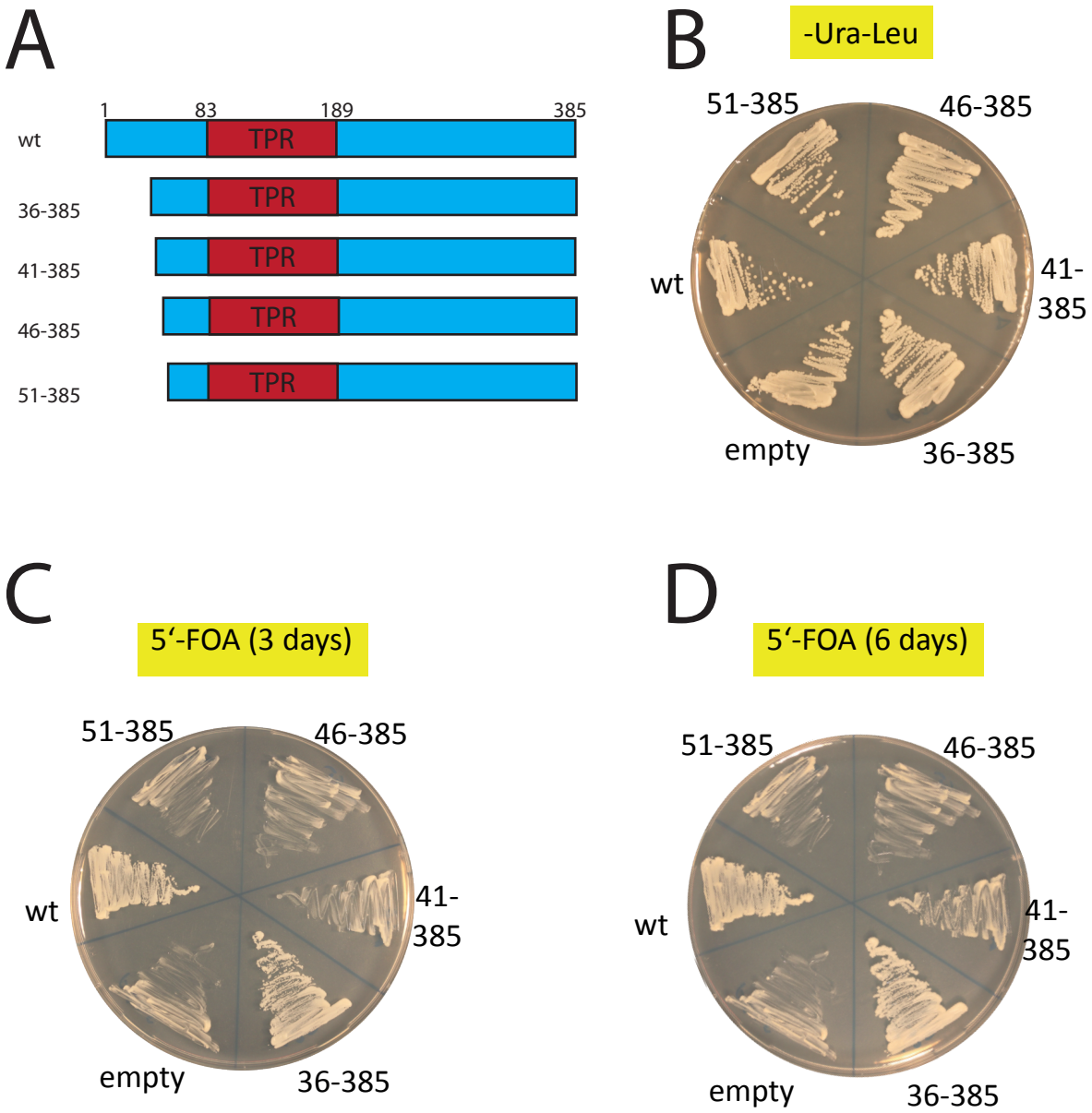

Figure 17: Amino acids N-terminal of the TPR domain contain the essential function of Cns1 *in vivo*. A) Schematic overview of truncation mutants of Cns1 lacking a varying number of amino acids from the N-terminus. B) *cns1*Δ [*CNS1*-URA3] strain expressing mutant versions from A) on a p425-GPD vector grown on -Ura-Leu plates. Cells were grown at 30°C for three days. C and D) strains from B were restreaked onto plates containing 5'-FOA and incubated at 30°C for 3 days and 6 days, respectively. Cns1^{wt} and empty vector were used as positive and negative controls, respectively.

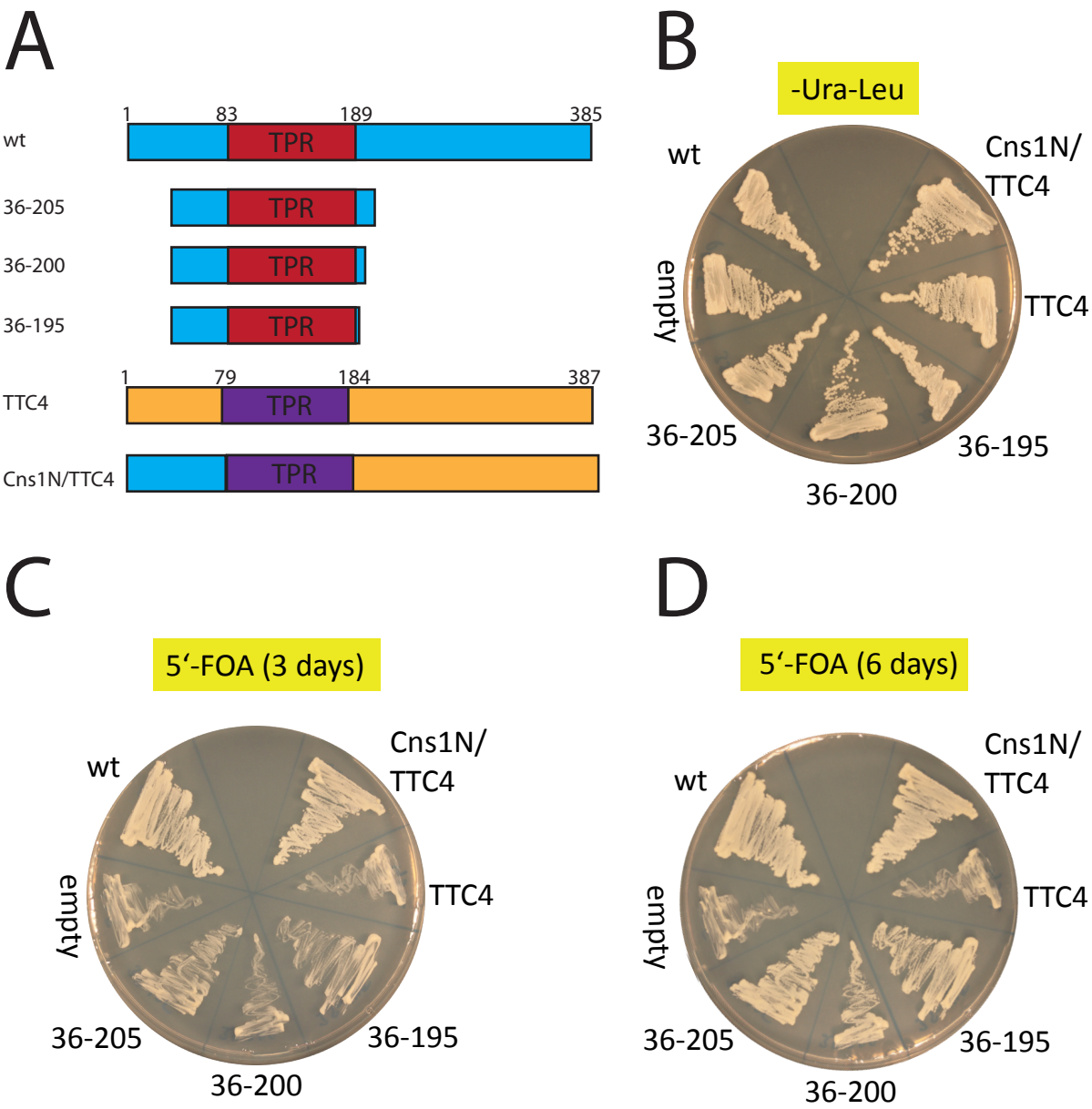

Figure 18: Shuffling of TPR and TTC4 mutants A) Schematic overview of truncation mutants of Cns1 lacking amino acids from N- and C-terminus and domain architecture of TTC4 and a Cns1N/TTC4 chimera mutant. B)*cns1*Δ [*CNS1*-URA3] strain expressing variants from A) on a p425-GPD vector grown on -Ura-Leu plates. Cells were grown at 30°C for three days. C and D) strains from B were restreaked onto plates containing 5'-FOA and incubated at 30°C for 3 days and 6 days, respectively. $Cns1^{wt}$ and empty vector were used as positive and negative controls, respectively.

4.2 Cns1 and its human orthologue TTC4 differ in their N-terminal domain

During the course of this work, in a high-throughput study, TTC4, the putative human orthologue of Cns1, was reported to complement a *cns1* yeast mutant *in vivo* (Kachroo et al., 2015). The domain architecture of TTC4 is shown in Figure 18A. Like Cns1, it contains a N-terminal domain, a TPR domain and a C-terminal domain. As shown in Figure 18C and D, TTC4 was not able to overcome the lethality of a *cns1* deletion using the 5'-FOA shuffling assay.

Protein sequence alignment of Cns1 and TTC4 revealed a strong sequence conservation in the TPR region, whereas the amino acids N-terminal and C-terminal of the TPR domain are less conserved (Figure 19).

Figure 19: Sequence alignment of Cns1 and TTC4 Protein sequences of Cns1 from *S. cerevisiae* and TTC4 from *H. sapiens* were aligned using mCoffee (http://tcoffee.crg.cat/)

TTC4 was reported to interact with Hsp90 (Crevel et al., 2008), and it is likely, that

this interaction is mediated by TTC4's TPR domain. Given the fact, that the results obtained so far suggest, that the essential function of Cns1 is encoded by the amino acids N-terminal of the TPR domain, one can reason that a chimera of the first 82 residues from Cns1 and TTC4 starting from the TPR (amino acid 79) might be able to overcome the lethality of a *CNS1* deletion. TTC4's TPR domain would here act as a hub to mediate Cns1 N-domain/Hsp90 interaction. Strikingly, Cns1N/TTC4 did not only suppress the lethality of *cns1*Δ, but also the mutant grew much better than Cns1$^{36\text{-}205}$, Cns1$^{36\text{-}200}$ and Cns1$^{36\text{-}195}$ (Figure 18C and D).

4.3 The essential function of Cns1 is associated with Hsp90, not Hsp70

It is already known, that a point mutant at the beginning of the Cns1's TPR domain (G90D) interferes with stable Hsp90 interaction *in vivo* and shows a temperature-sensitive growth defect as well as synthetic lethality with an Hsp90 allel lacking the C-terminal MEEVD motif (Tesic et al., 2003). The authors therefore speculated, that Cns1's essential function is dependent on Hsp90, but so far, no mutant completely lacking the TPR domain was tested.

Strikingly, Cns1$^{1\text{-}82}$ was able to support growth in the 5'-FOA shuffling assay, although the cells grew extremely poorly and growth was only visible after 5 days (Figure 20A-D). Comparison of this result with the mutants Cns1$^{1\text{-}200}$, Cns1$^{1\text{-}190}$, Cns1$^{1\text{-}185}$, which provided almost wildtype-like growth, leads to the assumption that the TPR domain of Cns1 is dispensable for the essential *in vivo* function, but its presence is strongly supporting growth.

Cns1 binds both, Hsp90 and Hsp70 *in vitro* via its TPR domain (Hainzl et al., 2004). Therefore, it is difficult to discriminate whether the improved growth of Cns1$^{1\text{-}190}$ compared to Cns1$^{1\text{-}82}$ is dependent on its ability to interact with Hsp90, Hsp70 or even both. The Hsp90/Hsp70 co-chaperone Sti1 contains three TPR domains with different interaction preferences for Hsp90 and Hsp70, respectively (Schmid et al., 2012; Scheufler et al., 2000). TPR1 binds only Hsp70, TPR2A only Hsp90 and TPR2B is able to bind both. As expected, Sti1 as well as as TPR1 were not able to suppress the lethality of a strain lacking *CNS1*. Fusion of the first 82 residues from Cns1 to TPR1 (Cns1$^{1\text{-}82\text{-}TPR1}$) showed a growth rate comparable to Cns1$^{1\text{-}82}$ (Figure 20A-D). Also constructs containing only

TPR2A and TPR2B were not able to suppress the *cns1*Δ lethality. Strikingly, fusion of the first 82 amino acids of Cns1 to TPR2A or TPR2B, improved growth of the cells and colonies were already visible after three days (Figure 20A and Figure 21A-C).
Although, no construct tested so far showed a growth defect in the *cns1*Δ [*CNS1-URA3*] strain on -Ura-Leu control plates, one can not exclude a possible negative effect of the mutants on cell growth, since the shuffling strains also over-expresses wildtype Cns1 from the GPD promoter, which in turn might compete with the mutants *in vivo*. Therefore, the wildtype strain BY4741 was transformed with plamids expressing several truncation variants of Cns1 (Figure 21D). Compared to the empty vector control, expression of $Cns1^{wt}$, $Cns1^{1\text{-}190}$, $Cns1^{1\text{-}82}$ and $Cns1^{169\text{-}385}$ had no effect on the growth of BY4741. Interestingly, the $Cns1^{51\text{-}385}$ construct showed a strong dominant negative effect on cell growth that was reversed by deletion of the C-terminal domain ($Cns1^{51\text{-}190}$). Again, theses findings underline the importance of of Cns1's N-terminal segment for its *in vivo* function and, moreover, they suggest a cooparative mechanism between N-, TPR- and C-domain *in vivo*.

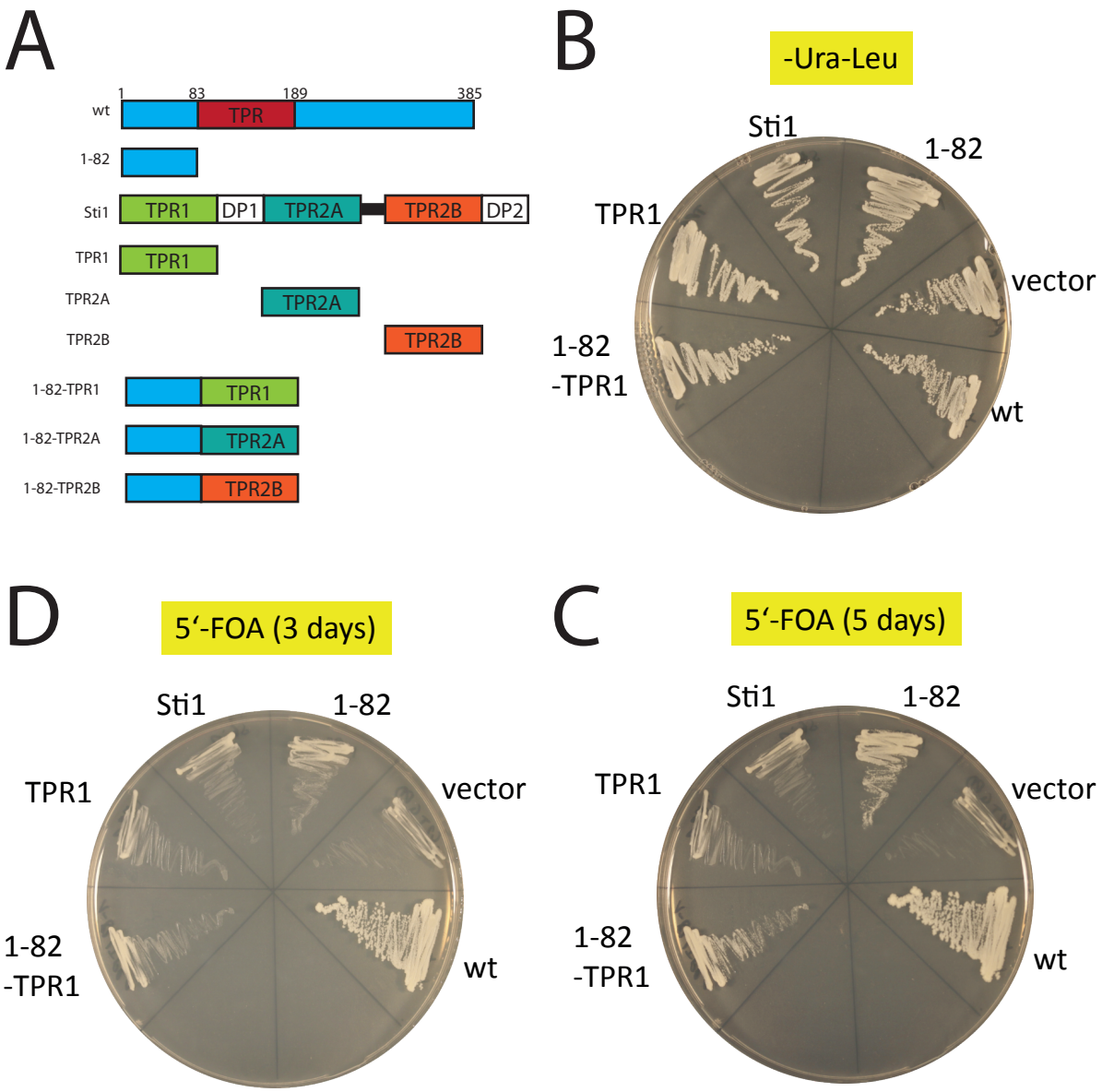

Figure 20: Cns1 N-domain fusion to TPR1 from Sti1 does not improve growth A) Schematic overview of Sti1's domain architecture and Cns1 chimera mutants with single Sti1 TPR domains. B)*cns1*Δ [*CNS1*-URA3] strain expressing variants from A) on a p425-GPD vector grown on -Ura-Leu plates. Cells were grown at 30°C for three days. C and D) strains from B were restreaked onto plates containing 5'-FOA and incubated at 30°C for 3 days and 5 days, respectively. $Cns1^{wt}$ and empty vector were used as positive and negative controls, respectively.

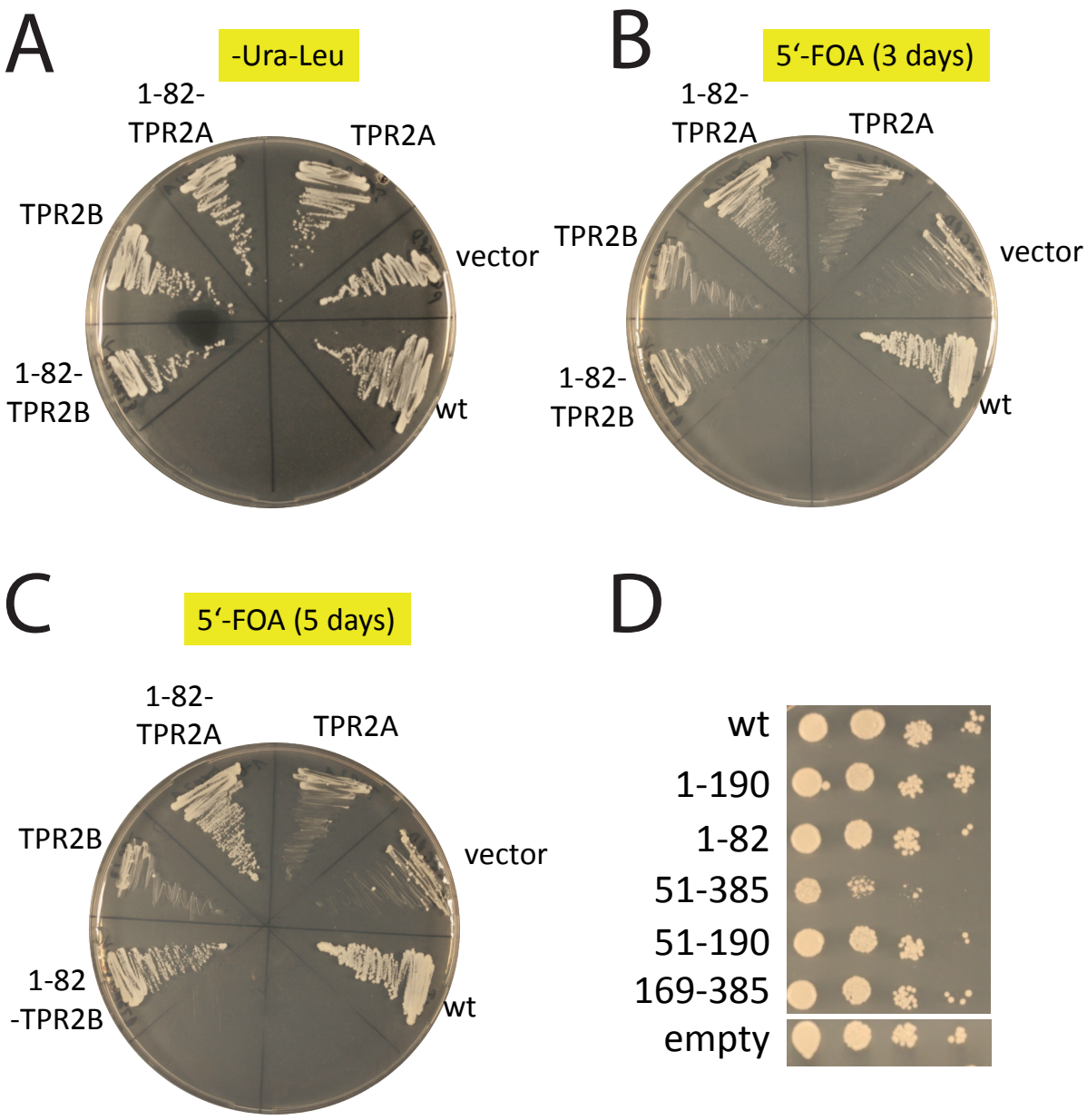

Figure 21: Cns1 N-domain fusion to Hsp90 binding TPR domains improves growth A)*cns1*Δ [*CNS1*-URA3] strain expressing variants from Figure 20A on a p425-GPD vector grown on -Ura-Leu plates. Cells were grown at 30°C for three days. B and C) strains from A were restreaked onto plates containing 5'-FOA and incubated at 30°C for 3 days and 5 days, respectively. $Cns1^{wt}$ and empty vector were used as positive and negative controls, respectively. D) Overexpression of Cns1 truncation variants in BY4741. -Leu plates were incubated at 30°C for 2 days.

Although the results obtained with the fusion proteins of the Cns1 N-domain with the three TPR domains from Sti1 suggest a genetic interaction between Cns1 and Hsp90, but not Hsp70, the observed effects could still be "off-target" effects.

Therefore, a direct fusion of the first 82 residues from Cns1 to Hsp90 and Hsp70, respectively, could provide helpful insights into the effect of the Cns1 N-domain on these two chaperones. As expected, expression of Hsc82 or Ssa1 under the control of the GPD promoter was not able to suppress the lethality of *cns1*Δ. Strikingly, the Hsc82-1-82 chimera (Cns1 N-terminal segment fused to the C-terminus of Hsp90) supported growth already after three days of incubation on 5'-FOA plates, whereas the Ssa1-1-82 chimera did not (Figure 22A-C). Note, that the $Cns^{1\text{-}82}$ and the Ssa1-1-82 chimera showed comparable (slow) growth after five days (data not shown), indicating that the Cns1 N-domain is functional when fused to Ssa1, albeit it is not improving growth of the *cns1*Δ strain. Interestingly, it seems that the position of the fusion to Hsp90 is not of importance, since fusion to the N-terminus of Hsp90 (1-82-Hsc82) shows a comparable growth rate to Hsc82-1-82 (Figure 22A-C). Moreover, both constructs are able to serve as the single source of Hsp90 in a Hsp90-shuffling mutant, indicating, that the chimera do not compromise general Hsp90 function (Figure 23).

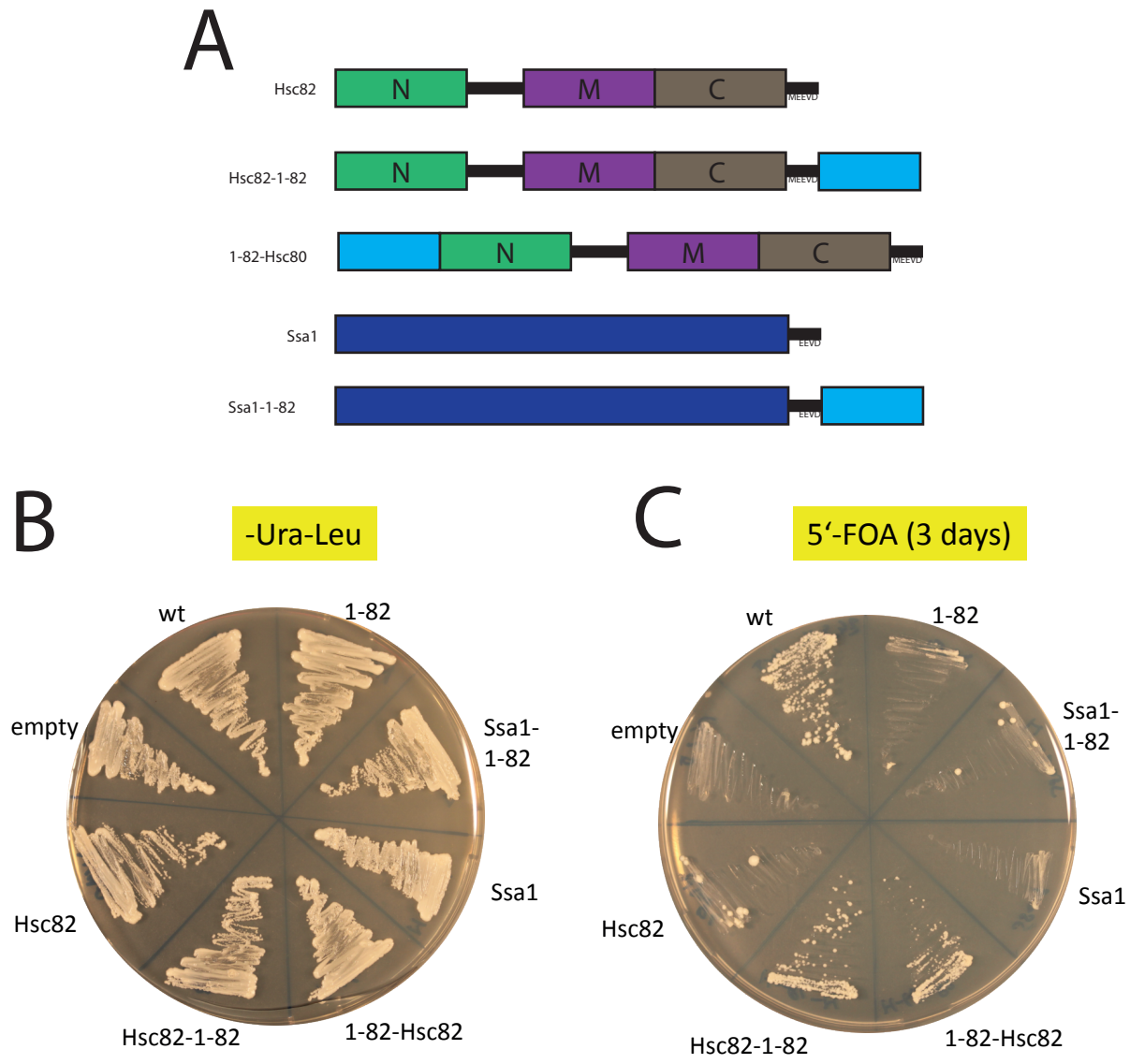

Figure 22: Direct fusion of the Cns1 N-domain to Hsp90 improves growth A) Schematic overview of the domain architecture of Hsp90 (Hsc82), Hsp70 (Ssa1) and chimera proteins between Cns1's N-terminal domain and Hsp90 and Hsp70. B) *cns1*Δ [*CNS1*-URA3] strain expressing variants from A) on a p425-GPD vector grown on -Ura-Leu plates. Cells were grown at 30°C for three days. C) strains from B were restreaked onto plates containing 5'-FOA and incubated at 30°C for 3 days. $Cns1^{wt}$ and empty vector were used as positive and negative controls, respectively.

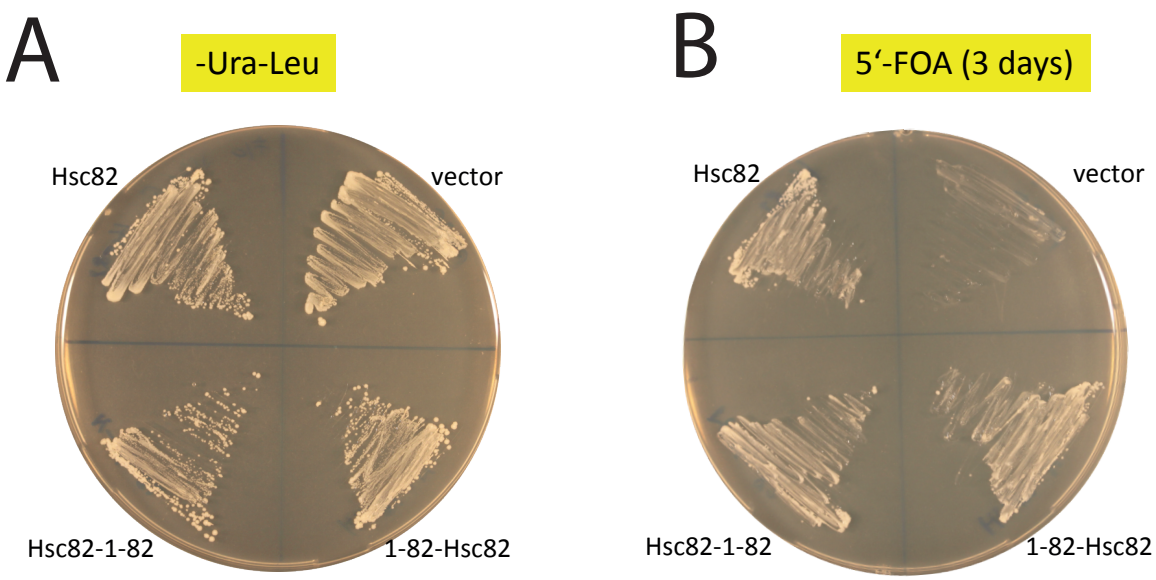

Figure 23: Cns1/Hsc82 chimera can serve as the single source of Hsp90 in yeast *hsc82*Δ *hsp82*Δ strain A) A *hsc82*Δ *hsp82*Δ double deletion strain carrying *HSP82* on a *URA3* plasmid was transformed with Hsp90- and Hsp90-chimera plasmids described in Figure 23A. Cells were grown at 30°C for 2 days. B) Strains from A) were restreaked onto 5'-FOA-containing plates and grown for 3 day at 30°C. Hsc82 wildtype and empty vector were used as positive and negative controls, respectively.

4.4 TTC4 is able to replace Cns1 at lower temperatures

Since the replacement of Cns1 by TTC4 was not successful so far, this question was readdressed by carrying out the 5'-FOA shuffling assay at lower temperatures. Again, TTC4 was not able to replace Cns1 at 30°C. $Cns1^{wt}$, $Cns1^{1\text{-}190}$, $Cns1^{1\text{-}82}$ and Cns1N/TTC4 served as positive controls in this assay, whereas empty vector was used as negative control. Interestingly, $Cns^{1\text{-}82}$ showed an increased growth rate at 23°C compared to 30°C. Strikingly, TTC4 was able to suppress the lethality of *cns1*Δ at 23°C (Figure 24A and B). These data indicate, that the essential function of Cns1 is conserved from yeast to man and confirms data presented in a recent high-throughput study (Kachroo et al., 2015).

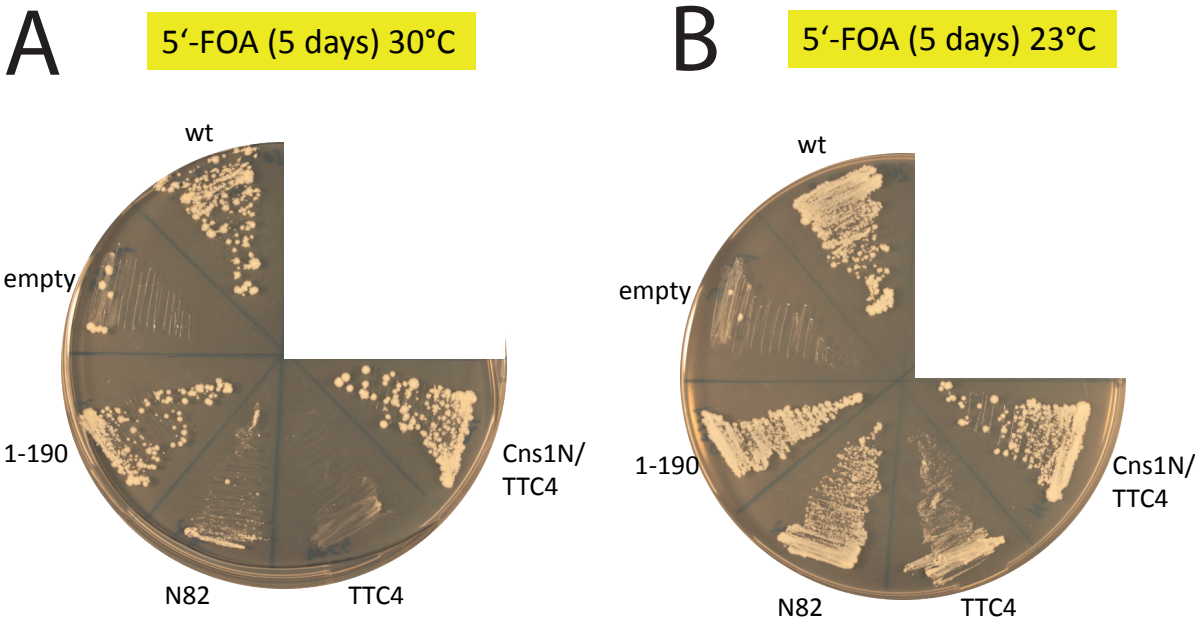

Figure 24: TTC4 can replace Cns1 at reduced temperature. *cns1*Δ [*CNS1*-URA3] strain expressing Cns1 variants, TTC4 and the Cns1N/TTC4 chimera from p425-GPD as indicated grown on 5'-FOA containing plates for 5 days at 30°C (A) and 23°C (B). $Cns1^{wt}$ and empty vector were used as positive and negative controls, respectively

4.5 Cns1 binds to Hsp90 independent of nucleotides and does not stimulate its ATPase activity *in vitro*

The *in vivo* analysis of the single Cns1 domains using the 5'-FOA shuffling method provides a good starting point for subsequent *in vitro* analyses. Especially, the chimera proteins of the Cns1 N-domain with the TPR domains from Sti1, Hsp90 and Hsp70 suggest that Cns1 functions in concert with Hsp90. Therefore, the focus of the *in vitro* analysis is on this chaperone.

First, Cns1 interaction with Hsp90 was probed using analytical ultracentrifugation (aUC). Since Cys-labeling led to strong protein aggregation and the labeled protein did not bind Hsp90 in aUC experiments (data not shown), random labeling of Lys residues was used. It is noteworthy, that a labeling efficiency of over 2 prevents binding of Cns1 to Hsp90. Therefore, the protein was labeled only to a degree of approx. 0.7 to maintain Hsp90 binding *in vitro*.

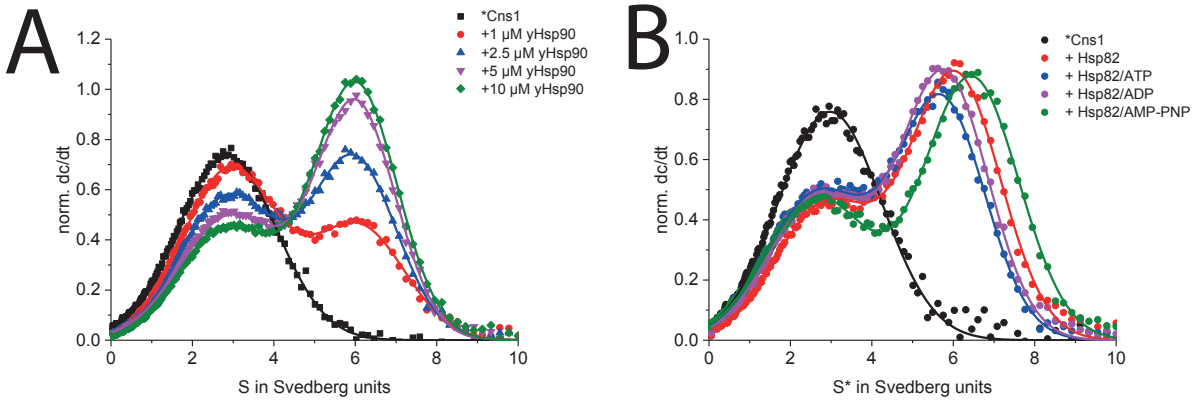

Figure 25: Binding of Cns1 to Hsp90 in presence and absence of nucleotides Analytical ultracentrifugation was performed with ATTO488-labeled Cns1, sedimentation was detected by the fluorescence optical system. Data were analysed using SedView and fitted according to the Gauss equation. A) 500nM ATTO488-labeled Cns1 was incubated with increasing amounts of yHsp90 as indicated and analyzed by aUC. B) 500 nM *Cns1, 10 µM yHsp90 and 2 mM nucleotides as indicated were mixed and analyzed by aUC.

500 nM of labeled Cns1 (*Cns1) was mixed with increasing amounts of Hsp90 (Figure 25A). *Cns1 alone showed a maximum at around 3S, which fits to the size of an approx.

45 kD protein and also shows, that Cns1 is a monomer in solution. Addition of Hsp90 led to the appearance of a second peak around 6S, indicating complex formation between Hsp90 and Cns1. Moreover, addition of 5 µM Hsp90 led to a strong 6S peak, that only increased slightly when 10 µM Hsp90 were added, indicating the binding reaction being saturated.

Moreover, no additional peaks at higher Svedberg values could be observed. This finding suggests, that only one Cns1 molecule per Hsp90 dimer is bound at a time.
Some co-chaperones like Sti1 and Sba1 preferentially bind to the open or closed conformation of Hsp90, respectivly (see introduction). Therefore, Cns1 binding to Hsp90 without nucleotide and in the presence of ATP, ADP and AMP-PNP was tested. As shown in Figure 25B, Cns1 binds to all Hsp90 nucleotide states tested. The slight shift from about 6S to 7S in the presence of AMP-PNP is due to the faster sedimentation of Hsp90 in the closed state (Li et al., 2013).
These results indicate, that binding of Cns1 to Hsp90 is independent of nucleotides, and confirm previous results (Lars Mitschke, PhD thesis).

Next, the effect of different Cns1 mutants on the ATPase activity of Hsp90 was investigated in more detail (Figure 26). $Cns1^{wt}$ did not alter the ATPase activity of Hsp90, confirming the results obtained by Hainzl et al. (2004). Also the viable mutants $Cns1^{36\text{-}385}$, $Cns1^{1\text{-}190}$, $Cns1^{1\text{-}82}$ and $Cns1^{36\text{-}205}$ as well as TTC4 and the chimera Cns1N/TTC4 did not alter Hsp90's ATPase activity. In addition, also the dominant negative $Cns1^{51\text{-}385}$ mutant did not affect the Hsp90 ATPase, indicating that the growth defect of the mutant is not due to inhibiting Hsp90 function in general. Interestingly, although very high concentrations of Cns1 were used in this assay (15µM), no effect on the Hsp90 ATPase could be observed. GR-LBD and Sti1 were used as positive controls for ATPase inhibition (Richter et al., 2003; Lorenz et al., 2014), whereas Aha1 was used as a positive control for ATPase stimulation (Lotz et al., 2003). All three proteins already have an effect at 5-fold lower doses (3µM used here).
Taking the low abundance of Cns1 *in vivo* into account (Ghaemmaghami et al., 2003), it is unlikely, that the co-chaperone regulates Hsp90's ATPase in the cell.

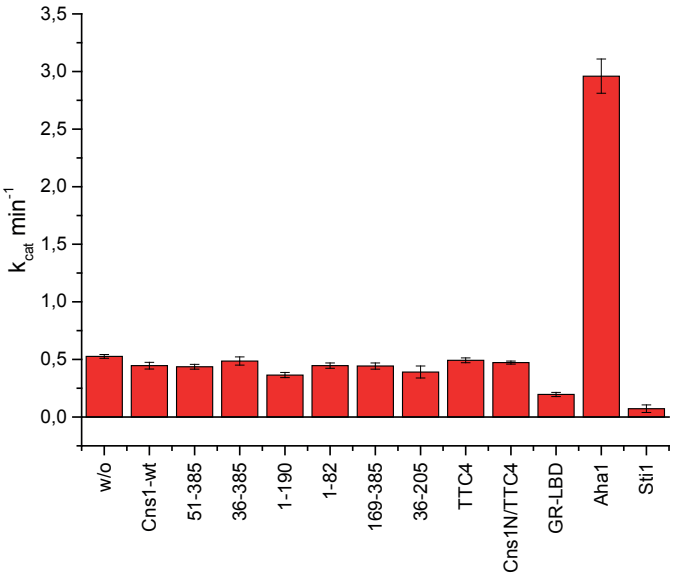

Figure 26: Influence of Cns1 and Cns1 truncation mutants on the ATPase activity of Hsp90 ATPase assays were carried out using a ATP-regenerating system. 3 µM yHsp90 were incubated with Cns1 constructs (15µM), TTC4 constructs (15 µM) or GR-LBD, Aha1 and Sti1 (3 µM) as controls as indicated. Assays were performed at 30°C and were started by the addition of ATP to a final concentration of 500 µM. Purified GR-LBD, Aha1 and Sti1 were kind gifts from Daniel Rutz.

4.6 Cns1 binds Hsp90 via its TPR domain

Cns1 is known to stably interact with Hsp90's C-terminal MEEVD motif via its TPR domain (Tesic et al., 2003; Hainzl et al., 2004). As shown in Figure 25A, Cns1 forms a complex with Hsp90 in a concentration-dependent manner. To test the ability of Cns1 mutants to bind Hsp90, a competitive binding assay was established to address this question. Again, a complex between *Cns1 and Hsp90 was formed *in vitro*. Addition of purified, unlabeled Cns1 constructs should lead to a disruption of the *Cns1-Hsp90 complex, if there was competition for Hsp90 binding. This hypothesis was confirmed by adding a 20-fold molar excess of unlabeled $Cns1^{wt}$ over labeled Cns1 protein to the preformed *Cns1-Hsp90 complex, which led to a strong disruption of the 6S peak and an increase of the 3S peak, representing the free monomer of labeled Cns1 (Figure 27A). Next, the Cns1 truncation versions $Cns1^{1\text{-}190}$, $Cns1^{1\text{-}82}$, $Cns1^{36\text{-}385}$, $Cns1^{51\text{-}385}$, $Cns1^{169\text{-}385}$ and $^{36\text{-}205}$ were tested. As expected, only the constructs that contained the entire TPR domain of Cns1 were able to disrupt a preformed *Cns1-Hsp90 complex (Figure 27A and B). Interestingly, disruption of the complex by the dominant negative mutant $Cns1^{51\text{-}385}$ was more pronounced than the disruption by $Cns1^{1\text{-}190}$, suggesting, that the ability to

bind Hsp90 alone does not correlate with *in vivo* function of the protein. This is further underlined by the finding that Cns1$^{1\text{-}82}$ and Cns1$^{169\text{-}385}$ showed opposite effects in the 5'-FOA shuffling assay, although they are not able to disrupt a *Cns1-Hsp90 complex *in vitro*.

Additionally, also TTC4 and the chimera Cns1N/TTC4 were investigated using the aUC competition assay. As shown in Figure 27B, both TTC4 and Cns1N/TTC4 were able to disrupt the *Cns1-Hsp90 complex, although to a decreased degree compared to Cns1^{wt}. Thus, again the viability of Cns1N/TTC4 compared to the inviability of TTC4 observed in the 5'-FOA shuffling assay at 30°C does not correlate with the ability to bind Hsp90 *in vitro*.

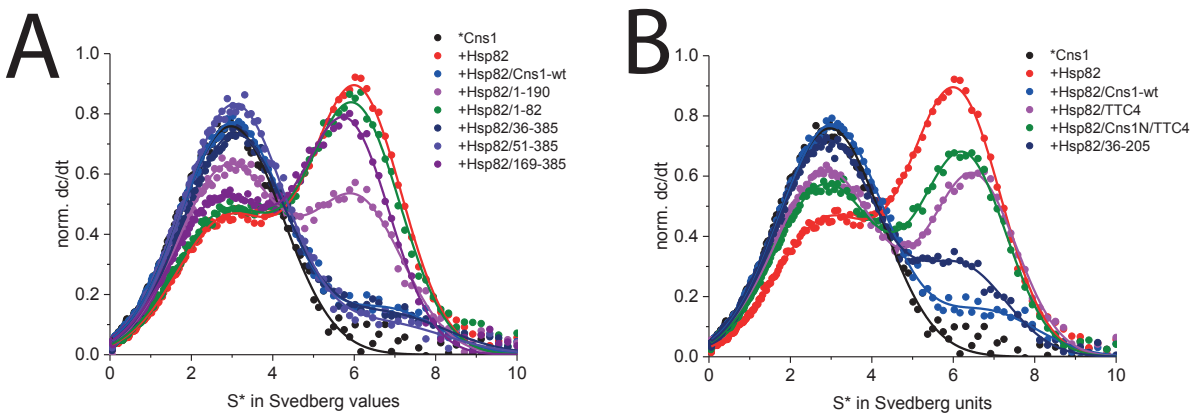

Figure 27: Binding of Cns1 truncation mutants to yHsp90 Analytical ultracentrifugation was performed with ATTO488-labeled Cns1, sedimentation was detected by the fluorescence optical system. Data were analysed using SedView and fitted according to the Gauss equation. A) 500nM *Cns1 was incubated with 10 µM yHsp90, and unlabeled Cns1 variants (10 µM) were added as indicated. B) 500nM *Cns1 was incubated with 10 µM yHsp90 and unlabeled Cns1 variants and TTC4 constructs (10 µM) were added as indicated. In both panels *Cns1, *Cns1+yHsp90 and *Cns1+yHsp90+Cns1^{wt} are shown as controls for better clarity.

4.7 The minimal Cns1$^{1\text{-}82}$ construct is partially disordered *in vitro*

To get a deeper insight into the structural properties of Cns1 and mutants thereof, CD spectroscopy was performed to get an overview of their general folding properties. Cns1^{wt}, Cns1$^{1\text{-}190}$, Cns1$^{36\text{-}385}$, Cns1$^{36\text{-}205}$, Cns1$^{51\text{-}385}$ and Cns1$^{169\text{-}385}$ all showed correct folding (Figure 28A). Moreover, no difference between TTC4 and Cns1N/TTC4 could

be observed using CD spectroscopy (Figure 28B), indicating, that there is also no general folding defect of the proteins that would correlate with the *in vivo* function. Also temperature stability of the purified constructs did not correlate with *in vivo* function (data not shown). Interestingly, the minimal viable construct Cns1$^{1\text{-}82}$ showed properties of an unstructured protein (Figure 28A), with low ellipticity above 210 nm and a minimum at around 200 nm. Therefore, it is tempting to speculate, that the essential domain of Cns1 might at least to some extent lack secondary structure.

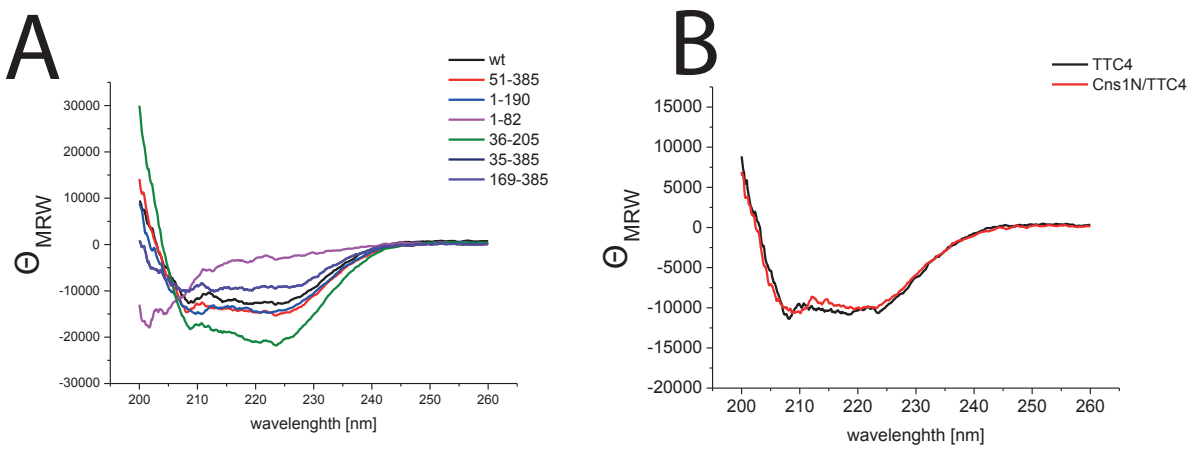

Figure 28: CD spectra of Cns1 and TTC4 constructs. CD spectra were recorded from 260 to 200 nm with 10 accumulations at 20°C. A) Cns1 and truncation mutants of Cns1 were analyzed using CD spectroscopy. B) TTC4 and the chimera mutant Cns1N/TTC4 were analyzed by CD spectroscopy.

4.8 Crystallization of Cns1 and TTC4

To further extend the insight into the structural properties of Cns1, protein crystallization experiments were performed in cooperation with Astrid König, Dr. Eva Huber and Prof. Dr. Michael Groll (Lehrstuhl für Biochemie, Technische Universität München). Several constructs were tested and protein concentrations up to 120 mg/mL were used. Four constructs yielded diffracting protein crystals (Figure 29), namely Cns1$^{36\text{-}220}$, Cns1$^{70\text{-}220}$, Cns1$^{221\text{-}385}$ and the C-terminal domain of TTC4 (TTC4$^{217\text{-}387}$) (Figure 29).

Unfortunately, the only crystal of a construct that is also expected to fulfill Cns1's *in vivo* function (Cns1$^{36\text{-}220}$), was not reproducible and it was not possible to solve the structure so far, since indexing and space group determination by XDS failed, although the crystal

diffracted to a resolution of about 3.2 Å (data not shown). Moreover, it was also not possible to solve the structure of native Cns1$^{70\text{-}220}$ due to phasing problems. After heavy metal soakings the crystals showed only limited resolution (Table 24). SeMet labeling of this construct was not possible due to the absence of methionine residues.

Table 24: X-ray data collection and refinement statistics for Cns1$^{70\text{-}220}$

	Cns1$^{70\text{-}220}$	**Cns1$^{70\text{-}220}$ Pt**
Crystal parameters		
Space group	P622	P622
	(Screws unknown)	(Screws unknown)
Cell constants	a= 118.4 Å	a= 69.3 Å
	b= 118.4 Å	b=69.3 Å
	c= 265.5 Å	c= 130.6 Å
CPs / AU[a]	probably 6-7	1
Data collection		
Beam line	ID29, ESRF	X06SA, SLS
Wavelength (Å)	0.972385	1.07122
Resolution range (Å)[b]	45-2.0	44-3.5
	(2.1-2.0)	(3.6-3.5)
No. oberservations	411062	15267
No. unique reflections [c]	74779*	4368[#]
Completeness (%)[b]	99.8 (99.7)	99.7 (98.3)
R_{merge} (%)[b, d]	8.9 (63.0)	7.6 (75.9)
I/σ(I)[b]	11.4 (3.0)	6.6 (1.5)

[a] Asymmetric unit

[b] The values in parentheses for resolution range, completeness, R_{merge} and I/σ(I) correspond to the highest resolution shell

[c] Data reduction was carried out with XS and from a single crystal. * Friedel pairs were treated as identical reflections. [#] Friedel pairs were treated as individual reflections

[d] $R_{merge}(I) = \Sigma_{hkl}\Sigma_j \mid I(hkl)_j - \langle I(hkl)\rangle \mid / \Sigma_{hkl}\ \Sigma_j\ I(hkl)_j$, where $I(hkl)_j$ is the j^{th} measurement of the intensity of reflection hkl and $\langle I(hkl)\rangle$ is the average intensity

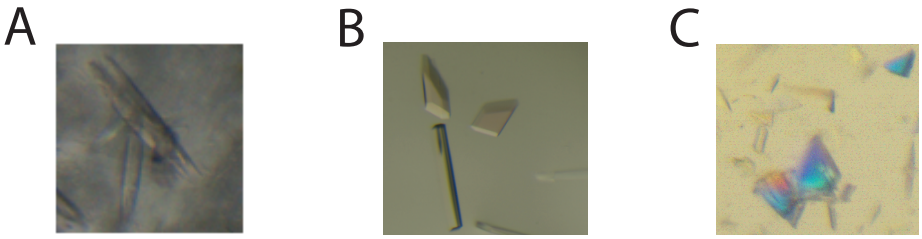

Figure 29: Protein crystals of Cns1 and TTC4 A) Protein crystal of Cns1$^{70\text{-}220}$, B) Cns1$^{221\text{-}385}$ and C) TTC4$^{217\text{-}387}$

The structure of the Cns1 C-domain has been solved in the lab before (Otmar Hainzl, PhD thesis). The construct used in the previous work was slightly different from the construct used in this thesis (Cns1$^{218\text{-}385}$ compared to Cns1$^{221\text{-}385}$) and, unfortunately, the original measurement data were not available anymore. Using SeMet labeling and protein crystallization trials, reproduction of protein crystals of the Cns1 C-domain and structure determination were successful (Table 25, Figure 30A). Note, that the structure was basically the same for this work and the previously solved structure (data not shown). Since Cns1$^{221\text{-}385}$ crystals grew very fast (overnight), crystallization of the C-terminal domain of Cns1's human orthologue TTC4 was attempted.
Like Cns1$^{221\text{-}385}$ crystals, TTC4$^{217\text{-}387}$ crystals grew overnight. Strikingly, using the Cns1$^{221\text{-}385}$ structure as a search model, it was possible to solve the structure of TTC4$^{217\text{-}387}$, already indicating a high similarity between the two structures (Figure 30B). Comparison of the two structures reveals a central core of the domain consisting of several tightly packed β-sheets surrounded by three to four α-helices. Although the precise *in vivo* function of both C-terminal domains is unclear so far, the growth defects observed for mutants lacking amino acids from the N-terminus and the C-terminal domain of Cns1 (e.g. Cns1$^{36\text{-}205}$), suggests an important contribution to the proper *in vivo* function of the full-length protein by the crystallized domains.

Table 25: X-ray data collection and refinement statistics for Cns1$^{221\text{-}385}$ and TTC4$^{217\text{-}387}$

	Cns1$^{221\text{-}385}$ SeMet	**TTC4$^{217\text{-}387}$**
Crystal parameters		
Space group	$P2_12_12_1$	C2
Cell constants	a= 44.9 Å	a= 44.9 Å
	b= 81.6 Å	b=81.6 Å
	c= 100.6 Å	c= 100.6 Å
CPs / AU[a]	2	1
Data collection		
Beam line	X06DA, SLS	ID30B, ESRF
Wavelength (Å)	0.97939	0.97856
Resolution range (Å)[b]	40-2.1	45-1.65
	(2.2-2.1)	(1.75-1.65)
No. oberservations	283690	60396
No. unique reflections [c]	41661#	2042*
Completeness (%)[b]	100.0 (100.0)	97.7 (97.9)
R_{merge} (%)[b, d]	8.2 (51.0)	4.4 (57.7)
$I/\sigma(I)$[b]	15.7 (3.5)	12.8 (1.9)
Refinement (REFMAC5)		
Resolution range (Å)	15-2.1	15-1.65
No. refl. working set	21074	19400
No. refl. test set	1109	1021
No. non hydrogen	2765	1354
Solvent (H_2O)	89	96
R_{work}/R_{free} (%)[e]	27.2/28.8	16.76/19.66
r.m.s.d. bond (Å)/(°)[f]	0.005/1.221	0.004/1.136
Average B-factor (Å^2)	38.8	43.0
Ramachandran Plot (%)	97.6/1.2/1.2	93.3/0.7/0.0

[a] Asymmetric unit

[b] The values in parentheses for resolution range, completeness, R_{merge} and $I/\sigma(I)$ correspond to the highest resolution shell

[c] Data reduction was carried out with XS and from a single crystal. # Friedel pairs were treated as individual reflections. * Friedel pairs were treated as identical reflections.

[d] $R_{merge}(I) = \Sigma_{hkl}\Sigma_j \mid I(hkl)_j - \langle I(hkl)\rangle \mid / \Sigma_{hkl}\ \Sigma_j\ I(hkl)_j$, where $I(hkl)_j$ is the j^{th} measurement of the intensity of reflection hkl and $\langle I(hkl)\rangle$ is the average intensity

[e] $R = \Sigma_{hkl} \mid |F_{obs}| - |F_{calc}| \mid / \Sigma_{hkl}\ |F_{obs}|$, where R_{free} is calculated without a sigma cut off for a randomly chosen 5% of reflections, which were not used for structure refinement, and R_{work} is calculated for the remaining reflections

[f] Deviations from ideal bond legths/angles

[g] Number of residues in favoured region / allowed region / outlier region

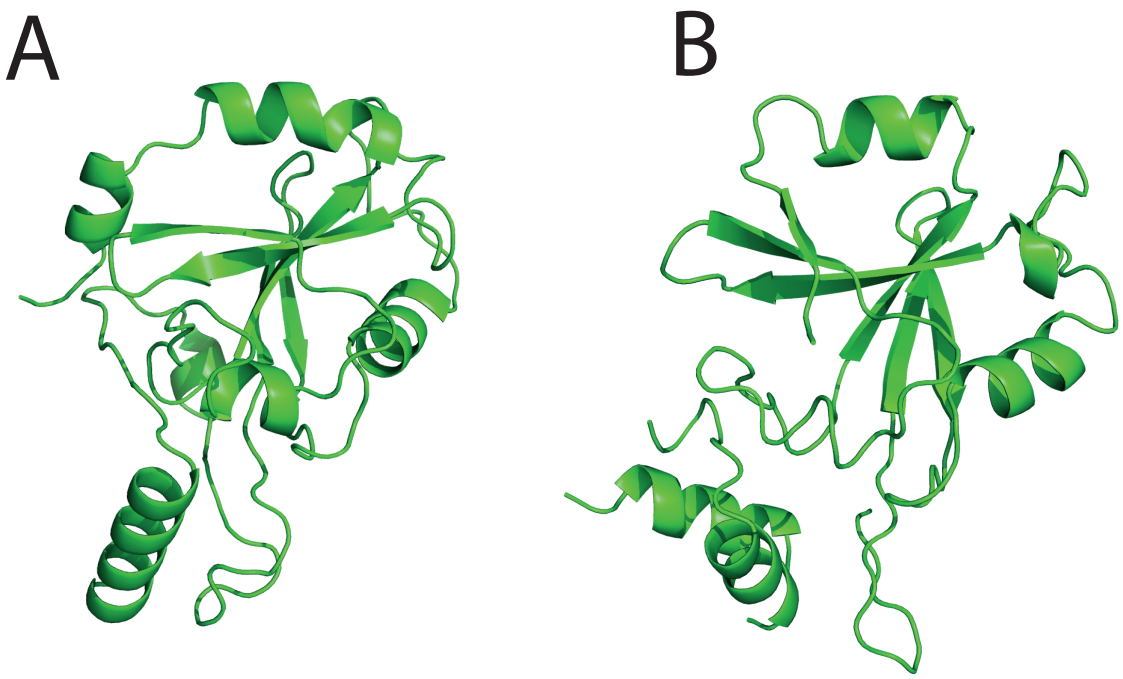

Figure 30: Crystal structures of the C-terminal domains of Cns1 and TTC4 A) Ribbon model of the crystal structure of Cns1$^{221\text{-}385}$. B) Ribbon model of the crystal structure of TTC4$^{217\text{-}387}$.

4.9 SAXS reveals partial disorder in the Cns1 N-terminal domain

Since protein crystallization and structure determination so far was only successful for $Cns1^{221\text{-}385}$, SAXS measurements in cooperation with Assoz. Prof. Mag. Dr.rer.nat. Tobias Madl (Technische Universität München and Medizinische Universität Graz) were performed. The crystal structure of the C-terminal domain of Cns1 starts at amino acid 221. Therefore, amino acid 220 was used as a domain barrier for SAXS measurements. For further *in vivo* and *in vitro* analysis of the used constructs see also section 4.15.

For $Cns1^{wt}$, two maxima could be observed in the SAXS radial density distribution P(R). This indicates that Cns1 consists of two major folded domains and that a fixed domain orientation is likely (Figure 31A). The first maximum corresponds approx. to the Rg of the isolated domains and the second maximum is related to the distance between the centers of mass of the two domains.

Analysis of the C-terminal domain construct $Cns1^{221\text{-}385}$ led to a single maximum (Figure 31B) confirming the single domain architecture of this construct in the crystal structure. Also the $Cns1^{1\text{-}220}$ construct showed a single maximum in SAXS analysis (Figure 31A), but, in addition, a tail (80-110 Å) characteristic for disordered regions was observed. Interestingly, this tail is lost in the $Cns1^{36\text{-}220}$ construct indicating a loss of the disordered region, which is even more exacerbated in $Cns1^{70\text{-}220}$. Interestingly, comparison of $Cns1^{36\text{-}220}$ with $Cns1^{70\text{-}220}$ reveals a fine structure at R$\sim$ 55Å, indicating that the amino acids adjacent to the TPR domain might be structured (Figure 31A and C).
Next, Cns1-Hsp90 complexes were analysed using SAXS. The total molecular mass increases up to a 1:1 molar ratio (1 molecule Cns1 per dimer Hsp90), and is not further increased by excess Cns1 (2:1 and 3:1 ratio per Hsp90 dimer), indicating, that one molecule Cns1 binds per Hsp90 dimer (Figure 31D). These data confirm the results obtained by aUC.
Finally, an *ab initio* model of Cns^{wt} was calculated using the program DAMMIF (50 runs, cluster analysis) (Franke and Svergun, 2009). The models were converged to a single density and the results are presented in Figure 31E. The $Cns1^{221\text{-}385}$ crystal structure and a calculated model of the TPR domain (starting at amino acid 55) using the

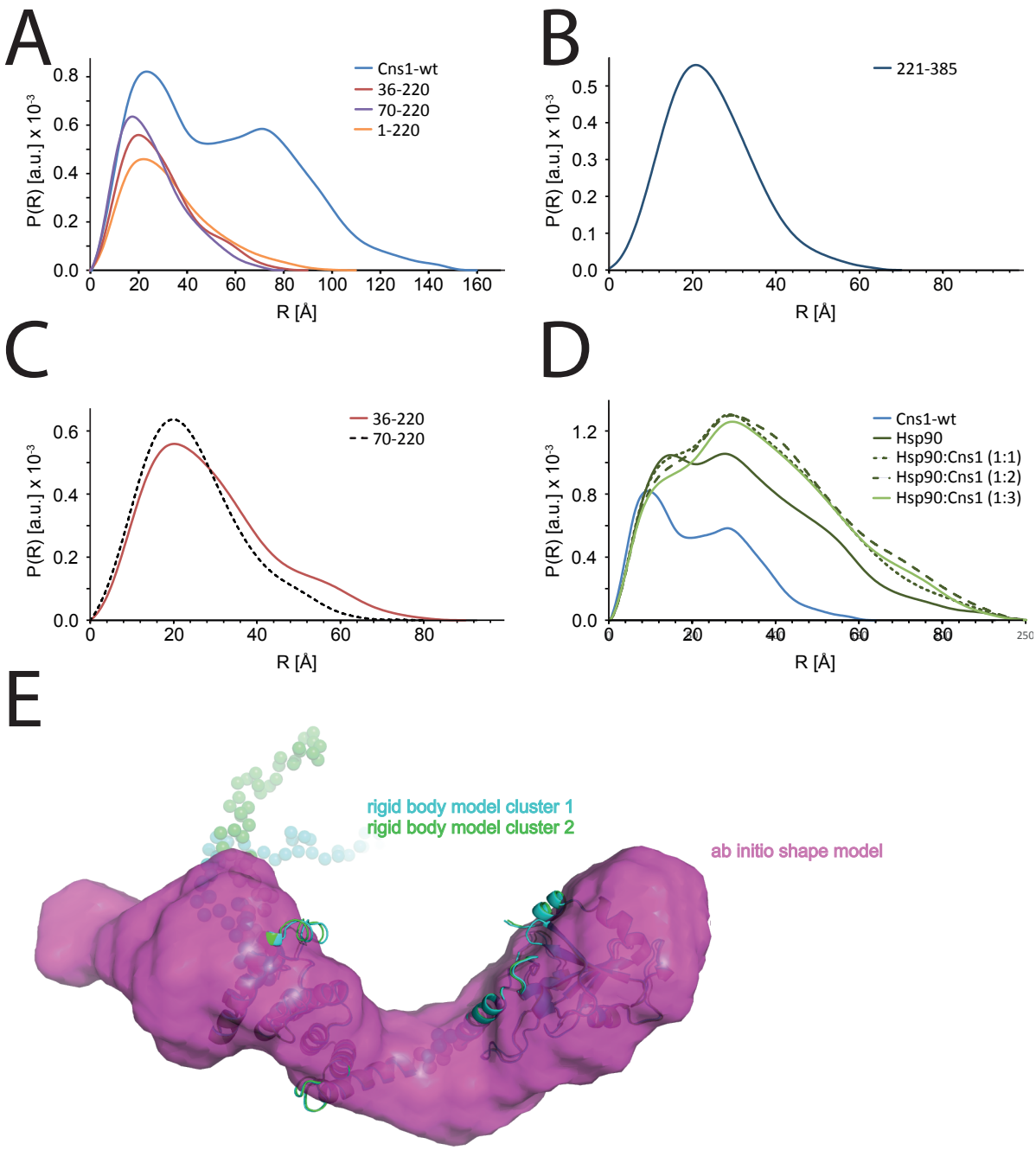

Figure 31: Structural analysis of Cns1 and its domains by SAXS A) SAXS radial density distributions measurements of $Cns1^{wt}$ and Cns1 truncation mutants. B) SAXS measurement of $Cns1^{221\text{-}385}$. C) Magnification of $Cns1^{36\text{-}220}$ and $Cns1^{70\text{-}220}$ from A). D) SAXS analysis $Cns1^{wt}$ in complex with yHsp90. Ratios indicate Hsp90(dimer):Cns1(monomer) E) *Ab initio* model of $Cns1^{wt}$ shown with the crystal structure of the Cns1 C-terminal domain $Cns1^{221\text{-}385}$ and a calculated model of the TPR domain.

program CORAL (Petoukhov et al., 2012) were fitted into their putative positions. The first 54 residues and 5 residues connecting the TPR and the C-terminal domain were kept flexible and modeled by dummy atoms. Interestingly, also the *ab initio* calculated model suggests a fixed domain orientation.

4.10 ^{15}N-NMR experiments reveal partial disorder in the essential Cns1 N-domain

As already described in this work, CD and SAXS data suggest an at least partial disorder in Cns1's first 82 amino acids, which contain the essential residues for *in vivo* function of the protein. To get in-depth insight into this putative disordered region, NMR spectroscopy was performed in cooperation with Dr. Lee Freiburger and Prof. Dr. Michael Sattler (Lehrstuhl für Biomolekulare NMR-Spektroskopie, Technische Universität München).
SAXS analysis of Cns1$^{1\text{-}220}$ revealed a putative disordered region that disappeared in Cns1$^{36\text{-}220}$. Therefore, uniformely ^{15}N-labeled variants of these two constructs were used for further analysis by NMR.
^{1}H, ^{15}N HSQC NMR spectra of Cns1$^{36\text{-}220}$ showed well-dispersed peaks, indicating this construct is structured (Figure 32, red). For Cns1$^{1\text{-}220}$ a large number of sharp, additional peaks appeared in the center (^{1}H frequencies 8-8.5 ppm) of the spectrum (Figure 32, black), indicative for a disordered region. Taken together, the results obtained by CD spectroscopy, SAXS and NMR strongly support the idea, that the essential N-terminal domain of Cns1 is at least partially unfolded.

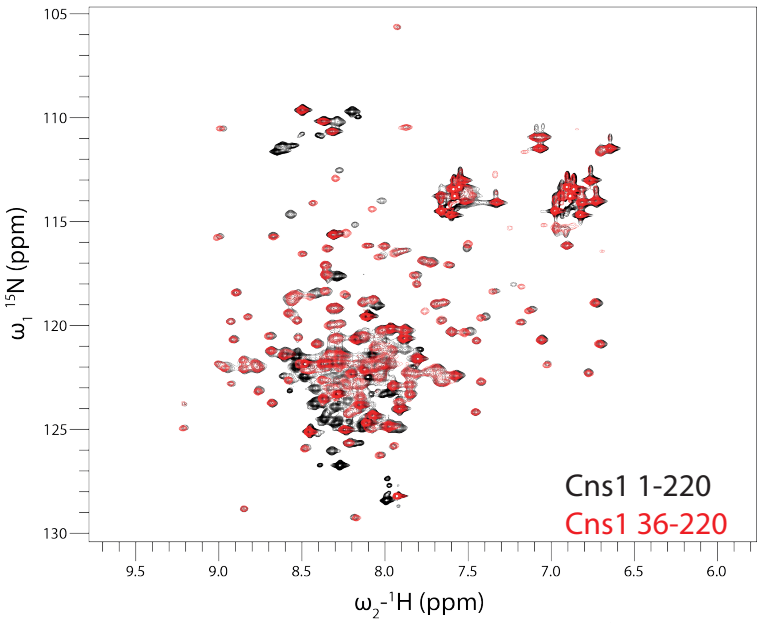

Figure 32: ^{1}H, ^{15}N HSQC NMR spectra of Cns1$^{1\text{-}220}$ and Cns1$^{36\text{-}220}$. Uniformly ^{15}N-labeld constructs of Cns1$^{1\text{-}220}$ (black) and Cns1$^{36\text{-}220}$ (red) were analyzed using NMR spectroscopy.

4.11 Cpr7 is a the only multi copy suppressor of a temperature-sensitive *cns1* mutant identified in a genome-wide screen

Although 5'-FOA shuffling led to the identification of the minimal Cns1 domain required for the *in vivo* function of the protein, the question why deletion of *CNS1* is lethal, remained unanswered. Tesic et al. (2003) already identified Cpr7 as a multi-copy-suppressor of a temperature-sensitive *cns1* allel (*cns1-1*). Since it is not clear, whether there are any other multi-copy-suppressors of this mutant, a new screen was carried out, using a commercially available library (Dharmacon) that contains almost the entire yeast genome on ∼1,500 plasmids (5-7 genes under their endogenous promoter per plasmid; 97% on the physical level and approximately 95% on the functional level). For screening, the *cns1-1* mutant strain was tranformed with the plasmid library or an empty vector as control, plated onto -Leu plates for plasmid selection and incubated for 24 h at 25°C to allow the cells to recover and to express the genes encoded on the plasmids. 2 plates from the library transformation were kept at 25°C to determine the transformation efficiency, whereas the rest of the library and the vector transformants were shifted to 37°C to screen for suppressors. Since there was some background growth even at the non-permissive temperature, only colonies that grew faster than the background and faster than the empty vector control were considered as suppressors. These colonies were restreaked onto -Leu plates and incubated at 37°C for 48 h to confirm the phenotype. Finally, plasmids were preped from yeast, retransformed into *E. coli* for plasmid amplification and sequenced.

The screen yielded ∼4,500 transformants, covering the library approximately three times. The plasmids identified as multi copy suppressors of the *cns1-1* mutation are listed in Table 26. As expected, plasmids containing *CNS1* and *CPR7* were identified, indicating that the screen was successful. Unfortunately, no other suppressor gene could be identified using this screening method. Also when the screen was repeated only *CNS1* and *CPR7* containing plasmids were recovered (data not shown).

As proof of principle and to further confirm the suppressor effect of Cpr7, one of the identified plasmids was freshly retransformed into the *cns1-1* strain and tested at 25°C, 30°C and 37°C. Emtpy vector served as control.

Table 26: Suppressor plasmids recovered from the MCS screen

plasmid	**inserts**
1	YJR030C GEA1 **CPR7** [RAV1] [PET191]*
2	[RIB7]& RPB5 **CNS1** SLI15 ICS2 AMN1 [YBR159W]*
3	YJR030C GEA1 **CPR7** [RAV1] [PET191]*
4	YJR030C GEA1 **CPR7** [RAV1] [PET191]*
5	YJR030C GEA1 **CPR7** [RAV1] [PET191]*
6	[GEA1]* **CPR7** RAV1 PET191 [RAD26]*
7	[GEA1]* **CPR7** RAV1 PET191 [RAD26]*
8	YJR030C GEA1 **CPR7** [RAV1] [PET191]*
9	[GEA1]* **CPR7** RAV1 PET191 [RAD26]*

As expected, the plasmid was able to cure the growth defect of the *cns1-1* mutant strain at the non-permissive temperature (Figure 33). Taken together, data from Tesic et al. (2003) and this study suggest, that, besides *CNS1* wildtype sequence, only a single multi-copy-suppressor of the *cns1-1* mutation exits, which is *CPR7*.

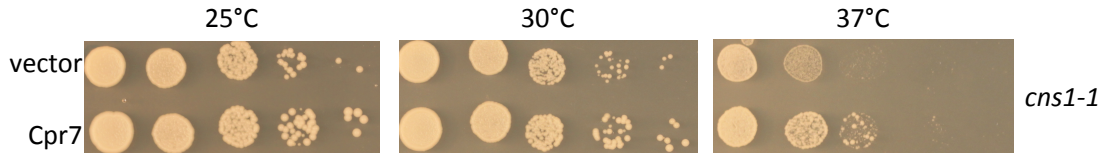

Figure 33: Multi copy suppression of the temperature-sensitive phenotype of the *cns1-1* strain by high copy *CPR7* Cells were spotted in 10-fold serial dilutions and incubated at 25°C, 30°C and 37°C as indicated. Empty vector was used as a control, plasmid 5 from the screen was used for *CPR7* overexpression.

4.12 Synthetic Genetic Array (SGA) screening of *cpr7*Δ and a strain containing *CNS1* under a doxycycline-regulateable promoter

The SGA technology is a versatile tool for large scale screening of yeast double mutants (Tong and Boone, 2006, 2007). Since it is already known, that Cns1 and Cpr7 have overlapping functions *in vivo* (Marsh et al., 1998; Tesic et al., 2003), a robot-based screen using a *CPR7* deletion strain and a strain carrying *CNS1* under the doxycycline-regulatable tet07 promoter (tet07-*CNS1*; Mnaimneh et al., 2004) as baits was carried out. The screens described here were performed in cooperation with Jochen Rech and Prof. Dr. Stefan Jentsch (Max-Planck-Institut für Biochemie, Martinsried).

Figure 34 gives an overview over the method used. In brief, a query mutant is crossed with the entire deletion collection of non-essential genes in a robot-based screen. After sporulation, haploid, single mutant and double mutant selection, the obtained double mutants can be scored as synthetically lethal, synthetic sick, neutral or positive genetic interactors. Note, that in the tet07-*CNS1* screen, after double mutant selection, cells were replica-plated onto plates containing 10 µg/mL doxycycline to repress *CNS1* expression, before scoring could be carried out.

Synthetic lethal and synthetic sick interactors of *cpr7*Δ are listed in Table 27 and 28, respectively.

In the *cns1* screen, only one synthetic sick interactor (*get2*Δ) could be identified. This might be due to the only weak growth response of *CNS1* repression upon doxycycline treatment.

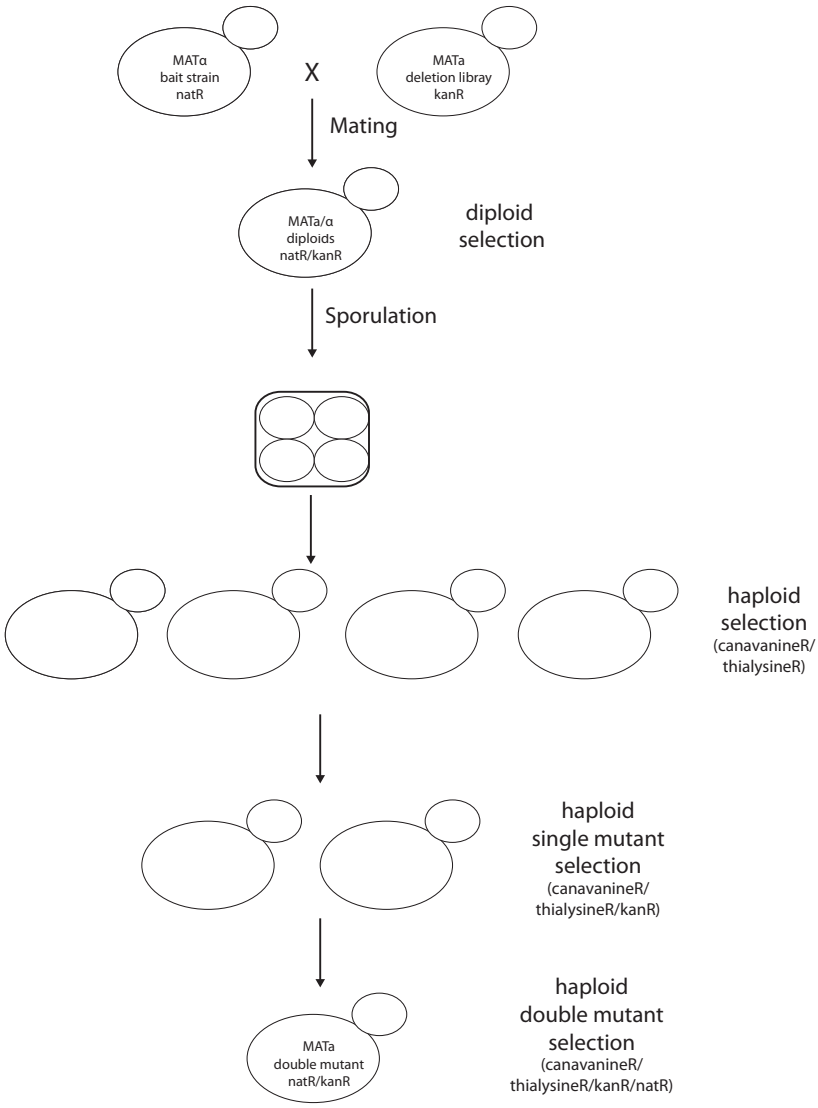

Figure 34: Overview over a typical SGA screen A bait/query mutant is systematically crossed with the entire yeast deletion collection. Diploids are selected and sporulated. After haploid, single mutant and double mutant selection steps, synthetic genetic interaction is scored.

Table 27: Synthetic lethal interactors of *cpr7*Δ

gene	**negative genetic interaction with *cpr7*Δ in other studies**		
ccs1			
cog5	Costanzo et al., 2010		
cog8	Costanzo et al., 2010		
csg2			
get2	Costanzo et al., 2010	Kiktev et al., 2012	Pan et al., 2006
gim1	Tong et al., 2004		
hrd1			
sac1	Beltrao et al., 2009		
tlg2	Costanzo et al., 2010	Dixon et al., 2008	
vps51	Costanzo et al., 2010		
vps53			

Table 28: Synthetic sick interactors of *cpr7*Δ

gene	**negative genetic interaction with *cpr7*Δ in other studies**			
aco2				
atf2				
avt1				
bem1				
cax4				
ccw12				
cdc50				
cdh1				
csf1				
ctf4				
ctr1				
did4				
dlt1				
ggc1				
gim3	Tong et al., 2004			
gis3				
gly1				
gup1				
gyp1	Costanzo et al., 2010	Dixon et al., 2008	Tong et al., 2004	Lafourcade et al., 2004

Synthetic sick interactors of *cpr7*Δ

hgh1	Costanzo et al., 2010			
hsc82	Costanzo et al., 2010	Duina et al., 1998	Duina et al., 1996a	Bali et al., 2003
hst3				
ilv1				
irs4	Costanzo et al., 2010			
isa2				
ltv1				
mdm10				
mnn10	Collins et al., 2007			
mrpl17				
mrpl4				
mtc1				
mtc4				
mtc6				
npl3	Moehle et al., 2012			
pac10	Tong et al., 2004			
pep12				
pfk1				
pho85				
pos5				
rad50				
rcy1				

Synthetic sick interactors of *cpr7*Δ

rgp1				
ric1	Collins et al., 2007	Costanzo et al., 2010		
rpl39				
rpn4				
rpo41				
rrg1				
rud3	Costanzo et al., 2010	Dixon et al., 2008		
scs7	Costanzo et al., 2010			
shp1				
sif2				
sit1				
snf6				
snf7				
snf8				
sod1				
spe2				
sps4				
sti1	Costanzo et al., 2010	Moosavi et al., 2010	Duina et al., 1996a	Flom et al., 2005
swf1	Costanzo et al., 2010			
tef4				
thi4				
tpd3				

trs85	
vam10	
vma1	
vma21	Finnigan et al., 2011
vma22	
vma6	
vma7	
vps16	
vps20	
vps25	
vps52	
whi2	
YBR196C-A	
ydj1	Costanzo et al., 2010
yel045c	
ygl081w	
yjl175w	
ykl118w	
yll020c	
yme1	
ynl198c	
yor302w	

yor331c		
ypl260w		
ypr153w		
ypt6	Collins et al., 2007	Dixon et al., 2008

4.13 Identification of physical interactors of Cns1 *in vivo*

As described above, SGA screening is a suitable method to identify synthetic genetic interactors on the whole genome level. A drawback is that it does not always identify direct targets or physical interactors of a query mutant, but is likely to identify pathways which lie up-stream, down-stream or in parallel to the process the query mutant is acting on. Hence, it is crucial to identify physical interactors *in vivo*.

Therefore, pull-down assays of selected GFP-tagged Cns1 variants (Figure 35A) using anti-GFP agarose beads (ChromoTek) were performed. The constructs were selected due to their behaviour in the shuffling assays, upon overexpression and *in vitro* Hsp90 binding. $Cns1^{wt}$ and $Cns1^{1\text{-}190}$ support growth *in vivo* and bind Hsp90 *in vitro*, $Cns1^{1\text{-}82}$ is the minimal construct that renders cells viable, but does not bind Hsp90 *in vitro*, $Cns1^{50\text{-}385}$ is inviable in the shuffling assay, its overexpression shows a dominant negative effect in wildtype yeast, but it is able to bind Hsp90 *in vitro*. $Cns1^{169\text{-}385}$ is inviable in the shuffling assay and does not bind Hsp90 *in vitro*.

All constructs were cloned into p425-GPD as C-terminal GFP fusions ($Cns1^{wt\text{-}GFP}$, $Cns1^{1\text{-}190\text{-}GFP}$, $Cns1^{1\text{-}82\text{-}GFP}$, $Cns1^{51\text{-}385\text{-}GFP}$, $Cns1^{169\text{-}385\text{-}GFP}$). A vector only expressing GFP was used as control (Figure 35A). The plasmids were transformed into BY4741, cells were grown to mid-log phase, harvasted and pull-down experiments were carried out as described in Materials and Methods.

The GFP control showed only little background (Figure 35B), indicating that the conditions used are specific. As expected, the TPR-containing constructs $Cns1^{wt\text{-}GFP}$, $Cns1^{1\text{-}190\text{-}GFP}$ and $Cns1^{51\text{-}385\text{-}GFP}$ were able to interact with Hsp90 in the pull-down assay (Figure 35B) as confirmed by mass spectrometry (data not shown). In addition, many other bands appeared in the pull-downs with Cns1 constructs containing the C-terminal domain. Analysis by mass spectrometry identified proteins from both the large and the small ribosomal subunit (data not shown). These data are in agreement with findings published during the course of this work (Tenge et al., 2015), in which Cns1 was reported to interact with the intact ribosome via its C-terminal domain.

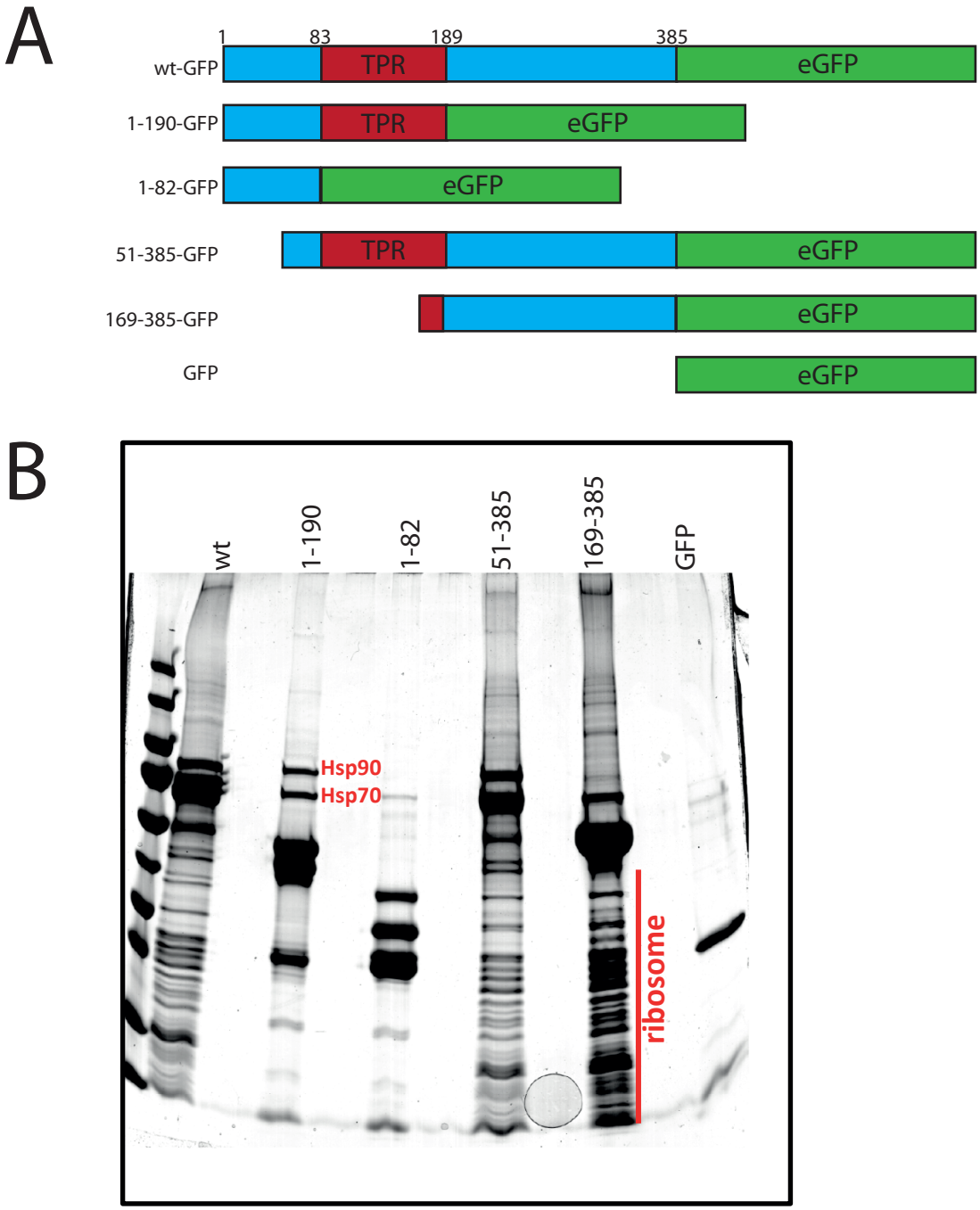

Figure 35: Pull-down of GFP-tagged Cns1 variants A) Schematic overview over GFP-tagged Cns1 variants. B) Constructs from A) were expressed from a p425-GPD plasmid in BY4741 and pull-down experiments were carried out using anti-GFP agarose beads. GFP was used as a control. Contrast was increased using Adobe Photoshop applying a linear filter.

Interestingly, Cns1$^{1\text{-}190\text{-}GFP}$ and Cns1$^{1\text{-}82\text{-}GFP}$ were not stably interacting with the ribosome and only Cns1$^{1\text{-}190\text{-}GFP}$ interacted with Hsp90, confirming the data obtained by aUC, that the TPR domain is important for Hsp90 interaction. Although additional bands appeared in both pull-downs, none of them was a specific interactor but degradation products of the GFP-fusion proteins as identified by mass spectrometry (data not shown).

4.14 A putative role for Cns1 in ribosome biogenesis

Analysis of *CNS1* expression data using the SPELL database (http://spell.yeastgenome.org; 3rd Aug 2016) revealed a strong enrichment of GO terms associated with ribosome biogenesis (top 10 GO terms: nucleolus, ribosome biogenesis, ribonucleoprotein complex biogenesis, rRNA processing, rRNA metabolic process, preribosome, ncRNA processing, ncRNA metabolic process, nuclear lumen, RNA processing).
Interestingly, the *cns1-1* mutant and *cpr7*Δ strain were reported to be hypersensitive to the translation inhibitor hygromycin B (Tenge et al., 2015; Albanèse et al., 2006). In order to test whether this sensitivity of the *cns1-1* mutant strain was allel-specific or a more general phenotype of cells impaired in Cns1 function, hygromycin B sensitivity of the tet07-*CNS1* strain was tested. As shown in Figure 36, only the combinaion of sublethal doses of doxycycline and hygromycin B led to a strong growth defect in the tet07-*CNS1* strains, whereas the isogenic wildtype R1158 remained unaffected, suggesting that hygB sensitivity is a general phenotype of *cns1* mutants.

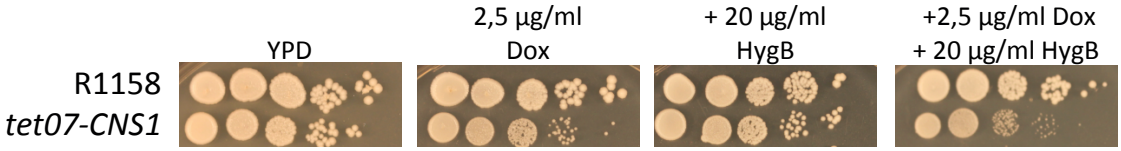

Figure 36: Hygromycin B sensitivity of the tet07-*CNS1* mutant tet07-*CNS1* and the isogenic wildtype R1158 were spotted onto YPD plates and plates containing doxycyclin and/or hygromycin B at indicated concentrations. Plates were incubated at 30°C for 2 days.

Although Cns1 is able to bind to the ribosome via its C-terminal domain and *cns1* mutants show hygromycin B sensitivity, a general role for Cns1 in translation is unlikely

due to the protein's low abundance in the cell.
Given the fact, that Cns1 is strongly co-regulated with genes involved in ribosome biogenesis and binds the ribosome via its C-terminal domain, a possible role of Cns1 in this process was investigated in more detail.
Ribosome biogenesis is a complex process in which over 200 assembly factors and 76 small nucleolar RNAs are involved (reviewed in Woolford and Baserga (2013)). In general, ribosome biogenesis starts in the nucleuolus and precursors are transported under constant processing via the nucleus to the cytoplasm, where the final maturation steps take place (Woolford and Baserga (2013)).
One widely used method is to monitor the localization of GFP-tagged proteins from the large and small ribosomal subunit, respectively. A block in ribosome biogenesis leads to a retention of these proteins in the nucleus depending on the subunit affacted. The advantage of this method is, that not only nuclear biogenesis defects, but also cytoplasmic ribosome biogenesis defects can be observed due to failure of biogenesis factor recycling to the nucleus (Bécam et al., 2001; Senger et al., 2001; Kallstrom et al., 2003; Hedges et al., 2005; West et al., 2005; Demoinet et al., 2007; Meyer et al., 2007; Pertschy et al., 2007; Lo et al., 2010).
Therefore, Rpl25-GFP (Hurt et al., 1999; Hedges et al., 2005) and Rps2-GFP (Milkereit et al., 2003) were used in combination with the *cns1-1* temperature-sensitive mutant to investigate putative defects in ribosome biogenesis. Although different timepoints after the shift to the non-permissive temperature and even short recovery at the permissive temperature were tested, there was no change in Rpl25-GFP and Rps2-GFP localization at the permissive temperature (25°C, data not shown) and neither was there at the nonpermissive temperature (37°C, Figure 37).
Another method to investigate ribosome function is ribosome fractionation on a sucrose gradient. This analysis can provide valuable insight into the translational status of a cell (Esposito et al., 2010), but can also be used to investigate ribosome biogenesis (Ripmaster et al., 1993).
For example, the appearance of half-mers or 80S and larger peaks with a slight shoulder, indicates 40S subunits awaiting 60S subunit joining and therefore are indicators for defects in 60S ribosome biogenesis (e.g. West et al., 2005). Increase of 60S subunits and loss of 40S subunits are hallmarks of defects in 40S biogenesis (e.g. Loar et al., 2004). Performing the experiments in the absence of cycloheximide allows the analysis of the rate of polysome run-off, which indicates whether or not elongation is altered (Esposito

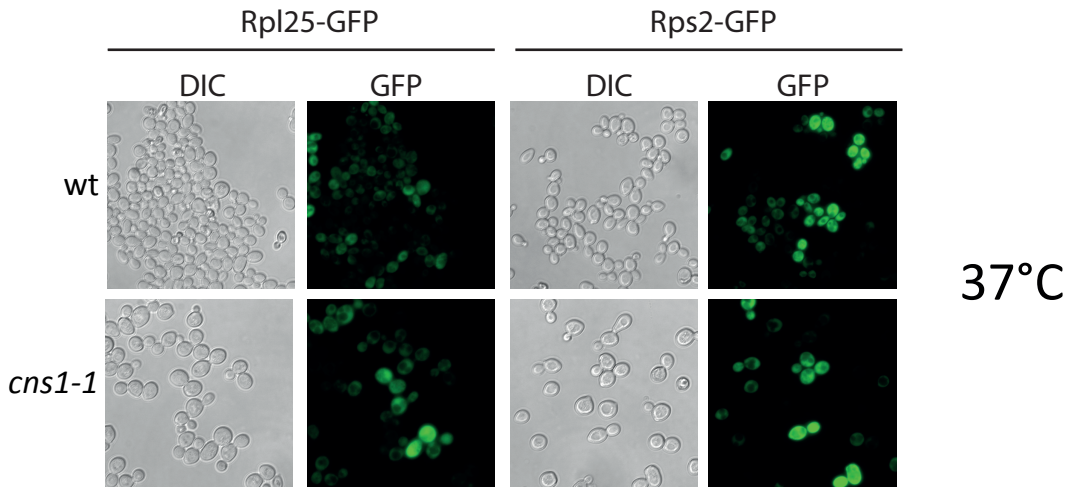

Figure 37: Localization of Rpl25-GFP and Rps2-GFP in wildtype and *cns1-1* BY4741 and *cns1-1* expressing Rpl25-GFP and Rps2-GFP, respectively, were pre-grown at 25°C before they were shifted to 37°C for 6h. Pictures were taken using DIC and GFP filters.

et al., 2010; Anand et al., 2003). Moreover, defects in translation initiation lead to a loss of polysomes and accumulation of the 80S fraction (Nielsen et al., 2004).

Ribosome fractionation was carried out in cooperation with Timm Hassemer in the lab of Prof. Dr. Ulrich Hartl (Max-Planck-Institut für Biochemie, Martinsried). Wildtype yeast grown at 25°C was used as a control. The temperature-sensitive *cns1-1* strain was either grown at the permissive temperature (25°C) or shifted to the non-permissive temperature (37°C) for 6h. Interestingyl, the *cns1-1* mutant showed a decrease of the 80S monosome peak of around 50% already under permissive conditions compared to wildtype. In addition, the polysome fraction was decreased slightly (Figure 38). The 40S and 60S fractions did not seem to be affected. Surprisingly, the ribosome profile of the *cns1-1* strain grown at the non-permissive temperature did not show any difference compared to the mutant strain under permissive conditions. There was no effect on polysome run-off, 40S, 60S or 80S accumulation and no halfmers were observed. Note, that the experiment was carried out in the absence of cycloheximide, so in general polysome run-off is possible.

Taken together, since neither Rpl25-GFP and Rps2-GFP localization were affected, nor the polysome profile changed in the *cns1-1* mutant, it is unlikely that translation in general or ribosome biogenesis are affected by Cns1.

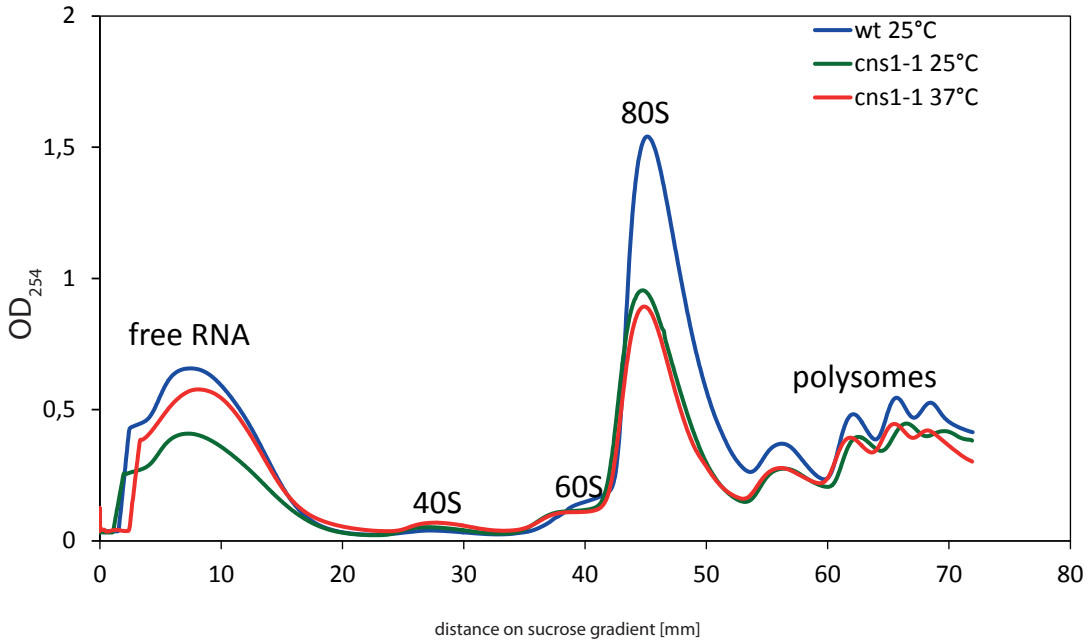

Figure 38: Ribosome fractionation of wildtype and *cns1-1* BY4741 and *cns1-1* were grown at 25°C or at the non-permissive temperature (37°C). Lysates were fractionated on 7-47% sucrose gradients and ribosome profiles were recorded at 254 nm.

4.15 Cooperative co-chaperone function of the Cns1 N- and C-terminal domains in the absence of a TPR domain

Due to the fact that a Cns1 construct lacking the first 35 amino acids and the entire C-terminal domain ($Cns1^{36\text{-}205}$) showed a strong growth defect in 5'-FOA shuffling assays, it is tempting to speculate that there could be a functional cooperation between the N-terminal and C-terminal domains of the co-chaperone. In addition, although Cns1 does not seem to play a major role in ribosome biogenesis or translation, the targeting to the ribosome via its C-terminal domain might still be of importance, when the N-terminal segment is shortened.

Therefore, the constructs already used for the SAXS measurements and protein crystallization ($Cns1^{1\text{-}220}$ and $Cns1^{221\text{-}385}$) were cloned into p425-GPD (Figure 39A). As expected cells expressing $Cns1^{1\text{-}220}$ as the single source of Cns1 were viable, whereas $Cns1^{221\text{-}385}$ was not able to support growth (Figure 39B-C). Next, the first 82 amino acids of Cns1, which represent a minimal construct for *in vivo* function, were connected to several constructs lacking the N-terminal segment and the TPR domain using

a $(GAAAA)_5$-linker (Figure 39A). Cells only expressing the C-terminal domain constructs $Cns1^{191\text{-}385}$ and $Cns^{221\text{-}385}$ were inviable, whereas cells expressing $Cns1^{1\text{-}82\text{-}L}$ (L... linker) showed only poor growth comparable to $Cns1^{1\text{-}82}$ (see earlier results). Strikingly, the constructs where the Cns1 N-domain was linked to the C-domain via the $(GAAAA)_5$-linker ($Cns1^{1\text{-}82\text{-}L\text{-}169\text{-}385}$, $Cns1^{1\text{-}82\text{-}L\text{-}191\text{-}385}$ and $Cns1^{1\text{-}82\text{-}L\text{-}221\text{-}385}$) showed an increased growth rate compared to $Cns1^{1\text{-}82\text{-}L}$. Moreover the $Cns1^{1\text{-}82\text{-}L\text{-}191\text{-}220}$ construct did not improve growth compared to $Cns1^{1\text{-}82\text{-}L}$, indicating that the cooperation between N- and C-terminal segments is depending on $Cns1^{1\text{-}82}$ and $Cns1^{221\text{-}385}$, the construct of which the crystal structure was determined (Figure 39).

Based on the results above, $Cns1^{1\text{-}220}$, $Cns1^{221\text{-}385}$, the constructs used for SAXS and NMR measurements $Cns1^{36\text{-}220}$ and the linker construct $Cns1^{1\text{-}82\text{-}L\text{-}221\text{-}385}$ were purified. CD spectroscopy revealed normal folding for all constructs (Figure 40A). Interestingly, $Cns1^{1\text{-}82\text{-}L\text{-}221\text{-}385}$ showed a slightly stronger signal below 205 nm compared to $Cns1^{221\text{-}385}$, probably indicating an increase of disordered regions (likely resulting from the linker and the Cns1 N-domain).
To investigate *in vitro* interaction of these constructs with Hsp90, the previously established competitive binding assay using aUC was performed. As expected, the TPR containing constructs $Cns1^{wt}$(positive control), $Cns1^{1\text{-}220}$ and $Cns1^{36\text{-}220}$ were able to disrupt a preformed *Cns1-Hsp90 complex to about the same extent. In line with the previously obtained results for $Cns1^{169\text{-}385}$, $Cns1^{221\text{-}385}$ was not able to disrupt the complex. Interestingly, also the linker construct $Cns1^{1\text{-}82\text{-}L\text{-}221\text{-}385}$ failed to do so (Figure 40B). Thus, one can conclude that stable binding of Cns1 to Hsp90 *in vitro* is not detrimental for the protein to be functional *in vivo*.

4.16 Integration of Cns1 into the Hsp90 (co-)chaperone cycle

Hsp90 is regulated by many different co-chaperones (see introduction) and it is known, that it is able to form heterotrimeric complexes with them during the progression of the chaperone cycle (Li et al., 2011, 2013). For this reason, whether Cns1 was able to form heterotrimeric complexes with other co-chaperones *in vitro*, is crucial to understand its role in the chaperone cycle. To address this question, a *Cns1-Hsp90 complex was formed

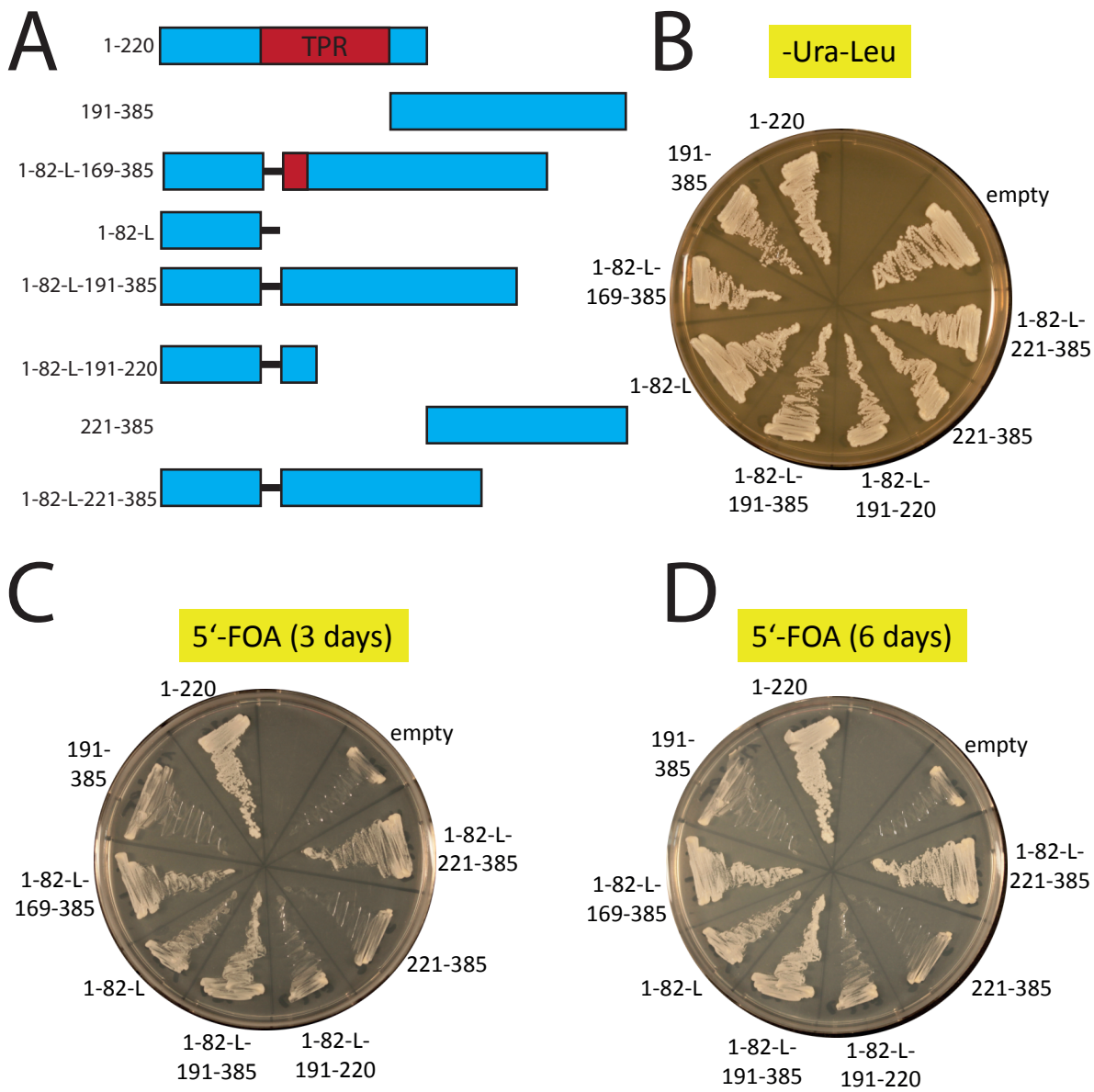

Figure 39: Cooperative co-chaperone function of the Cns1 N- and C-terminal domains in the absence of a TPR domain A) Schematic overview of Cns1 truncation mutants and Cns1 domain mutants which are connected by a flexible linker B) *cns1*Δ [*CNS1*-URA3] strain expressing variants from A) on a p425-GPD vector grown on -Ura-Leu plates. Cells were grown at 30°C for three days. C and D) strains from B were restreaked onto plates containing 5'-FOA and incubated at 30°C for 3 days and 6 days, respectively. $Cns1^{wt}$ and empty vector were used as positive and negative controls, respectively.

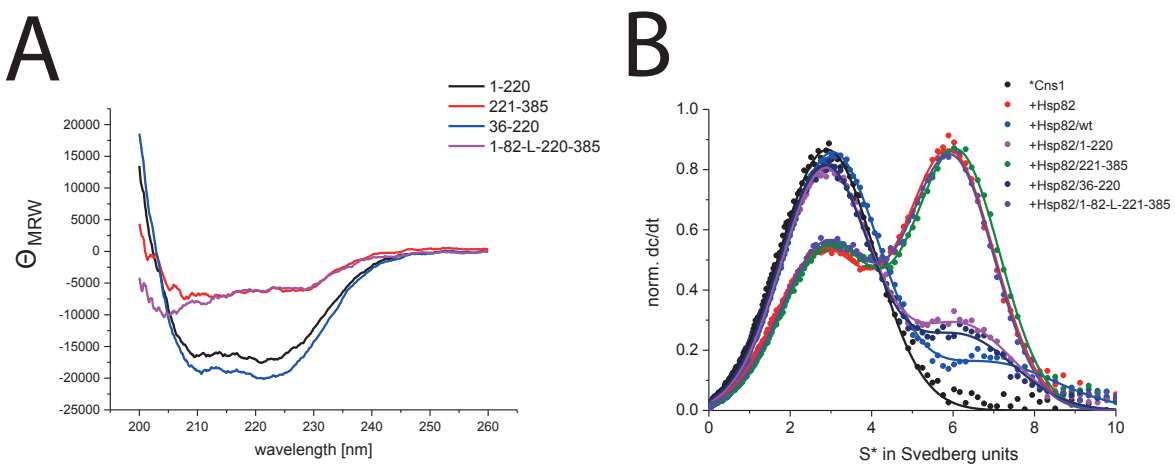

Figure 40: *In vitro* characterization of Cns1 truncation- and linker-mutants. A) CD spectra of Cns1 truncation and Cns1 linker mutants were recorded from 260 to 200 nm with 10 accumulations at 20°C. B) 500 nM *Cns1 was incubated with 10 µM yHsp90, and unlabeled Cns1 variants (10 µM) were added as indicated. *Cns1, *Cns1+yHsp90 and *Cns1+yHsp90+Cns1^{wt} are shown as controls for better clarity.

in vitro and a 20-fold excess of co-chaperones was added. As shown before Cns1^{wt} was able to disrupt the complex. Moreover, all tested co-chaperones known to bind Hsp90 at the NTD or MD (Sgt1, Sba1, Aha1 and Hch1) were able to form heterotrimeric complexes with *Cns1 and Hsp90 (Figure 41). The TPR containing co-chaperones Cpr6, Sti1 and Ppt1 completely disrupted the preformed *Cns1-Hsp90 complex, whereas Cpr7, which is known to have overlapping function with Cns1 *in vivo*, only partly disrupted the complex and additionally led to the appearance of a peak at around 7.5S, indicating the formation of a heterotrimeric complex. Whether these effects are due to different binding affinities of the various TPR domains to Hsp90 needs further clarification using titration assays.

In a currently ongoing Master thesis, the tet07-*CNS1* bait strain used in the SGA screen, was used in a more direct genetic interaction screen using random spore analysis (Tong and Boone, 2006) with the Hsp90 co-chaperone knock-out strains and a *cdc37*-DAmP mutant. Note, that a *sgt1*-DAmP mutant strain could not be included due to technical reasons. Interestingly, the tet07-*CNS1* strain only showed a negative genetic interaction with *cpr7*Δ upon downregulation of *CNS1* expression by adding doxycycline, but no other Hsp90 co-chaperone (Figure 42). These data also confirm the synthetic lethal phenotype of a *cns1-1 cpr7*Δ double mutant (Tesic et al., 2003).

The combination of the *in vitro* data with the random spore analysis based investiga-

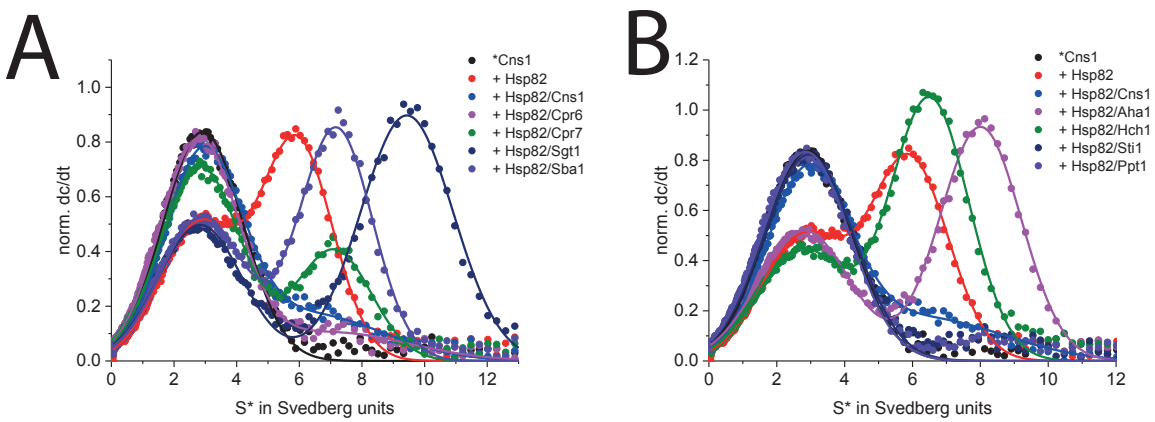

Figure 41: Heterotrimeric complex formation of Cns1, Hsp90 and other Hsp90 co-chaperones A and B) 500 nM *Cns1 was incubated with 10 µM yHsp90, and unlabeled Hsp90 co-chaperones (10 µM) were added as indicated. In both panels *Cns1, *Cns1+yHsp90 and *Cns1+yHsp90+Cns1^{wt} are shown as controls for better clarity. Purified Hsp90 co-chaperones were kind gifts of Sandrine Stiegler and Priyanka Sahasrabudhe.

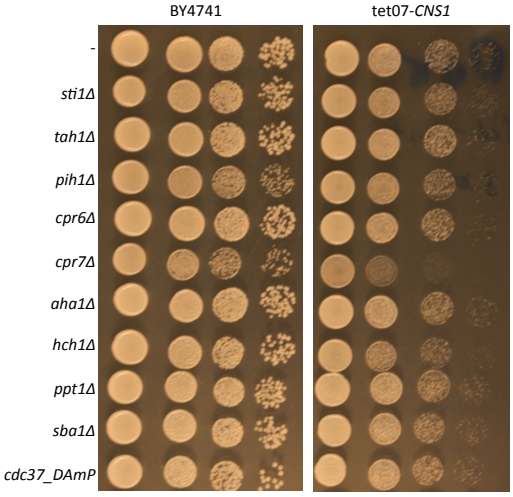

Figure 42: Genetic interaction of tet07-*CNS1* with Hsp90-co-chaperone mutant strains. BY4741 and Hsp90 co-chaperone mutant strains (left) or tet07-*CNS1* and double mutants with Hsp90 co-chaperone mutants as indicated (right), were spotted in 10-fold serial dilutions onto YPD plates containing 10 µg/mL doxycyclin. Plates were incubated at 30°C for 2 days (experiment carried out by Christopher Dodt, supervised master student)

tion of double mutants leads to the conclusion, that, although, several combinations of heterotrimeric complexes containing *Cns1, Hsp90 and an additional co-chaperone are possible *in vitro*, their role *in vivo* might be of less importance. The only exception to this seems to be Cpr7, which is a multi-copy-suppressor of the *cns1-1* mutant strain (this study and Tesic et al. (2003)). *cpr7*Δ shows a negative genetic interaction phenotype in *cns1 cpr7*Δ double mutants (this study and Tesic et al. (2003)) and is able to form a heterotrimeric *Cns1-Hsp90-Cpr7 complex *in vitro*, highlighting the importance of the genetic interactions.

5 Discussion

5.1 Functional characterization of Cns1 and its domains *in vivo*

In this thesis, 5'-FOA shuffling was successfully used to identify serveral Cns1 truncation mutants with various effects on their *in vivo* function and *in vitro* interaction with Hsp90. Deletion of the C-terminal domain has only a mild effect on cell viability, confirming already published results (Tesic et al., 2003). Moreover, it could be shown that even the last few amino acids of the TPR domain ($Cns1^{1\text{-}185}$) are dispensable *in vivo*. In addition, evidence is provided, that the deletion of the first 35 amino acids ($Cns1^{36\text{-}385}$) has no effect on cell growth, whereas the deletion of the first 40 amino acids ($Cns1^{41\text{-}385}$) leads to a strong growth defect. Interestingly, the truncation mutants $Cns1^{46\text{-}385}$ and $Cns1^{51\text{-}385}$ were not viable at all.
Mutants, in which Cns1 was lacking amino acids from the N-terminal segment and the entire C-terminal domain ($Cns1^{36\text{-}205}$, $Cns1^{36\text{-}200}$, $Cns1^{36\text{-}195}$), showed all a strong growth defect compared to $Cns1^{36\text{-}385}$. These data suggest, that both, the N-terminal and the C-terminal domain, are important for full *in vivo* function of $Cns1^{wt}$. This idea is further underlined by the finding that $Cns1^{51\text{-}385}$ overexpression results in a dominant negative effect on wildtype yeast, that is not observed when the construct is lacking the C-terminal domain ($Cns1^{51\text{-}190}$) or when the C-terminal domain alone is expressed ($Cns1^{169\text{-}385}$).

Cns1 was already known to bind Hsp90 and Hsp70 *in vitro* (Hainzl et al., 2004), but whether its essential *in vivo* function was dependent on Hsp90 or Hsp70 was not clear. Strikingly, further analysis of the N-terminal domain completely lacking the Cns1-TPR domain using 5'-FOA shuffling revealed, that the first 82 amino acids of Cns1 ($Cns1^{1\text{-}82}$) are sufficient to support growth of a *cns1*Δ strain, but the resulting mutants grew ex-

tremly poorly and it took them several days to form colonies.
Since the TPR domains of Sti1/HOP are known to specifically bind Hsp90 or Hsp70 (Scheufler et al., 2000; Schmid et al., 2012), respectively, with TPR1 binding Hsp70, TPR2A binding Hsp90 and TPR2B binding both, chimera mutants between $Cns1^{1\text{-}82}$ and the three Sti1 TPR domains were cloned. Remarkably, the fusion to the Hsp70-binding domain TPR1 ($Cns1^{1\text{-}82\text{-}TPR1}$), did not increase the growth rate compared to $Cns1^{1\text{-}82}$, but the $Cns1^{1\text{-}82\text{-}TPR2A}$ and $Cns1^{1\text{-}82\text{-}TPR2B}$ chimera showed an increased growth rate. These findings strongly suggested, that the essential *in vivo* function of Cns1 is dependent on Hsp90. To further confirm this effect, $Cns1^{1\text{-}82}$ was also fused directly to Hsp90 and Hsp70, respectively. Strikingly, only the direct fusion to Hsp90 increased the growth rate of the *cns1*Δ strain compared to $Cns1^{1\text{-}82}$. These findings further support the idea, that the essential Cns1 function is Hsp90-dependent *in vivo*. Interestingly, Tesic et al. (2003) showed a negative genetic interaction between a temperature-sensitive *cns1* mutant and a Hsp90 mutant lacking the C-terminal MEEVD motif, providing further evidence for the Hsp90-dependence of Cns1 function.

TTC4, the human orthologue of Cns1, was also studied using 5'-FOA shuffling. In initial experiments, TTC4 was not able to fulfill Cns1's essential function *in vivo*. Comparison of Cns1 and TTC4 by sequence alignment revealed a strong conservation of the amino acids encoding the TPR domain but more variability outside the TPR domain. Remarkably, a chimera where the N-domain of Cns1 was fused to the TPR domain of TTC4, supported full growth of the resulting mutant. Moreover, it could be shown, that TTC4 is able to overcome the deletion of *CNS1* at lower temperatures. In a recent high-throughput study (Kachroo et al., 2015), it was also reported, that TTC4 was able to suppress *cns1* mutants, but the authors did not use a complete deletion of *cns1*, but repressible-promoter and temperature-sensitive mutants. Thus, one can conclude that Cns1/TTC4 is conserved from yeast to man, although both proteins are slightly different in their N-terminal domain.

5.2 *In vitro* interaction of Cns1 and its domains with Hsp90

5'-FOA shuffling gave a good starting point for in-depth *in vitro* analysis of Cns1 and selected truncation mutants therof. Since the shuffling results strongly support the idea that Cns1's essential function is connected to Hsp90, the focus of the *in vitro* analysis was on this chaperone. None of the tested mutants had an effect on Hsp90's ATPase, confirming data published previously (Hainzl et al., 2004). Even the dominant-negative Cns1$^{51\text{-}385}$ construct did not have an effect, indicating that the mutant is not having a general negative effect on Hsp90 function. Moreover, Cns1 binding to Hsp90 was independent of nucleotides, suggesting, that Cns1 does not influence the classic Hsp90 chaperone cycle.

aUC revealed that only mutants containing the entire TPR domain were able to disrupt a preformed *Cns1-Hsp90 complex. This data provide evidence, that stable Hsp90-Cns1 interaction is achieved by the co-chaperone's TPR domain. The obtained data also go in line with results published previously (Tesic et al., 2003; Hainzl et al., 2004).

Strikingly, the ability to stably interact with Hsp90 *in vitro*, does not correlate with *in vivo* functionality of the single domains (Table 29). For example, Cns1$^{1\text{-}82}$ confers viabilty, but is not binding Hsp90 *in vitro* and Cns1$^{51\text{-}385}$ is inviable in the shuffling assay, leads to a dominant-negative effect when overexpressed in wildtype yeast, but binds Hsp90 *in vitro*. The C-terminal domain construct Cns1$^{169\text{-}385}$ is inviable in the shuffling assay, but does not lead to a dominant-negative effect upon overexpression and is not able to bind Hsp90 *in vitro*. Interestingly, Cns1$^{1\text{-}190}$ containing the Cns1 N-domain and the TPR domain, shows a good growth rate in the shuffling assay and is able to bind Hsp90 *in vitro*. This result, in combination with the findings from the shuffling assays (enhanced growth rate of Cns1$^{1\text{-}82\text{-}TPR2A}$, Cns1$^{1\text{-}82\text{-}TPR2B}$, Cns1$^{1\text{-}82\text{-}Hsc82}$, Cns1$^{Hsc82\text{-}1\text{-}82}$, Cns1N/TTC4), provides evidence, that stable interaction of the N-terminal segment of Cns1 with Hsp90 (under normal conditions mediated via a TPR domain) is important for the *in vivo* function. Since all shuffling constructs are expressed from the strong GPD-promoter, it is for example possible that *in vivo* Hsp90 and Cns1$^{1\text{-}82}$ act on the same client protein due to the high abundace of both proteins under the selected experimental conditions.

Table 29: Summary of shuffling and aUC results

construct	**viability**	**Hsp90 binding**
$Cns1^{wt}$	++++	+++
$Cns1^{1\text{-}190}$		
$Cns1^{wt}$	+++	+
$Cns1^{1\text{-}82}$	+	-
$Cns1^{36\text{-}385}$	+++	+++
$Cns1^{51\text{-}385}$	-	+++
$Cns1^{169\text{-}385}$	-	-
TTC4	∼	+
Cns1N/TTC4	+++	+
$Cns1^{36\text{-}205}$	++	++
$Cns1^{1\text{-}220}$	+++	++
$Cns1^{221\text{-}385}$	-	-
$Cns1^{1\text{-}82\text{-}L\text{-}221\text{-}385}$	++	-

The importance of the Cns1 N-domain interaction with Hsp90 is further supported by analysis of TTC4. TTC4 was only able to confer viability in the shuffling assay at lower temperatures, whereas the chimera mutant Cns1N/TTC4 showed almost wildtype-like growth at 30°C. Interestingly, Cns1N/TTC4, showed a similar affinity for Hsp90 compared to TTC4, and both proteins were folded, as confirmed by CD spectroscopy. Thus, again, the ability to stably interact with Hsp90 *in vitro* does not fully correlate with *in vivo* function.

5.3 Structural characterization of Cns1

All Cns1 constructs used showed correct folding as determined by CD spectroscopy except for $Cns1^{1\text{-}82}$, the minimal construct required for cell viability.
The C-terminal domain of Cns1 was crystallized successfully before (Otmar Hainzl, PhD thesis), but the original data were not available in the lab anymore. Recrystallization of SeMet-labeled $Cns1^{221\text{-}385}$ was successful, and showed the same structure as described in

the original work. Moreover, crystallization of TTC4's C-terminal domain was also successful. Strikingly, both constructs show a high structural similarity, underlined by the fact that the structure of Cns1$^{221\text{-}385}$ could be used to solve the structure of TTC4$^{217\text{-}387}$. The *in vivo* function of these structures is so far not clear, but there is evidence, that Cns1 interacts with the intact ribosome via its C-terminal domain (Tenge et al., 2015 and see below). Due to the fact that both structures are very similar, and that Cns1 and TTC4 are conserved from yeast to man, one can speculate that the function of their C-terminal domains might be similar.

Crystallization of several Cns1-TPR-domain constructs was successful, but structure determination was not successful so far. Alternatively, NMR spectroscopy may help to solve the structure of the TPR domain and the essential residues adjacent to the TPR domain (see below).

To get a general idea of Cns1's structural properties, SAXS measurements were carried out. These experiments suggested a two folded domain architecture for Cns1^{wt}. Interestingly, SAXS provided evidence for an unstructured tail in the construct Cns1$^{1\text{-}220}$, indicating a disordered region in the protein's structure. Strikingly, this tail was reduced in Cns1$^{36\text{-}220}$ uncovering a fine structure at around 60 Å (indicating a folded region), and absent in Cns1$^{70\text{-}220}$, suggesting, that the disordered region lies in the N-terminal region of Cns1, confirming the initial results obtained by CD spectroscopy.

Moreover, these data were confirmed by NMR spectroscopy. ^{1}H, ^{15}N HSQC NMR measurements gave well resolved spectra for Cns1$^{36\text{-}220}$, characteristic for a folded protein, whereas for Cns1$^{1\text{-}220}$ a large number of sharp, additional peaks appeared in the center of the spectrum, indicating that the first 35 amino acids lack structure in this construct. Since NMR spectroscopy led to well resolved spectra for Cns1$^{1\text{-}220}$ and Cns1$^{36\text{-}220}$, which contain the essential N-terminal residues in addition to the TPR domain, structure determination of one of these constructs by NMR is a powerful approach to get an in-depth insight into the structural properties of the essential part of Cns1.

In summary, structural analysis of Cns1 revealed, that the essential N-terminal segment of the protein is at least partly disordered. It is so far unclear what the exact function of the disordered region might be. The co-chaperone Sba1/p23, for example, contains a C-terminal disordered region, which is important for its chaperone function independent of Hsp90 (Weikl et al., 1999; Forafonov et al., 2008). However, using an *in vitro* assay, Cns1 showed no chaperone activity on its own (Hainzl et al., 2004).

5.4 High-throughput screenings to uncover genetic interactors of *cns1* and *cpr7*Δ mutants

Cns1 was originally identified as a multi-copy-suppressor of the slow growth phenotype of a *cpr7*Δ strain and a temperature-sensitive Hsp90 mutant (Dolinski et al., 1998; Marsh et al., 1998; Nathan et al., 1999). Moreover, Tesic et al. (2003) reported, that Cpr7 overexpression suppressed the growth defect of the temperature-sensitive *cns1-1* mutant. Since it was not clear whether there are other multi-copy-suppressors of the *cns1-1* mutant, that might have been missed in the previous publication, a new screen was carried out. Although the screen covered the used library approximately three times, no suppressor of the temperature-sensitive growth defect of *cns1-1* other than *CPR7* or *CNS1* could be identified. Therefore, one can conclude, that there is only one multi-copy-suppressor of the *cns1-1* mutant, which is *CPR7*. *cns1-1* carries a G90D mutation at the beginning of the TPR domain, which weakens Cns1-Hsp90 interaction *in vivo* (Tesic et al., 2003). Therefore, it is interesting, that another Hsp90 interacting protein is able to carry out Cns1's essential function. Maybe the construction of further ts-mutations, ideally in the essential N-terminal segment, might be useful for further multi-copy-suppressor screens, to find additional suppressors, e.g. putative client proteins that might interact with the N-terminal domain.

In addition to the multi-copy-suppressor screen, two SGA screens were carried out. In the first screen, a tet07-*CNS1* mutant was used as a bait. This screen resulted in only one hit, *get2*Δ. The reason for the low yield of genetic interactors is the slow response of the bait mutant to the addition of doxycycline. The cells manage to divide several times before the growth rate due to Cns1 depletion gets decreased. In SGA screens, the cells might simply be able to make enough division to reach stationary phase and are then missed in the data analysis.
Future screens, therefore, should be using the *cns1-1* mutant or a *cns1*-DAmP strain as bait.

Since Cpr7 is known to have overlapping functions with Cns1 *in vivo* (see above), *cpr7*Δ was used as bait strain in the second screen. Due to their overlapping function, overlapping genetic interactors are expected. Several hits have been reported before (listed in

Table 27 and 28), but many of them were new. The screen included genes from the Hsp90 machinery (*hsc82*Δ, *sti1*Δ), the Hsp70 machinery (*ydj1*Δ) as well as genes associated with translation (*rpg1*Δ, *tef4*Δ, *rpl39*Δ, *hgh1*Δ) and as largest group, vesicular transport (*tlg2*Δ, *get2*Δ, *sac1*Δ, *vps51*Δ, *cog8*Δ, *vps53*Δ, *cog5*Δ, *pep12*Δ, *gyp1*Δ, *tsr85*Δ, *swf1*Δ, *did4*Δ, *cax4*Δ, *rud3*Δ, *ypt6*Δ, *cdc50*Δ, *gup1*Δ, *vps20*Δ, *ric1*Δ, *vps25*Δ, *mtc1*Δ, *vps52*Δ, *vps16*Δ, *mnn10*Δ,...). Interestingly, there was also negative genetic interaction with three genes encoding subunits of the GimC/prefoldin chaperone machine (*gim1*Δ, *pac10*Δ *and gim3*Δ), a multi-subunit chaperone required for proper folding of tubulin (Geissler et al., 1998).

The negative genetic interaction between *cpr7*Δ and *sti1*Δ and *hsp90* mutants was reported previously (Duina et al., 1996a; Flom et al., 2005; Zuehlke and Johnson, 2012; Duina et al., 1998). Interestingly, there was also negative genetic interaction with *ydj1*Δ, which was also reported previously (Costanzo et al., 2010). Since it is known, that Sti1 acts as a central hub to connect Hsp70 with Hsp90 (Wegele et al., 2006), future studies will have to address the details of these interaction in more detail. One possible explanation is, that mutation of *STI1* or *YDJ1* reduces overall client transfer to the Hsp90 machinery, including Cpr7 and Cns1 substrates, and therefore shows a synthetic growth defect with *cpr7*Δ.

Also the genetic interaction with the chaperone prefoldin is of interest, how it is connected to the Hsp90 machinery is to date unclear.

Interestingly, most negative genetic interactors are involved in vesicular transport, although they are not part of a specific complex or step in trafficking, but rather distributed over many different trafficking stages. Hsp90 was reported to interact genetically and physically with genes and proteins involved in trafficking previously (McClellan et al., 2007; Zhao et al., 2005), but whether Cpr7 or Cns1 are specific co-chaperones for these processes is unknown. Table 30 lists the most abundant GO term hits (10 proteins per term threshold) obtained by processing the hits from Table 28 and 27 using Yeastmine (yeastmine.yeastgenome.org).

Future studies, using for example GFP-tagged marker proteins to monitor vesicular transport and *cpr7*Δ and *cns1* mutants will have to address a possbile involvement of Cns1 and/or Cpr7 in this process in more detail. Moreover, if vesicular transport is influenced by the two co-chaperones, it will be important to identify whether they act at a specific step or whether they have a more global role in this process. Still, it is

possible that the genetic interactions presented here, are caused by inhibiting processes upstream or downstream by mutating *cpr7* or *cns1*.

Table 30: Most abundant GO terms identified in the *cpr7*Δ SGA screen

GO term	**number of proteins**
transport	40
protein localization	28
establishment of protein localization	26
protein transport	25
vesicle-mediated transport	21
vacuolar transport	19
endosomal transport	12

A possible role in ribosome biogenesis/translation is discussed in more detail below.

5.5 The role of Cns1 in ribosome biogenesis and/or translation

Cns1 interacts with the intact ribosome via its C-terminal domain (this study; Tenge et al., 2015). In addition, Cpr7 was reported to interact with the ribosome as well (Tenge et al., 2015). The expression of *CNS1* is strongly co-regulated with genes involved in ribosome biogenesis. Moreover, *cns1* mutants and *cpr7*Δ are sensitive to hygromycin B treatment (this study; Tenge et al., 2015; Albanèse et al., 2006), an inhibitor of protein translation. Due to the low abundance of Cns1 in the cell (Ghaemmaghami et al., 2003), a general involvement in translation or co-translational folding is unlikely, since ribosomes are in large excess over the co-chaperone.
A possible involvement of Cns1 in ribosome biogenesis was investigated using two different approaches. First, the cellular localiziation of Rpl25-GFP and Rps2-GFP was used as a readout for impaired large and small ribosome subunit biogenesis defects, but no changes in protein localization could be observed. In addition, ribosome fractionation

was carried out. Again, no classical ribosome biogenesis defects were observed for the *cns1-1* mutant (no effect on 40S and 60S accumulation, no half-mer formation). The mutant showed a reduced amount of the 80S monosome peak already at the permissive temperature, but the effect was not more pronounced at the non-permissive temperature. The observed polysome profile (reduced 80S) is, interestingly, pheno-copying an effect of a *ssb1*Δ*ssb2*Δ double deletion strain (Koplin et al., 2010). Ssb1/2 is a complex involved in co-translational folding. Therefore, it might be worth to investigate a role of Cns1 in co-translational folding in more detail, by e.g. performing aggregate isolation from yeast (Koplin et al., 2010). Although a general role for Cns1 in cotranslational folding is unlikely due to its low abundace, it is worth to mention, that *cpr7*Δ pheno-copies many (co)-chaperone mutants involved in general folding (Ssa-family, Ssb-family, RAC, TRiC, GimC/prefoldin), but not mutants involved in the heat shock response (*cpr6*Δ, *sti1*Δ, *hsp82*Δ, *hsp104*Δ,...) (Albanèse et al., 2006).

Interestingly, stable interaction with the ribosome is not required for cell viability, since only Cns1 constructs containing the C-terminal domain were able to bind the ribosome in GFP-pull-down assays. Cns1$^{1\text{-}190\text{-}GFP}$ and Cns1$^{1\text{-}82\text{-}GFP}$ did not interact with the ribosome in these assays, but it is important to mention that Cns1$^{36\text{-}195}$ showed a strong growth defect in the shuffling assay, suggesting an important role for the C-terminal domain (and therefore ribosome binding) when the function of the N-terminal domain is somewhat compromised.

*get2*Δ, a subunit of the GET complex, responsible for the insertion of tail-anchored proteins into the ER membrane (Schuldiner et al., 2008), was the only hit found in the tet07-*CNS1* SGA screen and was as well found in the *cpr7*Δ screen. Interestingly, *get2*Δ was also reported as being hygromycin B sensitive in the same study (Schuldiner et al., 2008), as well as *pep12*Δ and *tlg2*Δ, two tail-anchored proteins, which were also found as negative genetic interactors of the *cpr7*Δ strain, but, so far, the connection between translation inhibition, vesicular trafficking and the Hsp90 machinery is not clear.

One possible explanation for the discrepancy between the genetic and the physical interactions is, that vesicular trafficking (in particular the secretory pathway) and ribosome biogenesis are connected by a feedback mechanism (Mizuta and Warner, 1994; Marion et al., 2004), in which a block in the secretory pathway down-regulates ribosomal gene transcription via the transcription factor Sfp1. It is also important to mention that many ribosome biogenesis factors are essential and therefore not included in the SGA analysis.

5.6 Cooperative co-chaperone function of Cns1's N- and C-terminal domains

As mentioned before, Cns1$^{36\text{-}195}$ showed a strong growth defect in the shuffling assay, indicating a possible cooperative *in vivo* function of Cns1's N- and C-terminal segments. Strikingly, a fusion protein between the N-terminal and the C-terminal domain (Cns1$^{1\text{-}82\text{-}L\text{-}221\text{-}385}$) improved growth compared to Cns1$^{1\text{-}82\text{-}L}$. Moreover, this construct was not able to disrupt a *Cns1-Hsp90 complex *in vitro*, confirming the effects described previously, that stable Hsp90 binding *in vitro*, does not fully correlate with protein function *in vivo*. Given the fact that the first 82 residues encode the essential function of the protein, whereas the C-terminal domain mediates ribosome binding, one can speculate, that the C-terminal domain might act as a targeting factor to the ribosome, where the N-terminal domain might fulfill its essential function in concert with Hsp90, which is recruited by Cns1's TPR domain. This model is further supported by the finding, that the Cns1$^{51\text{-}385}$ construct leads to a dominant-negative effect in wildtype yeast, although it is able to bind the ribosome as well as Hsp90, perhaps leading to a block in client maturation in the absence of the N-terminal domain.

5.7 The role of Cns1 in the Hsp90 (co)-chaperone cycle

During the progression of the reaction cycle, Hsp90 is able to form mixed complexes with various co-chaperones, some in a nucleotide-dependent way (Li et al., 2011, 2013). How Cns1 is integrated into the Hsp90 (co)-chaperone cycle, was not clear so far. Since Cns1 binds Hsp90 independent of the presence of nucleotides, it is unlikely, that Cns1 targets a specific conformation of Hsp90. Moreover, none of the tested Cns1 constructs affected Hsp90's ATPase activity, indicating, that Cns1 is not a general modulator of the Hsp90 (co)-chaperone cycle. Interestingly, although many different heterotrimeric complexes could be formed *in vitro*, only the *Cns1-Hsp90-Cpr7 complex seems to have relevance *in vivo*, since only negative genetic interaction between tet07-*CNS1* and *cpr7*Δ was observed in the presence of doxycycline, but with no other Hsp90 co-chaperone mutant.

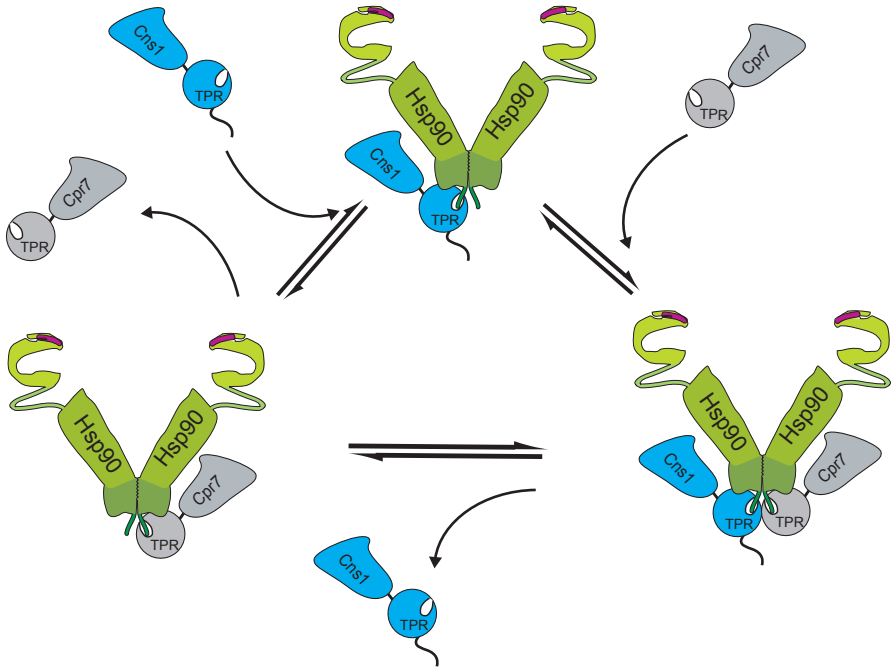

Figure 43: Model of the Cns1 domain architecture and function. Cns1 and Cpr7 both bind Hsp90 via their TPR domains. Although they are able to bind Hsp90 *in vitro* at the same time, it is also possible, that the reaction cycle works as a cascade, with sequential binding and release of the two co-chaperones.

Thus, one can conclude, also taking results published previously into account (Tesic et al., 2003; Tenge et al., 2015; Zuehlke and Johnson, 2012), that Cns1 and Cpr7, in concert with Hsp90, form a chaperone/co-chaperone machine on their own. Additional *in vitro* analyses, to further characterize mixed complexes of Cns1, Hsp90 and Cpr7, will be required to completely understand the nature of this chaperone machine. Moreover, *in vivo* pull-down assays could show whether the complexes observed *in vitro* also exist *in vivo*. It will be also important to see, whether Cns1 and Cpr7 are associating with Hsp90 preferentially in a heterotrimeric complex, or whether they interact with Hsp90 sequentially (Figure 43).

6 Summary and Outlook

In this thesis, the essential co-chaperone Cns1 was characterized by the combination of a broad range of *in vivo* and *in vitro* methods.
In-depth *in vivo* analysis revealed that the essential function of Cns1 is encoded by its N-terminal domain and CD spectroscopy, SAXS and NMR revealed, that this domain is partly disordered.
Moreover, it was shown that Cns1's TPR domain is essential for stably binding Hsp90. Although, crystallization of this domain was successful, structure determination failed so far. Since the spectra obtained by NMR spectroscopy of a uniformly ^{15}N-labeled TPR domain construct are promising, this method will be useful in future studies to solve the structure of Cns1's TPR domain.
In addition, it was shown, that the C-terminal domain is important for the *in vivo* function of Cns1. Crystallization and structure determination of it was successful. It was also possible to solve the structure of the C-terminal domain of the human orthologue TTC4, which shows a strong similarity to the C-domain of Cns1.

Although, a role for Cns1 in ribosome biogenesis was tested, its role in this process is unclear so far. Northern Blot analysis of rRNA maturation intermediates might be useful to further characterize a role for Cns1 in the process in more detail.
Figure 44 summarizes the domain architecture, folding properties and *in vivo* function of Cns1.
Genetic and biochemical analyses revealed a strong connection between Cns1, Cpr7 and Hsp90, but no other Hsp90 co-chaperones, suggesting that the three might form a chaperone machine independent of the so far characterized Hsp90 co-chaperone cycle. Future *in vitro* studies will have to address, whether the observed Cns1-Hsp90-Cpr7 complex is relevant *in vivo* or whether Cns1 and Cpr7 prefer to interact sequentially with Hsp90.
Moreover, triple mutants (e.g. tet07-*CNS1 cpr7*Δ + another Hsp90 co-chaperone) will be helpful to further characterize the core Cns1-Cpr7-Hsp90 machine. Additionally, this

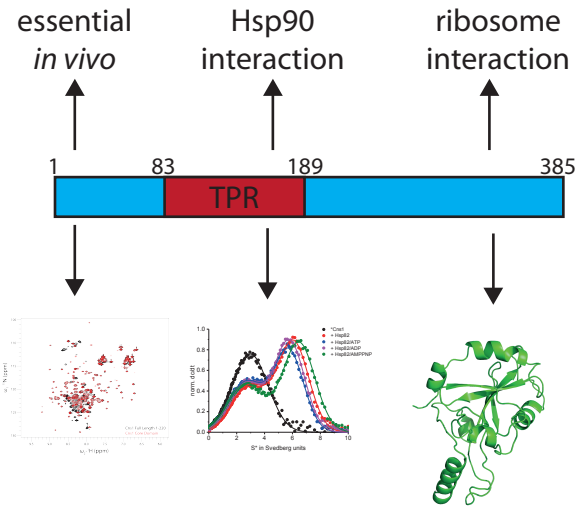

Figure 44: Model of Cns1 domain architecture and function. The partly disordered N-terminal region is essential *in vivo*. Cns1 binds Hsp90 via its central TPR domain, whereas the C-terminal domain is required for ribosome interaction.

approach can be extended to other chaperone classes of the cytosol (e.g. GimC/prefoldin, CCT/TRiC, Ssa-familiy, Ssb-family, RAC, NAC, etc.) to get a global understanding of the Cns1-chaperone interaction network in the cell.
Since the biggest group of negative genetic interactors in the *cpr7*Δ SGA screen are known to contribute to vesicular trafficking, monitoring GFP-mutants of marker proteins, which are known to mislocalize upon blocking intracellular trafficking, will be a useful approach to confirm or disprove a possible involvement of Cpr7 and/or Cns1 in this process.

In summary, the essential domain of Cns1 was identified and characterized *in vivo*. In addition, it was shown, that the C-terminal domain of Cns1 is important for full *in vivo* function, possibly by acting as a targeting factor to the ribosome. Moreover, it could be proven, that Cns1's essential function is connected to Hsp90, with which it interacts via its TPR domain. Finally, a model for a new Hsp90 co-chaperone machine, acting independently of the so far characterized Hsp90 chaperone cycle, emerges from genetic and biochemical interaction data, consisting of Cpr7, Hsp90 and Cns1 (Figure 43).

7 Abbreviations

Table 31: Abbreviations

5'-FOA	5-fluoroorotic acid
A	ampere
A_{280}	absorption at 280 nm
ADP	adenosine diphosphate
APS	ammoniumpersulfate
ATP	adenosine triphosphate
ATPase	ATP hydrolase
aUC	analytical ultracentrifugation
CD	circular dichroism
clonNAT	nourseothricin
CTD	carboxy terminal domain
Da	dalton
DMSO	dimethyl sulfoxide
DNA	deoxyribonucleic acid
dNTP	deoxynucleoside triphosphate
Dox	doxycyclin
DTT	dithiothreitol
E. coli	*Escherichia coli*
EDTA	ethylenediamine-tetraacetic acid
ε	molar extinction coefficient
ER	endoplasmic reticulum
FPLC	fast protein liquid chromatography
g	gram
G418	geneticin

GHKL	gyrase, hsp90, histidine kinase, mutL
GR	glucocorticoid receptor
h	hours
HAT	hydroxyapatite
HEPES	N-(2-hydroxyethyle)-piperazine-N´-2-ethanesulfonic acid
Hsp	heat shock protein
HygB	hygromycine B
I1	intermediate state 1
I2	intermediate state 2
IEC	ion exchange chromatography
IPTG	isopropyl-β-D-thiogalactopyranosid
k_{cat}	unimolecular rate constant
K_D	dissociation constant
L	liter
λ	wavelength
LB_0	lysogeny broth without antibiotics
LBD	ligand binding domain
LDH	lactate dehydrogenase
LiAc	lithium acetate
M	molar
M9	minimal medium
MD	middle domain
min	minutes
NAC	nascent chain associated complex
NAD(H)	nicotinamide adenine dinucleotide
NBD	nucleotide binding domain
NEF	nucleotide exchange factor
NHS	N-hydroxysuccinimide
NiNTA	nickel nitrilotriacetic acid
NMR	nuclear magnetic resonance
NTD	N-terminal domain

OD	optical density
PAGE	polyacrylamide gel electrophoresis
PCR	polymerase chain reaction
PEG	polyethylene glycol
PEP	phosphoenolpyruvate
pH	potentia hydrogenii
P_i	orthophosphate
pI	isoelectric point
PK	pyruvate kinase
PMSF	phenylmethylsulfonyl fluoride
PPIase	pepdidyl-prolyl-isomerase
PTM	post translational modification
RAC	ribosome associated complex
RNA	ribonucleic acid
Rpm	rounds per minute
RT	room temperature
s	second
S. cerevisiae	*Saccharomyces cerevisiae*
SAXS	small angle X-ray scattering
SBD	substrate binding domain
SDS	sodium dodecyl sulfate
SEC	size exclusion chromatography
SeMet	selenomethionine
sHSp	small heat shock protein
SLIC	sequence and ligation independent cloning
ssDNA	single strand DNA
TAE	TRIS acetate EDTA
TCEP	tris(2-carboxyethyl)phosphine
TEMED	N, N, N´,N´-tetramethylethylenediamine
TF	trigger factor
TPR	tetratricopeptide repeat
TRIS	trihydroxymethylaminomethan-hydrochloride

UV	ultraviolet
v/v	volt
VIS	visual
vSrc	viral Src kinase
w/v	weight per volume
YNB	yeast nitrogen base
YPD	yeast extract peptone dextrose
YT	yeast extract tryptone

8 Publications

Hofbauer Harald F., **Schopf Florian H.,** Schleifer Hannes, Knittelfelder, Oskar L., Pieber Bartholomäus, Rechberger Gerald N., Wolinski Heimo, Gaspar Maria L., Kappe C. Oliver, Stadlmann Johannes, Mechtler Karl, Zenz Alexandra, Lohner Karl, Tehlivets Oksana, Henry Susan A. and Kohlwein, Sepp D. Regulation of gene expression through a transcriptional repressor that senses acyl-chain length in membrane phospholipids. *Dev Cell*, 2014 Jun 23;29(6):729-39.

Zierer Bettina K., Rübbelke Martin, Tippel Franziska, Madl Tobias, **Schopf Florian H.**, Rutz Daniel A., Richter Klaus, Sattler Michael and Buchner Johannes. Importance of cycle timing for the function of the molecular chaperone Hsp90. *Nature Structural and Molecular Biology*, Aug 2016; *accepted*

References

Albanèse, V., Yam, A. Y.-W., Baughman, J., Parnot, C., and Frydman, J. (2006). Systems analyses reveal two chaperone networks with distinct functions in eukaryotic cells. *Cell 124*, 75–88.

Alexopoulos, J. A., Guarné, A., and Ortega, J. (2012). ClpP: a structurally dynamic protease regulated by AAA+ proteins. *Journal of structural biology 179*, 202–10.

Ali, J. A., Jackson, A. P., Howells, A. J., and Maxwell, A. (1993). The 43-kilodalton N-terminal fragment of the DNA gyrase B protein hydrolyzes ATP and binds coumarin drugs. *Biochemistry 32*, 2717–24.

Ali, M. M. U., Roe, S. M., Vaughan, C. K., Meyer, P., Panaretou, B., Piper, P. W., Prodromou, C., and Pearl, L. H. (2006). Crystal structure of an Hsp90-nucleotide-p23/Sba1 closed chaperone complex. *Nature 440*, 1013–7.

Anand, M., Chakraburtty, K., Marton, M. J., Hinnebusch, A. G., and Kinzy, T. G. (2003). Functional interactions between yeast translation eukaryotic elongation factor (eEF) 1A and eEF3. *The Journal of biological chemistry 278*, 6985–91.

Anfinsen, C. B. (1973). Principles that govern the folding of protein chains. *Science 181*, 223–30.

Aquilina, J. A., Benesch, J. L. P., Ding, L. L., Yaron, O., Horwitz, J., and Robinson, C. V. (2004). Phosphorylation of alphaB-crystallin alters chaperone function through loss of dimeric substructure. *The Journal of biological chemistry 279*, 28675–80.

Balchin, D., Hayer-Hartl, M., and Hartl, F. U. (2016). In vivo aspects of protein folding and quality control. *Science (New York, N.Y.) 353*, aac4354.

Bali, M., Zhang, B., Morano, K. A., and Michels, C. A. (2003). The Hsp90 molecular chaperone complex regulates maltose induction and stability of the Saccharomyces MAL gene transcription activator Mal63p. *The Journal of biological chemistry 278*, 47441–8.

Bali, P., Pranpat, M., Bradner, J., Balasis, M., Fiskus, W., Guo, F., Rocha, K., Kumaraswamy, S., Boyapalle, S., Atadja, P., Seto, E., and Bhalla, K. (2005). Inhibition of histone deacetylase 6 acetylates and disrupts the chaperone function of heat shock protein 90: a novel basis for antileukemia activity of histone deacetylase inhibitors. *The Journal of biological chemistry 280*, 26729–34.

Bécam, A. M., Nasr, F., Racki, W. J., Zagulski, M., and Herbert, C. J. (2001). Ria1p (Ynl163c), a protein similar to elongation factors 2, is involved in the biogenesis of the 60S subunit of the ribosome in Saccharomyces cerevisiae. *Molecular genetics and genomics : MGG 266*, 454–62.

Beissinger, M., Rutkat, K., and Buchner, J. (1999). Catalysis, commitment and encapsulation during GroE-mediated folding. *Journal of molecular biology 289*, 1075–92.

Beltrao, P., Trinidad, J. C., Fiedler, D., Roguev, A., Lim, W. A., Shokat, K. M., Burlingame, A. L., and Krogan, N. J. (2009). Evolution of phosphoregulation: comparison of phosphorylation patterns across yeast species. *PLoS biology 7*, e1000134.

Bertelsen, E. B., Chang, L., Gestwicki, J. E., and Zuiderweg, E. R. P. (2009). Solution conformation of wild-type E. coli Hsp70 (DnaK) chaperone complexed with ADP and substrate. *Proceedings of the National Academy of Sciences of the United States of America 106*, 8471–6.

Beyer, A. (1997). Sequence analysis of the AAA protein family. *Protein science : a publication of the Protein Society 6*, 2043–58.

Bledsoe, R. K., Montana, V. G., Stanley, T. B., Delves, C. J., Apolito, C. J., McKee, D. D., Consler, T. G., Parks, D. J., Stewart, E. L., Willson, T. M., Lambert, M. H., Moore, J. T., Pearce, K. H., and Xu, H. E. (2002). Crystal structure of the glucocorticoid receptor ligand binding domain reveals a novel mode of receptor dimerization and coactivator recognition. *Cell 110*, 93–105.

Boczek, E. E., Reefschläger, L. G., Dehling, M., Struller, T. J., Häusler, E., Seidl, A., Kaila, V. R. I., and Buchner, J. (2015). Conformational processing of oncogenic v-Src kinase by the molecular chaperone Hsp90. *Proceedings of the National Academy of Sciences of the United States of America 112*, E3189–98.

Borkovich, K. A., Farrelly, F. W., Finkelstein, D. B., Taulien, J., and Lindquist, S. (1989). hsp82 is an essential protein that is required in higher concentrations for growth of cells at higher temperatures. *Molecular and Cellular Biology 9*, 3919–30.

Bose, S., Weikl, T., Bügl, H., and Buchner, J. (1996). Chaperone function of Hsp90-associated proteins. *Science 274*, 1715–7.

Braakman, I. and Hebert, D. N. (2013). Protein folding in the endoplasmic reticulum. *Cold Spring Harbor perspectives in biology 5*, a013201.

Breter, H. J., Ferguson, J., Peterson, T. A., and Reed, S. I. (1983). Isolation and transcriptional characterization of three genes which function at start, the controlling event of the Saccharomyces cerevisiae cell division cycle: CDC36, CDC37, and CDC39. *Molecular and Cellular Biology 3*, 881–91.

Brinker, A., Pfeifer, G., Kerner, M. J., Naylor, D. J., Hartl, F. U., and Hayer-Hartl, M. (2001). Dual function of protein confinement in chaperonin-assisted protein folding. *Cell 107*, 223–33.

Brockwell, D. J. and Radford, S. E. (2007). Intermediates: ubiquitous species on folding energy landscapes? *Current opinion in structural biology 17*, 30–7.

Brugge, J. S. (1986). Interaction of the Rous sarcoma virus protein pp60src with the cellular proteins pp50 and pp90. *Current topics in microbiology and immunology 123*, 1–22.

Brugge, J. S., Erikson, E., and Erikson, R. L. (1981). The specific interaction of the Rous sarcoma virus transforming protein, pp60src, with two cellular proteins. *Cell 25*, 363–72.

Bukau, B. and Horwich, A. L. (1998). The Hsp70 and Hsp60 chaperone machines. *Cell 92*, 351–66.

Calloni, G., Chen, T., Schermann, S. M., Chang, H.-C., Genevaux, P., Agostini, F., Tartaglia, G. G., Hayer-Hartl, M., and Hartl, F. U. (2012). DnaK functions as a central hub in the E. coli chaperone network. *Cell reports 1*, 251–64.

Carroni, M., Kummer, E., Oguchi, Y., Wendler, P., Clare, D. K., Sinning, I., Kopp, J., Mogk, A., Bukau, B., and Saibil, H. R. (2014). Head-to-tail interactions of the coiled-coil domains regulate ClpB activity and cooperation with Hsp70 in protein disaggregation. *eLife 3*, e02481.

Cashikar, A. G., Duennwald, M., and Lindquist, S. L. (2005). A chaperone pathway in protein disaggregation. Hsp26 alters the nature of protein aggregates to facilitate reactivation by Hsp104. *The Journal of biological chemistry 280*, 23869–75.

Catlett, M. G. and Kaplan, K. B. (2006). Sgt1p is a unique co-chaperone that acts as a client adaptor to link Hsp90 to Skp1p. *The Journal of biological chemistry 281*, 33739–48.

Chadli, A., Bouhouche, I., Sullivan, W., Stensgard, B., McMahon, N., Catelli, M. G., and Toft, D. O. (2000). Dimerization and N-terminal domain proximity underlie the function of the molecular chaperone heat shock protein 90. *Proceedings of the National Academy of Sciences of the United States of America 97*, 12524–9.

Chakraborty, K., Chatila, M., Sinha, J., Shi, Q., Poschner, B. C., Sikor, M., Jiang, G., Lamb, D. C., Hartl, F. U., and Hayer-Hartl, M. (2010). Chaperonin-catalyzed rescue of kinetically trapped states in protein folding. *Cell 142*, 112–22.

Chen, S. and Smith, D. F. (1998). Hop as an adaptor in the heat shock protein 70 (Hsp70) and hsp90 chaperone machinery. *The Journal of Biological Chemistry 273*, 35194–200.

Cheng, M. Y., Hartl, F. U., Martin, J., Pollock, R. A., Kalousek, F., Neupert, W., Hallberg, E. M., Hallberg, R. L., and Horwich, A. L. (1989). Mitochondrial heat-shock protein hsp60 is essential for assembly of proteins imported into yeast mitochondria. *Nature 337*, 620–5.

Choe, Y.-J., Park, S.-H., Hassemer, T., Körner, R., Vincenz-Donnelly, L., Hayer-Hartl, M., and Hartl, F. U. (2016). Failure of RQC machinery causes protein aggregation and proteotoxic stress. *Nature 531*, 191–5.

Clare, D. K., Vasishtan, D., Stagg, S., Quispe, J., Farr, G. W., Topf, M., Horwich, A. L., and Saibil, H. R. (2012). ATP-triggered conformational changes delineate substrate-binding and -folding mechanics of the GroEL chaperonin. *Cell 149*, 113–23.

Collins, S. R., Miller, K. M., Maas, N. L., Roguev, A., Fillingham, J., Chu, C. S., Schuldiner, M., Gebbia, M., Recht, J., Shales, M., Ding, H., Xu, H., Han, J., Ingvarsdottir, K., Cheng, B., Andrews, B., Boone, C., Berger, S. L., Hieter, P., Zhang, Z., Brown, G. W., Ingles, C. J., Emili, A., Allis, C. D., Toczyski, D. P., Weissman, J. S., Greenblatt, J. F., and Krogan, N. J. (2007). Functional dissection of protein complexes involved in yeast chromosome biology using a genetic interaction map. *Nature 446*, 806–10.

Costanzo, M., Baryshnikova, A., Bellay, J., Kim, Y., Spear, E. D., Sevier, C. S., Ding, H., Koh, J. L. Y., Toufighi, K., Mostafavi, S., Prinz, J., St Onge, R. P., VanderSluis, B., Makhnevych, T., Vizeacoumar, F. J., Alizadeh, S., Bahr, S., Brost, R. L., Chen, Y., Cokol, M., Deshpande, R., Li, Z., Lin, Z.-Y., Liang, W., Marback, M., Paw, J., San Luis, B.-J., Shuteriqi, E., Tong, A. H. Y., van Dyk, N., Wallace, I. M., Whitney, J. A., Weirauch, M. T., Zhong, G., Zhu, H., Houry, W. A., Brudno, M., Ragibizadeh, S., Papp, B., Pál, C., Roth, F. P., Giaever, G., Nislow, C., Troyanskaya, O. G., Bussey, H., Bader, G. D., Gingras, A.-C., Morris, Q. D., Kim, P. M., Kaiser, C. A., Myers, C. L., Andrews, B. J., and Boone, C. (2010). The genetic landscape of a cell. *Science (New York, N.Y.) 327*, 425–31.

Cowtan, K. D. and Main, P. (1996). Phase combination and cross validation in iterated density-modification calculations. *Acta crystallographica. Section D, Biological crystallography 52*, 43–8.

Crevel, G., Bates, H., Huikeshoven, H., and Cotterill, S. (2001). The Drosophila Dpit47 protein is a nuclear Hsp90 co-chaperone that interacts with DNA polymerase alpha. *Journal of Cell Science 114*, 2015–25.

Crevel, G., Bennett, D., and Cotterill, S. (2008). The human TPR protein TTC4 is a putative Hsp90 co-chaperone which interacts with CDC6 and shows alterations in transformed cells. *PloS One 3*, e0001737.

Das, A. K., Cohen, P. W., and Barford, D. (1998). The structure of the tetratricopeptide repeats of protein phosphatase 5: implications for TPR-mediated protein-protein interactions. *The EMBO journal 17*, 1192–9.

de La Fortelle, E. and Bricogne, G. (1997). Methods Enzymol. *276*, 472–494.

de Zoeten, E. F., Wang, L., Butler, K., Beier, U. H., Akimova, T., Sai, H., Bradner, J. E., Mazitschek, R., Kozikowski, A. P., Matthias, P., and Hancock, W. W. (2011). Histone deacetylase 6 and heat shock protein 90 control the functions of Foxp3(+) T-regulatory cells. *Molecular and cellular biology 31*, 2066–78.

Demoinet, E., Jacquier, A., Lutfalla, G., and Fromont-Racine, M. (2007). The Hsp40 chaperone Jjj1 is required for the nucleo-cytoplasmic recycling of preribosomal factors in Saccharomyces cerevisiae. *RNA (New York, N.Y.) 13*, 1570–81.

Dey, B., Lightbody, J. J., and Boschelli, F. (1996). CDC37 is required for p60v-src activity in yeast. *Molecular biology of the cell 7*, 1405–17.

Dixon, S. J., Fedyshyn, Y., Koh, J. L. Y., Prasad, T. S. K., Chahwan, C., Chua, G., Toufighi, K., Baryshnikova, A., Hayles, J., Hoe, K.-L., Kim, D.-U., Park, H.-O., Myers, C. L., Pandey, A., Durocher, D., Andrews, B. J., and Boone, C. (2008). Significant conservation of synthetic lethal genetic interaction networks between distantly related eukaryotes. *Proceedings of the National Academy of Sciences of the United States of America 105*, 16653–8.

Dmitriev, R. I., Korneenko, T. V., Bessonov, A. a., Shakhparonov, M. I., Modyanov, N. N., and Pestov, N. B. (2007). Characterization of hampin/MSL1 as a node in the nuclear interactome. *Biochemical and Biophysical Research Communications 355*, 1051–7.

Dmitriev, R. I., Okkelman, I. a., Abdulin, R. a., Shakhparonov, M. I., and Pestov, N. B. (2009). Nuclear transport of protein TTC4 depends on the cell cycle. *Cell and Tissue Research 336*, 521–7.

Dolinski, K. J., Cardenas, M. E., and Heitman, J. (1998). CNS1 encodes an essential p60/Sti1 homolog in Saccharomyces cerevisiae that suppresses cyclophilin 40 mutations and interacts with Hsp90. *Molecular and Cellular Biology 18*, 7344–52.

Dollins, D. E., Warren, J. J., Immormino, R. M., and Gewirth, D. T. (2007). Structures of GRP94-nucleotide complexes reveal mechanistic differences between the hsp90 chaperones. *Molecular cell 28*, 41–56.

Douglas, N. R., Reissmann, S., Zhang, J., Chen, B., Jakana, J., Kumar, R., Chiu, W., and Frydman, J. (2011). Dual action of ATP hydrolysis couples lid closure to substrate release into the group II chaperonin chamber. *Cell 144*, 240–52.

Doyle, S. M., Genest, O., and Wickner, S. (2013). Protein rescue from aggregates by powerful molecular chaperone machines. *Nature reviews. Molecular cell biology 14*, 617–29.

Doyle, S. M., Shorter, J., Zolkiewski, M., Hoskins, J. R., Lindquist, S., and Wickner, S. (2007). Asymmetric deceleration of ClpB or Hsp104 ATPase activity unleashes protein-remodeling activity. *Nature structural & molecular biology 14*, 114–22.

Dubacq, C., Guerois, R., Courbeyrette, R., Kitagawa, K., and Mann, C. (2002). Sgt1p contributes to cyclic AMP pathway activity and physically interacts with the adenylyl cyclase Cyr1p/Cdc35p in budding yeast. *Eukaryotic cell 1*, 568–82.

Duina, A. A., Chang, H. C., Marsh, J. A., Lindquist, S., and Gaber, R. F. (1996). A cyclophilin function in Hsp90-dependent signal transduction. *Science 274*, 1713–5.

Duina, A. A., Kalton, H. M., and Gaber, R. F. (1998). Requirement for Hsp90 and a CyP-40-type cyclophilin in negative regulation of the heat shock response. *The Journal of biological chemistry 273*, 18974–8.

Duina, A. A., Marsh, J. A., and Gaber, R. F. (1996). Identification of two CyP-40-like cyclophilins in Saccharomyces cerevisiae, one of which is required for normal growth. *Yeast 12*, 943–52.

Dunker, A. K., Silman, I., Uversky, V. N., and Sussman, J. L. (2008). Function and structure of inherently disordered proteins. *Current opinion in structural biology 18*, 756–64.

Dunn, D. M., Woodford, M. R., Truman, A. W., Jensen, S. M., Schulman, J., Caza, T., Remillard, T. C., Loiselle, D., Wolfgeher, D., Blagg, B. S. J., Franco, L., Haystead, T. A., Daturpalli, S., Mayer, M. P., Trepel, J. B., Morgan, R. M. L., Prodromou, C., Kron, S. J., Panaretou, B., Stetler-Stevenson, W. G., Landas, S. K., Neckers, L., Bratslavsky, G., Bourboulia, D., and Mollapour, M. (2015). c-Abl Mediated Tyrosine Phosphorylation of Aha1 Activates Its Co-chaperone Function in Cancer Cells. *Cell reports 12*, 1006–18.

Dyballa, N. and Metzger, S. (2009). Fast and sensitive colloidal coomassie G-250 staining for proteins in polyacrylamide gels. *Journal of visualized experiments : JoVE*.

Ehrnsperger, M., Gräber, S., Gaestel, M., and Buchner, J. (1997). Binding of non-native protein to Hsp25 during heat shock creates a reservoir of folding intermediates for reactivation. *The EMBO journal 16*, 221–9.

Ellis, R. J. (2001). Macromolecular crowding: an important but neglected aspect of the intracellular environment. *Current opinion in structural biology 11*, 114–9.

Ellis, R. J. (2007). Protein misassembly: macromolecular crowding and molecular chaperones. *Advances in experimental medicine and biology 594*, 1–13.

Emsley, P., Lohkamp, B., Scott, W. G., and Cowtan, K. (2010). Features and development of Coot. *Acta crystallographica. Section D, Biological crystallography 66*, 486–501.

Esposito, A. M., Mateyak, M., He, D., Lewis, M., Sasikumar, A. N., Hutton, J., Copeland, P. R., and Kinzy, T. G. (2010). Eukaryotic polyribosome profile analysis. *Journal of visualized experiments : JoVE*.

Fairbanks, G., Steck, T. L., and Wallach, D. F. (1971). Electrophoretic analysis of the major polypeptides of the human erythrocyte membrane. *Biochemistry 10*, 2606–17.

Fanghänel, J. and Fischer, G. (2004). Insights into the catalytic mechanism of peptidyl prolyl cis/trans isomerases. *Frontiers in bioscience : a journal and virtual library 9*, 3453–78.

Ferbitz, L., Maier, T., Patzelt, H., Bukau, B., Deuerling, E., and Ban, N. (2004). Trigger factor in complex with the ribosome forms a molecular cradle for nascent proteins. *Nature 431*, 590–6.

Finka, A., Mattoo, R. U. H., and Goloubinoff, P. (2016). Experimental Milestones in the Discovery of Molecular Chaperones as Polypeptide Unfolding Enzymes. *Annual review of biochemistry 85*, 715–42.

Finnigan, G. C., Ryan, M., and Stevens, T. H. (2011). A genome-wide enhancer screen implicates sphingolipid composition in vacuolar ATPase function in Saccharomyces cerevisiae. *Genetics 187*, 771–83.

Fleckenstein, T., Kastenmüller, A., Stein, M. L., Peters, C., Daake, M., Krause, M., Weinfurtner, D., Haslbeck, M., Weinkauf, S., Groll, M., and Buchner, J. (2015). The Chaperone Activity of the Developmental Small Heat Shock Protein Sip1 Is Regulated by pH-Dependent Conformational Changes. *Molecular cell 58*, 1067–78.

Flom, G., Weekes, J., and Johnson, J. L. (2005). Novel interaction of the Hsp90 chaperone machine with Ssl2, an essential DNA helicase in Saccharomyces cerevisiae. *Current genetics 47*, 368–80.

Flom, G. A., Langner, E., and Johnson, J. L. (2012). Identification of an Hsp90 mutation that selectively disrupts cAMP/PKA signaling in Saccharomyces cerevisiae. *Current genetics 58*, 149–63.

Flotho, A. and Melchior, F. (2013). Sumoylation: a regulatory protein modification in health and disease. *Annual review of biochemistry 82*, 357–85.

Forafonov, F., Toogun, O. A., Grad, I., Suslova, E., Freeman, B. C., and Picard, D. (2008). p23/Sba1p protects against Hsp90 inhibitors independently of its intrinsic chaperone activity. *Molecular and cellular biology 28*, 3446–56.

Franke, D. and Svergun, D. I. (2009). DAMMIF , a program for rapid ab-initio shape determination in small-angle scattering. *Journal of Applied Crystallography 42*, 342–346.

Franzmann, T. M., Menhorn, P., Walter, S., and Buchner, J. (2008). Activation of the chaperone Hsp26 is controlled by the rearrangement of its thermosensor domain. *Molecular cell 29*, 207–16.

Freeman, B. C., Toft, D. O., and Morimoto, R. I. (1996). Molecular chaperone machines: chaperone activities of the cyclophilin Cyp-40 and the steroid aporeceptor-associated protein p23. *Science 274*, 1718–20.

Frydman, J. (2001). Folding of newly translated proteins in vivo: the role of molecular chaperones. *Annual review of biochemistry 70*, 603–47.

Gaiser, A. M., Kretzschmar, A., and Richter, K. (2010). Cdc37-Hsp90 complexes are responsive to nucleotide-induced conformational changes and binding of further cofactors. *The Journal of Biological Chemistry 285*, 40921–32.

Gautschi, M., Lilie, H., Fünfschilling, U., Mun, A., Ross, S., Lithgow, T., Rücknagel, P., and Rospert, S. (2001). RAC, a stable ribosome-associated complex in yeast formed by the DnaK-DnaJ homologs Ssz1p and zuotin. *Proceedings of the National Academy of Sciences of the United States of America 98*, 3762–7.

Gautschi, M., Mun, A., Ross, S., and Rospert, S. (2002). A functional chaperone triad on the yeast ribosome. *Proceedings of the National Academy of Sciences of the United States of America 99*, 4209–14.

Geissler, S., Siegers, K., and Schiebel, E. (1998). A novel protein complex promoting formation of functional alpha- and gamma-tubulin. *The EMBO journal 17*, 952–66.

Georgopoulos, C. and Welch, W. J. (1993). Role of the major heat shock proteins as molecular chaperones. *Annual Review of Cell Biology 9*, 601–34.

Ghaemmaghami, S., Huh, W.-K., Bower, K., Howson, R. W., Belle, A., Dephoure, N., O'Shea, E. K., and Weissman, J. S. (2003). Global analysis of protein expression in yeast. *Nature 425*, 737–41.

Gietz, R. D. and Woods, R. A. (2002). Transformation of yeast by lithium acetate/single-stranded carrier DNA/polyethylene glycol method. *Methods in enzymology 350*, 87–96.

Glover, J. R. and Lindquist, S. (1998). Hsp104, Hsp70, and Hsp40: a novel chaperone system that rescues previously aggregated proteins. *Cell 94*, 73–82.

Goloubinoff, P., Mogk, A., Zvi, A. P., Tomoyasu, T., and Bukau, B. (1999). Sequential mechanism of solubilization and refolding of stable protein aggregates by a bichaperone network. *Proceedings of the National Academy of Sciences of the United States of America 96*, 13732–7.

Graf, C., Lee, C.-T., Eva Meier-Andrejszki, L., Nguyen, M. T. N., and Mayer, M. P. (2014). Differences in conformational dynamics within the Hsp90 chaperone family reveal mechanistic insights. *Frontiers in molecular biosciences 1*, 4.

Graf, C., Stankiewicz, M., Kramer, G., and Mayer, M. P. (2009). Spatially and kinetically resolved changes in the conformational dynamics of the Hsp90 chaperone machine. *The EMBO Journal 28*, 602–13.

Grallert, H. and Buchner, J. (2001). Review: a structural view of the GroE chaperone cycle. *Journal of structural biology 135*, 95–103.

Grenert, J. P., Johnson, B. D., and Toft, D. O. (1999). The importance of ATP binding and hydrolysis by hsp90 in formation and function of protein heterocomplexes. *The Journal of Biological Chemistry 274*, 17525–33.

Gruber, R. and Horovitz, A. (2016). Allosteric Mechanisms in Chaperonin Machines. *Chemical reviews 116*, 6588–606.

Gupta, A. J., Haldar, S., Miličić, G., Hartl, F. U., and Hayer-Hartl, M. (2014). Active cage mechanism of chaperonin-assisted protein folding demonstrated at single-molecule level. *Journal of molecular biology 426*, 2739–54.

Hainzl, O., Lapina, M. C., Buchner, J., and Richter, K. (2009). The charged linker region is an important regulator of Hsp90 function. *The Journal of Biological Chemistry 284*, 22559–67.

Hainzl, O., Wegele, H., Richter, K., and Buchner, J. (2004). Cns1 is an activator of the Ssa1 ATPase activity. *The Journal of Biological Chemistry 279*, 23267–73.

Hainzl, O. K. W. (2008). *Charakterisierung des Cochaperons Cns1 und Funktionsanalyse des molekularen Chaperons Hsp90*. Ph. D. thesis, Technische Universität München.

Hanahan, D. (1983). Studies on transformation of Escherichia coli with plasmids. *Journal of molecular biology 166*, 557–80.

Harrell, J. M., Murphy, P. J. M., Morishima, Y., Chen, H., Mansfield, J. F., Galigniana, M. D., and Pratt, W. B. (2004). Evidence for glucocorticoid receptor transport on microtubules by dynein. *The Journal of biological chemistry 279*, 54647–54.

Hartl, F. U., Bracher, A., and Hayer-Hartl, M. (2011). Molecular chaperones in protein folding and proteostasis. *Nature 475*, 324–32.

Hartl, F. U. and Hayer-Hartl, M. (2002). Molecular chaperones in the cytosol: from nascent chain to folded protein. *Science 295*, 1852–8.

Hartl, F. U. and Hayer-Hartl, M. (2009). Converging concepts of protein folding in vitro and in vivo. *Nature Structural & Molecular Biology 16*, 574–81.

Hartson, S. D. and Matts, R. L. (2012). Approaches for defining the Hsp90-dependent proteome. *Biochimica et Biophysica Acta 1823*, 656–67.

Haslbeck, M., Franzmann, T., Weinfurtner, D., and Buchner, J. (2005). Some like it hot: the structure and function of small heat-shock proteins. *Nature structural & molecular biology 12*, 842–6.

Haslbeck, M., Miess, A., Stromer, T., Walter, S., and Buchner, J. (2005). Disassembling protein aggregates in the yeast cytosol. The cooperation of Hsp26 with Ssa1 and Hsp104. *The Journal of biological chemistry 280*, 23861–8.

Haslbeck, M., Walke, S., Stromer, T., Ehrnsperger, M., White, H. E., Chen, S., Saibil, H. R., and Buchner, J. (1999). Hsp26: a temperature-regulated chaperone. *The EMBO journal 18*, 6744–51.

Hayer-Hartl, M., Bracher, A., and Hartl, F. U. (2016). The GroEL-GroES Chaperonin Machine: A Nano-Cage for Protein Folding. *Trends in biochemical sciences 41*, 62–76.

Hayes, D. B. and Stafford, W. F. (2010). SEDVIEW, real-time sedimentation analysis. *Macromolecular bioscience 10*, 731–5.

Hedges, J., West, M., and Johnson, A. W. (2005). Release of the export adapter, Nmd3p, from the 60S ribosomal subunit requires Rpl10p and the cytoplasmic GTPase Lsg1p. *The EMBO journal 24*, 567–79.

Hessling, M., Richter, K., and Buchner, J. (2009). Dissection of the ATP-induced conformational cycle of the molecular chaperone Hsp90. *Nature Structural & Molecular Biology 16*, 287–93.

Holtkamp, W., Kokic, G., Jäger, M., Mittelstaet, J., Komar, A. A., and Rodnina, M. V. (2015). Cotranslational protein folding on the ribosome monitored in real time. *Science (New York, N.Y.) 350*, 1104–7.

Horwich, A. L., Farr, G. W., and Fenton, W. A. (2006). GroEL-GroES-mediated protein folding. *Chemical reviews 106*, 1917–30.

Horwich, A. L. and Fenton, W. A. (2009). Chaperonin-mediated protein folding: using a central cavity to kinetically assist polypeptide chain folding. *Quarterly reviews of biophysics 42*, 83–116.

Horwich, A. L., Neupert, W., and Hartl, F. U. (1990). Protein-catalysed protein folding. *Trends in Biotechnology 8*, 126–31.

Horwitz, J. (1992). Alpha-crystallin can function as a molecular chaperone. *Proceedings of the National Academy of Sciences of the United States of America 89*, 10449–53.

Hurt, E., Hannus, S., Schmelzl, B., Lau, D., Tollervey, D., and Simos, G. (1999). A novel in vivo assay reveals inhibition of ribosomal nuclear export in ran-cycle and nucleoporin mutants. *The Journal of cell biology 144*, 389–401.

Jaenicke, R. (1987). Folding and association of proteins. *Progress in Biophysics and Molecular Biology 49*, 117–237.

Jakob, U. and Buchner, J. (1994). Assisting spontaneity: the role of Hsp90 and small Hsps as molecular chaperones. *Trends in biochemical sciences 19*, 205–11.

Jeng, W., Lee, S., Sung, N., Lee, J., and Tsai, F. T. F. (2015). Molecular chaperones: guardians of the proteome in normal and disease states. *F1000Research 4*.

Jeong, J.-Y., Yim, H.-S., Ryu, J.-Y., Lee, H. S., Lee, J.-H., Seen, D.-S., and Kang, S. G. (2012). One-step sequence- and ligation-independent cloning as a rapid and versatile cloning method for functional genomics studies. *Applied and environmental microbiology 78*, 5440–3.

Joab, I., Radanyi, C., Renoir, M., Buchou, T., Catelli, M. G., Binart, N., Mester, J., and Baulieu, E. E. (1984). Common non-hormone binding component in non-transformed chick oviduct receptors of four steroid hormones. *Nature 308*, 850–3.

Johnson, B. D., Schumacher, R. J., Ross, E. D., and Toft, D. O. (1998). Hop modulates Hsp70/Hsp90 interactions in protein folding. *The Journal of Biological Chemistry 273*, 3679–86.

Johnson, J. L. (2012). Evolution and function of diverse Hsp90 homologs and cochaperone proteins. *Biochimica et biophysica acta 1823*, 607–13.

Johnson, J. L. and Toft, D. O. (1994). A novel chaperone complex for steroid receptors involving heat shock proteins, immunophilins, and p23. *The Journal of Biological Chemistry 269*, 24989–93.

Kabsch, W. (2010). XDS. *Acta crystallographica. Section D, Biological crystallography 66*, 125–32.

Kachroo, A. H., Laurent, J. M., Yellman, C. M., Meyer, A. G., Wilke, C. O., and Marcotte, E. M. (2015). Evolution. Systematic humanization of yeast genes reveals conserved functions and genetic modularity. *Science (New York, N.Y.) 348*, 921–5.

Kaiser, C. M., Goldman, D. H., Chodera, J. D., Tinoco, I., and Bustamante, C. (2011). The ribosome modulates nascent protein folding. *Science (New York, N.Y.) 334*, 1723–7.

Kallstrom, G., Hedges, J., and Johnson, A. (2003). The putative GTPases Nog1p and Lsg1p are required for 60S ribosomal subunit biogenesis and are localized to the nucleus and cytoplasm, respectively. *Molecular and cellular biology 23*, 4344–55.

Kampinga, H. H., Brunsting, J. F., Stege, G. J., Konings, A. W., and Landry, J. (1994). Cells overexpressing Hsp27 show accelerated recovery from heat-induced nuclear protein aggregation. *Biochemical and biophysical research communications 204*, 1170–7.

Kampinga, H. H. and Craig, E. A. (2010). The HSP70 chaperone machinery: J proteins as drivers of functional specificity. *Nature reviews. Molecular cell biology 11*, 579–92.

Kang, H., Sayner, S. L., Gross, K. L., Russell, L. C., and Chinkers, M. (2001). Identification of amino acids in the tetratricopeptide repeat and C-terminal domains of protein phosphatase 5 involved in autoinhibition and lipid activation. *Biochemistry 40*, 10485–90.

Karagöz, G. E., Duarte, A. M. S., Ippel, H., Uetrecht, C., Sinnige, T., van Rosmalen, M., Hausmann, J., Heck, A. J. R., Boelens, R., and Rüdiger, S. G. D. (2011). N-terminal domain of human Hsp90 triggers binding to the cochaperone p23. *Proceedings of the National Academy of Sciences of the United States of America 108*, 580–5.

Kiktev, D. A., Patterson, J. C., Müller, S., Bariar, B., Pan, T., and Chernoff, Y. O. (2012). Regulation of chaperone effects on a yeast prion by cochaperone Sgt2. *Molecular and cellular biology 32*, 4960–70.

Kim, Y. E., Hipp, M. S., Bracher, A., Hayer-Hartl, M., and Hartl, F. U. (2013). Molecular chaperone functions in protein folding and proteostasis. *Annual review of biochemistry 82*, 323–55.

Kirschke, E., Goswami, D., Southworth, D., Griffin, P. R., and Agard, D. A. (2014). Glucocorticoid receptor function regulated by coordinated action of the Hsp90 and Hsp70 chaperone cycles. *Cell 157*, 1685–97.

Kitagawa, K., Skowyra, D., Elledge, S. J., Harper, J. W., and Hieter, P. (1999). SGT1 encodes an essential component of the yeast kinetochore assembly pathway and a novel subunit of the SCF ubiquitin ligase complex. *Molecular cell 4*, 21–33.

Kityk, R., Kopp, J., Sinning, I., and Mayer, M. P. (2012). Structure and dynamics of the ATP-bound open conformation of Hsp70 chaperones. *Molecular cell 48*, 863–74.

Koplin, A., Preissler, S., Ilina, Y., Koch, M., Scior, A., Erhardt, M., and Deuerling, E. (2010). A dual function for chaperones SSB-RAC and the NAC nascent polypeptide-associated complex on ribosomes. *The Journal of cell biology 189*, 57–68.

Kosolapov, A. and Deutsch, C. (2009). Tertiary interactions within the ribosomal exit tunnel. *Nature structural & molecular biology 16*, 405–11.

Kovacs, J. J., Murphy, P. J. M., Gaillard, S., Zhao, X., Wu, J.-T., Nicchitta, C. V., Yoshida, M., Toft, D. O., Pratt, W. B., and Yao, T.-P. (2005). HDAC6 regulates Hsp90 acetylation and chaperone-dependent activation of glucocorticoid receptor. *Molecular cell 18*, 601–7.

Kozin, M. B. and Svergun, D. I. (2001). Automated matching of high- and low-resolution structural models. *Journal of Applied Crystallography 34*, 33–41.

Kramer, G., Rauch, T., Rist, W., Vorderwülbecke, S., Patzelt, H., Schulze-Specking, A., Ban, N., Deuerling, E., and Bukau, B. (2002). L23 protein functions as a chaperone docking site on the ribosome. *Nature 419*, 171–4.

Krukenberg, K. A., Förster, F., Rice, L. M., Sali, A., and Agard, D. A. (2008). Multiple conformations of E. coli Hsp90 in solution: insights into the conformational dynamics of Hsp90. *Structure (London, England : 1993) 16*, 755–65.

Kumar, N., Gaur, D., Gupta, A., Puri, A., and Sharma, D. (2015). Hsp90-Associated Immunophilin Homolog Cpr7 Is Required for the Mitotic Stability of [URE3] Prion in Saccharomyces cerevisiae. *PLoS genetics 11*, e1005567.

Kumsta, C. and Jakob, U. (2009). Redox-regulated chaperones. *Biochemistry 48*, 4666–76.

Lafourcade, C., Galan, J.-M., Gloor, Y., Haguenauer-Tsapis, R., and Peter, M. (2004). The GTPase-activating enzyme Gyp1p is required for recycling of internalized membrane material by inactivation of the Rab/Ypt GTPase Ypt1p. *Molecular and cellular biology 24*, 3815–26.

Lai, B. T., Chin, N. W., Stanek, A. E., Keh, W., and Lanks, K. W. (1984). Quantitation and intracellular localization of the 85K heat shock protein by using monoclonal and polyclonal antibodies. *Molecular and Cellular Biology 4*, 2802–10.

Lancaster, D. L., Dobson, C. M., and Rachubinski, R. A. (2013). Chaperone proteins select and maintain [PIN+] prion conformations in Saccharomyces cerevisiae. *The Journal of biological chemistry 288*, 1266–76.

Lavery, L. A., Partridge, J. R., Ramelot, T. A., Elnatan, D., Kennedy, M. A., and Agard, D. A. (2014). Structural asymmetry in the closed state of mitochondrial Hsp90 (TRAP1) supports a two-step ATP hydrolysis mechanism. *Molecular cell 53*, 330–43.

Lee, G. J., Pokala, N., and Vierling, E. (1995). Structure and in vitro molecular chaperone activity of cytosolic small heat shock proteins from pea. *The Journal of biological chemistry 270*, 10432–8.

Lee, G. J., Roseman, A. M., Saibil, H. R., and Vierling, E. (1997). A small heat shock protein stably binds heat-denatured model substrates and can maintain a substrate in a folding-competent state. *The EMBO journal 16*, 659–71.

Lee, S., Choi, J.-M., and Tsai, F. T. F. (2007). Visualizing the ATPase cycle in a protein disaggregating machine: structural basis for substrate binding by ClpB. *Molecular cell 25*, 261–71.

Lee, S., Sielaff, B., Lee, J., and Tsai, F. T. F. (2010). CryoEM structure of Hsp104 and its mechanistic implication for protein disaggregation. *Proceedings of the National Academy of Sciences of the United States of America 107*, 8135–40.

Lee, S., Sowa, M. E., Watanabe, Y.-h., Sigler, P. B., Chiu, W., Yoshida, M., and Tsai, F. T. F. (2003). The structure of ClpB: a molecular chaperone that rescues proteins from an aggregated state. *Cell 115*, 229–40.

Levinthal, C. (1968). Are there pathways for protein folding? *Journal de Chimie Physique et de Physico-Chimie Biologique 65*, 44–45.

Li, J., Richter, K., and Buchner, J. (2011). Mixed Hsp90-cochaperone complexes are important for the progression of the reaction cycle. *Nature Structural & Molecular Biology 18*, 61–6.

Li, J., Richter, K., Reinstein, J., and Buchner, J. (2013). Integration of the accelerator Aha1 in the Hsp90 co-chaperone cycle. *Nature Structural & Molecular Biology 20*, 326–31.

Li, J., Soroka, J., and Buchner, J. (2012). The Hsp90 chaperone machinery: conformational dynamics and regulation by co-chaperones. *Biochimica et Biophysica Acta 1823*, 624–35.

Liberek, K., Lewandowska, A., and Zietkiewicz, S. (2008). Chaperones in control of protein disaggregation. *The EMBO journal 27*, 328–35.

Lin, Z., Madan, D., and Rye, H. S. (2008). GroEL stimulates protein folding through forced unfolding. *Nature structural & molecular biology 15*, 303–11.

Lo, K.-Y., Li, Z., Bussiere, C., Bresson, S., Marcotte, E. M., and Johnson, A. W. (2010). Defining the pathway of cytoplasmic maturation of the 60S ribosomal subunit. *Molecular cell 39*, 196–208.

Loar, J. W., Seiser, R. M., Sundberg, A. E., Sagerson, H. J., Ilias, N., Zobel-Thropp, P., Craig, E. A., and Lycan, D. E. (2004). Genetic and biochemical interactions among Yar1, Ltv1 and Rps3 define novel links between environmental stress and ribosome biogenesis in Saccharomyces cerevisiae. *Genetics 168*, 1877–89.

Lorenz, O. R., Freiburger, L., Rutz, D. A., Krause, M., Zierer, B. K., Alvira, S., Cuéllar, J., Valpuesta, J. M., Madl, T., Sattler, M., and Buchner, J. (2014). Modulation of the Hsp90 chaperone cycle by a stringent client protein. *Molecular cell 53*, 941–53.

Lotz, G. P., Lin, H., Harst, A., and Obermann, W. M. J. (2003). Aha1 binds to the middle domain of Hsp90, contributes to client protein activation, and stimulates the ATPase activity of the molecular chaperone. *The Journal of Biological Chemistry 278*, 17228–35.

Lum, R., Tkach, J. M., Vierling, E., and Glover, J. R. (2004). Evidence for an unfolding/threading mechanism for protein disaggregation by Saccharomyces cerevisiae Hsp104. *The Journal of biological chemistry 279*, 29139–46.

MacLean, M. and Picard, D. (2003). Cdc37 goes beyond Hsp90 and kinases. *Cell Stress & Chaperones 8*, 114–9.

Mandal, A. K., Lee, P., Chen, J. a., Nillegoda, N., Heller, A., DiStasio, S., Oen, H., Victor, J., Nair, D. M., Brodsky, J. L., and Caplan, A. J. (2007). Cdc37 has distinct roles in protein kinase quality control that protect nascent chains from degradation and promote posttranslational maturation. *The Journal of Cell Biology 176*, 319–28.

Marion, R. M., Regev, A., Segal, E., Barash, Y., Koller, D., Friedman, N., and O'Shea, E. K. (2004). Sfp1 is a stress- and nutrient-sensitive regulator of ribosomal protein gene expression. *Proceedings of the National Academy of Sciences of the United States of America 101*, 14315–22.

Marozkina, N. V., Yemen, S., Borowitz, M., Liu, L., Plapp, M., Sun, F., Islam, R., Erdmann-Gilmore, P., Townsend, R. R., Lichti, C. F., Mantri, S., Clapp, P. W., Randell, S. H., Gaston, B., and Zaman, K. (2010). Hsp 70/Hsp 90 organizing protein as a nitrosylation target in cystic fibrosis therapy. *Proceedings of the National Academy of Sciences of the United States of America 107*.

Marsh, J. A., Kalton, H. M., and Gaber, R. F. (1998). Cns1 is an essential protein associated with the hsp90 chaperone complex in Saccharomyces cerevisiae that can restore cyclophilin 40-dependent functions in cpr7Delta cells. *Molecular and Cellular Biology 18*, 7353–9.

Mayer, M. P. (2010). Gymnastics of molecular chaperones. *Molecular cell 39*, 321–31.

Mayer, M. P. and Bukau, B. (2005). Hsp70 chaperones: cellular functions and molecular mechanism. *Cellular and molecular life sciences : CMLS 62*, 670–84.

Mayer, M. P. and Le Breton, L. (2015). Hsp90: breaking the symmetry. *Molecular cell 58*, 8–20.

Mayer, M. P., Nikolay, R., and Bukau, B. (2002). Aha, another regulator for hsp90 chaperones. *Molecular Cell 10*, 1255–6.

Mayer, M. P., Prodromou, C., and Frydman, J. (2009). The Hsp90 mosaic: a picture emerges. *Nature Structural & Molecular Biology 16*, 2–6.

Mayr, C., Richter, K., Lilie, H., and Buchner, J. (2000). Cpr6 and Cpr7, two closely related Hsp90-associated immunophilins from Saccharomyces cerevisiae, differ in their functional properties. *The Journal of Biological Chemistry 275*, 34140–6.

McClellan, A. J., Tam, S., Kaganovich, D., and Frydman, J. (2005). Protein quality control: chaperones culling corrupt conformations. *Nature cell biology 7*, 736–41.

McClellan, A. J., Xia, Y., Deutschbauer, A. M., Davis, R. W., Gerstein, M., and Frydman, J. (2007). Diverse cellular functions of the Hsp90 molecular chaperone uncovered using systems approaches. *Cell 131*, 121–35.

McCoy, A. J., Grosse-Kunstleve, R. W., Adams, P. D., Winn, M. D., Storoni, L. C., and Read, R. J. (2007). Phaser crystallographic software. *Journal of applied crystallography 40*, 658–674.

McHaourab, H. S., Godar, J. A., and Stewart, P. L. (2009). Structure and mechanism of protein stability sensors: chaperone activity of small heat shock proteins. *Biochemistry 48*, 3828–37.

McLaughlin, S. H., Smith, H. W., and Jackson, S. E. (2002). Stimulation of the weak ATPase activity of human hsp90 by a client protein. *Journal of molecular biology 315*, 787–98.

McLaughlin, S. H., Sobott, F., Yao, Z.-p., Zhang, W., Nielsen, P. R., Grossmann, J. G., Laue, E. D., Robinson, C. V., and Jackson, S. E. (2006). The co-chaperone p23 arrests the Hsp90 ATPase cycle to trap client proteins. *Journal of Molecular Biology 356*, 746–58.

Merz, F., Boehringer, D., Schaffitzel, C., Preissler, S., Hoffmann, A., Maier, T., Rutkowska, A., Lozza, J., Ban, N., Bukau, B., and Deuerling, E. (2008). Molecular mechanism and structure of Trigger Factor bound to the translating ribosome. *The EMBO journal 27*, 1622–32.

Meyer, A. E., Hung, N.-J., Yang, P., Johnson, A. W., and Craig, E. A. (2007). The specialized cytosolic J-protein, Jjj1, functions in 60S ribosomal subunit biogenesis. *Proceedings of the National Academy of Sciences of the United States of America 104*, 1558–63.

Meyer, P., Prodromou, C., Hu, B., Vaughan, C., Roe, S. M., Panaretou, B., Piper, P. W., and Pearl, L. H. (2003). Structural and functional analysis of the middle segment of hsp90: implications for ATP hydrolysis and client protein and cochaperone interactions. *Molecular cell 11*, 647–58.

Meyer, P., Prodromou, C., Liao, C., Hu, B., Roe, S. M., Vaughan, C. K., Vlasic, I., Panaretou, B., Piper, P. W., and Pearl, L. H. (2004). Structural basis for recruitment of the ATPase activator Aha1 to the Hsp90 chaperone machinery. *The EMBO journal 23*, 1402–10.

Mickler, M., Hessling, M., Ratzke, C., Buchner, J., and Hugel, T. (2009). The large conformational changes of Hsp90 are only weakly coupled to ATP hydrolysis. *Nature Structural & Molecular Biology 16*, 281–6.

Milkereit, P., Strauss, D., Bassler, J., Gadal, O., Kühn, H., Schütz, S., Gas, N., Lechner, J., Hurt, E., and Tschochner, H. (2003). A Noc complex specifically involved in the formation and nuclear export of ribosomal 40 S subunits. *The Journal of biological chemistry 278*, 4072–81.

Mishra, P. and Bolon, D. N. A. (2014). Designed Hsp90 heterodimers reveal an asymmetric ATPase-driven mechanism in vivo. *Molecular cell 53*, 344–50.

Mitschke, L. (2012). *Functional analysis of the co-chaperones Aha1 and Cns1 from S. cerevisiae*. Ph. D. thesis, Technische Universität München.

Mizuta, K. and Warner, J. R. (1994). Continued functioning of the secretory pathway is essential for ribosome synthesis. *Molecular and cellular biology 14*, 2493–502.

Mnaimneh, S., Davierwala, A. P., Haynes, J., Moffat, J., Peng, W.-T., Zhang, W., Yang, X., Pootoolal, J., Chua, G., Lopez, A., Trochesset, M., Morse, D., Krogan, N. J., Hiley, S. L., Li, Z., Morris, Q., Grigull, J., Mitsakakis, N., Roberts, C. J., Greenblatt, J. F., Boone, C., Kaiser, C. A., Andrews, B. J., and Hughes, T. R. (2004). Exploration of essential gene functions via titratable promoter alleles. *Cell 118*, 31–44.

Moehle, E. A., Ryan, C. J., Krogan, N. J., Kress, T. L., and Guthrie, C. (2012). The yeast SR-like protein Npl3 links chromatin modification to mRNA processing. *PLoS genetics 8*, e1003101.

Mollapour, M., Bourboulia, D., Beebe, K., Woodford, M. R., Polier, S., Hoang, A., Chelluri, R., Li, Y., Guo, A., Lee, M.-J., Fotooh-Abadi, E., Khan, S., Prince, T., Miyajima, N., Yoshida, S., Tsutsumi, S., Xu, W., Panaretou, B., Stetler-Stevenson, W. G., Bratslavsky, G., Trepel, J. B., Prodromou, C., and Neckers, L. (2014). Asymmetric Hsp90 N domain SUMOylation recruits Aha1 and ATP-competitive inhibitors. *Molecular cell 53*, 317–29.

Mollapour, M., Tsutsumi, S., Donnelly, A. C., Beebe, K., Tokita, M. J., Lee, M.-J., Lee, S., Morra, G., Bourboulia, D., Scroggins, B. T., Colombo, G., Blagg, B. S., Panaretou, B., Stetler-Stevenson, W. G., Trepel, J. B., Piper, P. W., Prodromou, C., Pearl, L. H., and Neckers, L. (2010). Swe1Wee1-dependent tyrosine phosphorylation of Hsp90 regulates distinct facets of chaperone function. *Molecular cell 37*, 333–43.

Mollapour, M., Tsutsumi, S., Kim, Y. S., Trepel, J., and Neckers, L. (2011). Casein kinase 2 phosphorylation of Hsp90 threonine 22 modulates chaperone function and drug sensitivity. *Oncotarget 2*, 407–17.

Mollapour, M., Tsutsumi, S., Truman, A. W., Xu, W., Vaughan, C. K., Beebe, K., Konstantinova, A., Vourganti, S., Panaretou, B., Piper, P. W., Trepel, J. B., Prodromou, C., Pearl, L. H., and Neckers, L. (2011). Threonine 22 phosphorylation attenuates Hsp90 interaction with cochaperones and affects its chaperone activity. *Molecular cell 41*, 672–81.

Moosavi, B., Wongwigkarn, J., and Tuite, M. F. (2010). Hsp70/Hsp90 co-chaperones are required for efficient Hsp104-mediated elimination of the yeast [PSI(+)] prion but not for prion propagation. *Yeast (Chichester, England) 27*, 167–79.

Morishima, Y., Kanelakis, K. C., Silverstein, A. M., Dittmar, K. D., Estrada, L., and Pratt, W. B. (2000). The Hsp organizer protein hop enhances the rate of but is not essential for glucocorticoid receptor folding by the multiprotein Hsp90-based chaperone system. *The Journal of biological chemistry 275*, 6894–900.

Motohashi, K., Watanabe, Y., Yohda, M., and Yoshida, M. (1999). Heat-inactivated proteins are rescued by the DnaK.J-GrpE set and ClpB chaperones. *Proceedings of the National Academy of Sciences of the United States of America 96*, 7184–9.

Muñoz, I. G., Yébenes, H., Zhou, M., Mesa, P., Serna, M., Park, A. Y., Bragado-Nilsson, E., Beloso, A., de Cárcer, G., Malumbres, M., Robinson, C. V., Valpuesta, J. M., and Montoya, G. (2011). Crystal structure of the open conformation of the mammalian chaperonin CCT in complex with tubulin. *Nature structural & molecular biology 18*, 14–9.

Nathan, D. F., Vos, M. H., and Lindquist, S. (1999). Identification of SSF1, CNS1, and HCH1 as multicopy suppressors of a Saccharomyces cerevisiae Hsp90 loss-of-function mutation. *Proceedings of the National Academy of Sciences of the United States of America 96*, 1409–14.

Neuwald, A. F., Aravind, L., Spouge, J. L., and Koonin, E. V. (1999). AAA+: A class of chaperone-like ATPases associated with the assembly, operation, and disassembly of protein complexes. *Genome research 9*, 27–43.

Nielsen, K. H., Szamecz, B., Valásek, L., Jivotovskaya, A., Shin, B.-S., and Hinnebusch, A. G. (2004). Functions of eIF3 downstream of 48S assembly impact AUG recognition and GCN4 translational control. *The EMBO journal 23*, 1166–77.

Nillegoda, N. B., Kirstein, J., Szlachcic, A., Berynskyy, M., Stank, A., Stengel, F., Arnsburg, K., Gao, X., Scior, A., Aebersold, R., Guilbride, D. L., Wade, R. C., Morimoto, R. I., Mayer, M. P., and Bukau, B. (2015). Crucial HSP70 co-chaperone complex unlocks metazoan protein disaggregation. *Nature 524*, 247–51.

Nilsson, O. B., Hedman, R., Marino, J., Wickles, S., Bischoff, L., Johansson, M., Müller-Lucks, A., Trovato, F., Puglisi, J. D., O'Brien, E. P., Beckmann, R., and von Heijne, G. (2015). Cotranslational Protein Folding inside the Ribosome Exit Tunnel. *Cell reports 12*, 1533–40.

Nørby, J. G. (1988). Coupled assay of Na+,K+-ATPase activity. *Methods in enzymology 156*, 116–9.

Obermann, W. M., Sondermann, H., Russo, A. A., Pavletich, N. P., and Hartl, F. U. (1998). In vivo function of Hsp90 is dependent on ATP binding and ATP hydrolysis. *The Journal of cell biology 143*, 901–10.

O'Brien, E. P., Christodoulou, J., Vendruscolo, M., and Dobson, C. M. (2011). New scenarios of protein folding can occur on the ribosome. *Journal of the American Chemical Society 133*, 513–26.

Ostermann, J., Horwich, A. L., Neupert, W., and Hartl, F. U. (1989). Protein folding in mitochondria requires complex formation with hsp60 and ATP hydrolysis. *Nature 341*, 125–30.

Oughtred, R., Chatr-aryamontri, A., Breitkreutz, B.-J., Chang, C. S., Rust, J. M., Theesfeld, C. L., Heinicke, S., Breitkreutz, A., Chen, D., Hirschman, J., Kolas, N., Livstone, M. S., Nixon, J., O'Donnell, L., Ramage, L., Winter, A., Reguly, T., Sellam, A., Stark, C., Boucher, L., Dolinski, K., and Tyers, M. (2016). BioGRID: A Resource for Studying Biological Interactions in Yeast. *Cold Spring Harbor protocols 2016*, pdb.top080754.

Pan, X., Ye, P., Yuan, D. S., Wang, X., Bader, J. S., and Boeke, J. D. (2006). A DNA integrity network in the yeast Saccharomyces cerevisiae. *Cell 124*, 1069–81.

Panaretou, B., Prodromou, C., Roe, S. M., O'Brien, R., Ladbury, J. E., Piper, P. W., and Pearl, L. H. (1998). ATP binding and hydrolysis are essential to the function of the Hsp90 molecular chaperone in vivo. *The EMBO Journal 17*, 4829–36.

Panaretou, B., Siligardi, G., Meyer, P., Maloney, A., Sullivan, J. K., Singh, S., Millson, S. H., Clarke, P. a., Naaby-Hansen, S., Stein, R., Cramer, R., Mollapour, M., Workman, P., Piper, P. W., Pearl, L. H., and Prodromou, C. (2002). Activation of the ATPase activity of hsp90 by the stress-regulated cochaperone aha1. *Molecular Cell 10*, 1307–18.

Parsell, D. A., Kowal, A. S., Singer, M. A., and Lindquist, S. (1994). Protein disaggregation mediated by heat-shock protein Hsp104. *Nature 372*, 475–8.

Pearl, L. H. and Prodromou, C. (2006). Structure and mechanism of the Hsp90 molecular chaperone machinery. *Annual review of biochemistry 75*, 271–94.

Pearl, L. H., Prodromou, C., and Workman, P. (2008). The Hsp90 molecular chaperone: an open and shut case for treatment. *The Biochemical Journal 410*, 439–53.

Peattie, D. A., Harding, M. W., Fleming, M. A., DeCenzo, M. T., Lippke, J. A., Livingston, D. J., and Benasutti, M. (1992). Expression and characterization of human FKBP52, an immunophilin that associates with the 90-kDa heat shock protein and is a component of steroid receptor complexes. *Proceedings of the National Academy of Sciences of the United States of America 89*, 10974–8.

Pech, M., Spreter, T., Beckmann, R., and Beatrix, B. (2010). Dual binding mode of the nascent polypeptide-associated complex reveals a novel universal adapter site on the ribosome. *The Journal of biological chemistry 285*, 19679–87.

Peisker, K., Braun, D., Wölfle, T., Hentschel, J., Fünfschilling, U., Fischer, G., Sickmann, A., and Rospert, S. (2008). Ribosome-associated complex binds to ribosomes in close proximity of Rpl31 at the exit of the polypeptide tunnel in yeast. *Molecular biology of the cell 19*, 5279–88.

Pertschy, B., Saveanu, C., Zisser, G., Lebreton, A., Tengg, M., Jacquier, A., Liebminger, E., Nobis, B., Kappel, L., van der Klei, I., Högenauer, G., Fromont-Racine, M., and Bergler, H. (2007). Cytoplasmic recycling of 60S preribosomal factors depends on the AAA protein Drg1. *Molecular and cellular biology 27*, 6581–92.

Peschek, J., Braun, N., Rohrberg, J., Back, K. C., Kriehuber, T., Kastenmüller, A., Weinkauf, S., and Buchner, J. (2013). Regulated structural transitions unleash the chaperone activity of αB-crystallin. *Proceedings of the National Academy of Sciences of the United States of America 110*, E3780–9.

Petoukhov, M. V., Franke, D., Shkumatov, A. V., Tria, G., Kikhney, A. G., Gajda, M., Gorba, C., Mertens, H. D. T., Konarev, P. V., and Svergun, D. I. (2012). New developments in the ATSAS program package for small-angle scattering data analysis. *Journal of Applied Crystallography 45*, 342–350.

Pirkl, F. and Buchner, J. (2001). Functional analysis of the Hsp90-associated human peptidyl prolyl cis/trans isomerases FKBP51, FKBP52 and Cyp40. *Journal of molecular biology 308*, 795–806.

Pratt, W. B., Morishima, Y., and Osawa, Y. (2008). The Hsp90 chaperone machinery regulates signaling by modulating ligand binding clefts. *The Journal of Biological Chemistry 283*, 22885–9.

Pratt, W. B., Silverstein, A. M., and Galigniana, M. D. (1999). A model for the cytoplasmic trafficking of signalling proteins involving the hsp90-binding immunophilins and p50cdc37. *Cellular signalling 11*, 839–51.

Pratt, W. B. and Toft, D. O. (1997). Steroid receptor interactions with heat shock protein and immunophilin chaperones. *Endocrine Reviews 18*, 306–60.

Pratt, W. B. and Toft, D. O. (2003). Regulation of signaling protein function and trafficking by the hsp90/hsp70-based chaperone machinery. *Experimental Biology and Medicine 228*, 111–33.

Preissler, S. and Deuerling, E. (2012). Ribosome-associated chaperones as key players in proteostasis. *Trends in biochemical sciences 37*, 274–83.

Prodromou, C. (2012). The 'active life' of Hsp90 complexes. *Biochimica et biophysica acta 1823*, 614–23.

Prodromou, C., Panaretou, B., Chohan, S., Siligardi, G., O'Brien, R., Ladbury, J. E., Roe, S. M., Piper, P. W., and Pearl, L. H. (2000). The ATPase cycle of Hsp90 drives a molecular 'clamp' via transient dimerization of the N-terminal domains. *The EMBO Journal 19*, 4383–92.

Prodromou, C., Roe, S. M., O'Brien, R., Ladbury, J. E., Piper, P. W., and Pearl, L. H. (1997). Identification and structural characterization of the ATP/ADP-binding site in the Hsp90 molecular chaperone. *Cell 90*, 65–75.

Prodromou, C., Roe, S. M., Piper, P. W., and Pearl, L. H. (1997). A molecular clamp in the crystal structure of the N-terminal domain of the yeast Hsp90 chaperone. *Nature structural biology 4*, 477–82.

Prodromou, C., Siligardi, G., O'Brien, R., Woolfson, D. N., Regan, L., Panaretou, B., Ladbury, J. E., Piper, P. W., and Pearl, L. H. (1999). Regulation of Hsp90 ATPase activity by tetratricopeptide repeat (TPR)-domain co-chaperones. *The EMBO Journal 18*, 754–62.

Rakwalska, M. and Rospert, S. (2004). The ribosome-bound chaperones RAC and Ssb1/2p are required for accurate translation in Saccharomyces cerevisiae. *Molecular and cellular biology 24*, 9186–97.

Ratajczak, T., Ward, B. K., Cluning, C., and Allan, R. K. (2009). Cyclophilin 40: an Hsp90-cochaperone associated with apo-steroid receptors. *The international journal of biochemistry & cell biology 41*, 1652–5.

Reissmann, S., Joachimiak, L. A., Chen, B., Meyer, A. S., Nguyen, A., and Frydman, J. (2012). A gradient of ATP affinities generates an asymmetric power stroke driving the chaperonin TRIC/CCT folding cycle. *Cell reports 2*, 866–77.

Retzlaff, M., Hagn, F., Mitschke, L., Hessling, M., Gugel, F., Kessler, H., Richter, K., and Buchner, J. (2010). Asymmetric activation of the hsp90 dimer by its cochaperone aha1. *Molecular cell 37*, 344–54.

Richter, K., Haslbeck, M., and Buchner, J. (2010). The heat shock response: life on the verge of death. *Molecular cell 40*, 253–66.

Richter, K., Muschler, P., Hainzl, O., Reinstein, J., and Buchner, J. (2003). Sti1 is a non-competitive inhibitor of the Hsp90 ATPase. Binding prevents the N-terminal dimerization reaction during the atpase cycle. *The Journal of Biological Chemistry 278*, 10328–33.

Richter, K., Reinstein, J., and Buchner, J. (2002). N-terminal residues regulate the catalytic efficiency of the Hsp90 ATPase cycle. *The Journal of biological chemistry 277*, 44905–10.

Richter, K., Soroka, J., Skalniak, L., Leskovar, A., Hessling, M., Reinstein, J., and Buchner, J. (2008). Conserved conformational changes in the ATPase cycle of human Hsp90. *The Journal of biological chemistry 283*, 17757–65.

Richter, K., Walter, S., and Buchner, J. (2004). The Co-chaperone Sba1 connects the ATPase reaction of Hsp90 to the progression of the chaperone cycle. *Journal of Molecular Biology 342*, 1403–13.

Ripmaster, T. L., Vaughn, G. P., and Woolford, J. L. (1993). DRS1 to DRS7, novel genes required for ribosome assembly and function in Saccharomyces cerevisiae. *Molecular and cellular biology 13*, 7901–12.

Rivenzon-Segal, D., Wolf, S. G., Shimon, L., Willison, K. R., and Horovitz, A. (2005). Sequential ATP-induced allosteric transitions of the cytoplasmic chaperonin containing TCP-1 revealed by EM analysis. *Nature structural & molecular biology 12*, 233–7.

Roe, S. M., Ali, M. M. U., Meyer, P., Vaughan, C. K., Panaretou, B., Piper, P. W., Prodromou, C., and Pearl, L. H. (2004). The Mechanism of Hsp90 regulation by the protein kinase-specific cochaperone p50(cdc37). *Cell 116*, 87–98.

Rogalla, T., Ehrnsperger, M., Preville, X., Kotlyarov, A., Lutsch, G., Ducasse, C., Paul, C., Wieske, M., Arrigo, A. P., Buchner, J., and Gaestel, M. (1999). Regulation of Hsp27 oligomerization, chaperone function, and protective activity against oxidative stress/tumor necrosis factor alpha by phosphorylation. *The Journal of biological chemistry 274*, 18947–56.

Röhl, A., Tippel, F., Bender, E., Schmid, A. B., Richter, K., Madl, T., and Buchner, J. (2015). Hop/Sti1 phosphorylation inhibits its co-chaperone function. *EMBO reports 16*, 240–9.

Rüßmann, F., Stemp, M. J., Mönkemeyer, L., Etchells, S. A., Bracher, A., and Hartl, F. U. (2012). Folding of large multidomain proteins by partial encapsulation in the chaperonin TRiC/CCT. *Proceedings of the National Academy of Sciences of the United States of America 109*, 21208–15.

Saibil, H. R., Fenton, W. A., Clare, D. K., and Horwich, A. L. (2013). Structure and allostery of the chaperonin GroEL. *Journal of molecular biology 425*, 1476–87.

Sanchez, E. R., Toft, D. O., Schlesinger, M. J., and Pratt, W. B. (1985). Evidence that the 90-kDa phosphoprotein associated with the untransformed L-cell glucocorticoid receptor is a murine heat shock protein. *The Journal of biological chemistry 260*, 12398–401.

Sauer, R. T. and Baker, T. A. (2011). AAA+ proteases: ATP-fueled machines of protein destruction. *Annual review of biochemistry 80*, 587–612.

Scheibel, T., Neuhofen, S., Weikl, T., Mayr, C., Reinstein, J., Vogel, P. D., and Buchner, J. (1997). ATP-binding properties of human Hsp90. *The Journal of biological chemistry 272*, 18608–13.

Scheufler, C., Brinker, A., Bourenkov, G., Pegoraro, S., Moroder, L., Bartunik, H., Hartl, F. U., and Moarefi, I. (2000). Structure of TPR domain-peptide complexes: critical elements in the assembly of the Hsp70-Hsp90 multichaperone machine. *Cell 101*, 199–210.

Schmid, A. B., Lagleder, S., Gräwert, M. A., Röhl, A., Hagn, F., Wandinger, S. K., Cox, M. B., Demmer, O., Richter, K., Groll, M., Kessler, H., and Buchner, J. (2012). The architecture of functional modules in the Hsp90 co-chaperone Sti1/Hop. *The EMBO Journal 31*, 1506–17.

Schmidpeter, P. A. M. and Schmid, F. X. (2015). Prolyl isomerization and its catalysis in protein folding and protein function. *Journal of molecular biology 427*, 1609–31.

Schneider, T. R. and Sheldrick, G. M. (2002). Substructure solution with SHELXD. *Acta crystallographica. Section D, Biological crystallography 58*, 1772–9.

Schuh, S., Yonemoto, W., Brugge, J., Bauer, V. J., Riehl, R. M., Sullivan, W. P., and Toft, D. O. (1985). A 90,000-dalton binding protein common to both steroid receptors and the Rous sarcoma virus transforming protein, pp60v-src. *The Journal of biological chemistry 260*, 14292–6.

Schuldiner, M., Metz, J., Schmid, V., Denic, V., Rakwalska, M., Schmitt, H. D., Schwappach, B., and Weissman, J. S. (2008). The GET complex mediates insertion of tail-anchored proteins into the ER membrane. *Cell 134*, 634–45.

Scroggins, B. T. and Neckers, L. (2007). Post-translational modification of heat-shock protein 90: impact on chaperone function. *Expert opinion on drug discovery 2*, 1403–14.

Scroggins, B. T., Robzyk, K., Wang, D., Marcu, M. G., Tsutsumi, S., Beebe, K., Cotter, R. J., Felts, S., Toft, D., Karnitz, L., Rosen, N., and Neckers, L. (2007). An acetylation site in the middle domain of Hsp90 regulates chaperone function. *Molecular cell 25*, 151–9.

Seitz, T., Thoma, R., Schoch, G. A., Stihle, M., Benz, J., D'Arcy, B., Wiget, A., Ruf, A., Hennig, M., and Sterner, R. (2010). Enhancing the stability and solubility of the glucocorticoid receptor ligand-binding domain by high-throughput library screening. *Journal of molecular biology 403*, 562–77.

Senger, B., Lafontaine, D. L., Graindorge, J. S., Gadal, O., Camasses, A., Sanni, A., Garnier, J. M., Breitenbach, M., Hurt, E., and Fasiolo, F. (2001). The nucle(ol)ar Tif6p and Efl1p are required for a late cytoplasmic step of ribosome synthesis. *Molecular cell 8*, 1363–73.

Sharma, S., Chakraborty, K., Müller, B. K., Astola, N., Tang, Y.-C., Lamb, D. C., Hayer-Hartl, M., and Hartl, F. U. (2008). Monitoring protein conformation along the pathway of chaperonin-assisted folding. *Cell 133*, 142–53.

Shiau, A. K., Harris, S. F., Southworth, D. R., and Agard, D. A. (2006). Structural Analysis of E. coli hsp90 reveals dramatic nucleotide-dependent conformational rearrangements. *Cell 127*, 329–40.

Siligardi, G., Panaretou, B., Meyer, P., Singh, S., Woolfson, D. N., Piper, P. W., Pearl, L. H., and Prodromou, C. (2002). Regulation of Hsp90 ATPase activity by the co-chaperone Cdc37p/p50cdc37. *The Journal of Biological Chemistry 277*, 20151–9.

Smith, D. F. (1993). Dynamics of heat shock protein 90-progesterone receptor binding and the disactivation loop model for steroid receptor complexes. *Molecular Endocrinology 7*, 1418–29.

Smith, D. F., Stensgard, B. a., Welch, W. J., and Toft, D. O. (1992). Assembly of progesterone receptor with heat shock proteins and receptor activation are ATP mediated events. *The Journal of Biological Chemistry 267*, 1350–6.

Soroka, J., Wandinger, S. K., Mäusbacher, N., Schreiber, T., Richter, K., Daub, H., and Buchner, J. (2012). Conformational switching of the molecular chaperone Hsp90 via regulated phosphorylation. *Molecular Cell 45*, 517–28.

Sparrer, H., Rutkat, K., and Buchner, J. (1997). Catalysis of protein folding by symmetric chaperone complexes. *Proceedings of the National Academy of Sciences of the United States of America 94*, 1096–100.

Sreedhar, A. S., Kalmár, E., Csermely, P., and Shen, Y.-F. (2004). Hsp90 isoforms: functions, expression and clinical importance. *FEBS Letters 562*, 11–5.

Stankiewicz, M. and Mayer, M. P. (2012). The universe of Hsp90. *Biomolecular concepts 3*, 79–97.

Stebbins, C. E., Russo, A. A., Schneider, C., Rosen, N., Hartl, F. U., and Pavletich, N. P. (1997). Crystal structure of an Hsp90-geldanamycin complex: targeting of a protein chaperone by an antitumor agent. *Cell 89*, 239–50.

Su, G., Roberts, T., and Cowell, J. K. (1999). TTC4, a novel human gene containing the tetratricopeptide repeat and mapping to the region of chromosome 1p31 that is frequently deleted in sporadic breast cancer. *Genomics 55*, 157–63.

Svergun, D. I. (1992). Determination of the regularization parameter in indirect-transform methods using perceptual criteria. *Journal of Applied Crystallography 25*, 495–503.

Taguchi, H. (2015). Reaction Cycle of Chaperonin GroEL via Symmetric "Football" Intermediate. *Journal of molecular biology 427*, 2912–8.

Taipale, M., Jarosz, D. F., and Lindquist, S. (2010). HSP90 at the hub of protein homeostasis: emerging mechanistic insights. *Nature reviews. Molecular cell biology 11*, 515–28.

Taipale, M., Krykbaeva, I., Koeva, M., Kayatekin, C., Westover, K. D., Karras, G. I., and Lindquist, S. (2012). Quantitative analysis of HSP90-client interactions reveals principles of substrate recognition. *Cell 150*, 987–1001.

Taipale, M., Krykbaeva, I., Whitesell, L., Santagata, S., Zhang, J., Liu, Q., Gray, N. S., and Lindquist, S. (2013). Chaperones as thermodynamic sensors of drug-target interactions reveal kinase inhibitor specificities in living cells. *Nature biotechnology 31*, 630–7.

Taipale, M., Tucker, G., Peng, J., Krykbaeva, I., Lin, Z.-Y., Larsen, B., Choi, H., Berger, B., Gingras, A.-C., and Lindquist, S. (2014). A quantitative chaperone interaction network reveals the architecture of cellular protein homeostasis pathways. *Cell 158*, 434–48.

Tang, Y.-C., Chang, H.-C., Roeben, A., Wischnewski, D., Wischnewski, N., Kerner, M. J., Hartl, F. U., and Hayer-Hartl, M. (2006). Structural features of the GroEL-GroES nano-cage required for rapid folding of encapsulated protein. *Cell 125*, 903–14.

Tenge, V. R., Zuehlke, A. D., Shrestha, N., and Johnson, J. L. (2015). The Hsp90 cochaperones Cpr6, Cpr7, and Cns1 interact with the intact ribosome. *Eukaryotic cell 14*, 55–63.

Tesic, M., Marsh, J. a., Cullinan, S. B., and Gaber, R. F. (2003). Functional interactions between Hsp90 and the co-chaperones Cns1 and Cpr7 in Saccharomyces cerevisiae. *The Journal of Biological Chemistry 278*, 32692–701.

Tipton, K. A., Verges, K. J., and Weissman, J. S. (2008). In vivo monitoring of the prion replication cycle reveals a critical role for Sis1 in delivering substrates to Hsp104. *Molecular cell 32*, 584–91.

Tong, A. H. Y. and Boone, C. (2006). Synthetic genetic array analysis in Saccharomyces cerevisiae. *Methods in Molecular Biology 313*, 171–92.

Tong, A. H. Y. and Boone, C. (2007). 16 High-Throughput Strain Construction and Systematic Synthetic Lethal Screening in S. cerevisiae. In *Yeast Gene Analysis - Second Edition* (Second Edi ed.)., pp. 369–707.

Tong, A. H. Y., Lesage, G., Bader, G. D., Ding, H., Xu, H., Xin, X., Young, J., Berriz, G. F., Brost, R. L., Chang, M., Chen, Y., Cheng, X., Chua, G., Friesen, H., Goldberg, D. S., Haynes, J., Humphries, C., He, G., Hussein, S., Ke, L., Krogan, N., Li, Z., Levinson, J. N., Lu, H., Ménard, P., Munyana, C., Parsons, A. B., Ryan, O., Tonikian, R., Roberts, T., Sdicu, A.-M., Shapiro, J., Sheikh, B., Suter, B., Wong, S. L., Zhang, L. V., Zhu, H., Burd, C. G., Munro, S., Sander, C., Rine, J., Greenblatt, J., Peter, M., Bretscher, A., Bell, G., Roth, F. P., Brown, G. W., Andrews, B., Bussey, H., and Boone, C. (2004). Global mapping of the yeast genetic interaction network. *Science (New York, N.Y.) 303*, 808–13.

Tsutsumi, S., Mollapour, M., Graf, C., Lee, C.-T., Scroggins, B. T., Xu, W., Haslerova, L., Hessling, M., Konstantinova, A. a., Trepel, J. B., Panaretou, B., Buchner, J., Mayer, M. P., Prodromou, C., and Neckers, L. (2009). Hsp90 charged-linker truncation reverses the functional consequences of weakened hydrophobic contacts in the N domain. *Nature Structural & Molecular Biology 16*, 1141–7.

Tsutsumi, S., Mollapour, M., Prodromou, C., Lee, C.-T., Panaretou, B., Yoshida, S., Mayer, M. P., and Neckers, L. M. (2012). Charged linker sequence modulates eukaryotic heat shock protein 90 (Hsp90) chaperone activity. *Proceedings of the National Academy of Sciences of the United States of America 109*, 2937–42.

Vagin, A. A., Steiner, R. A., Lebedev, A. A., Potterton, L., McNicholas, S., Long, F., and Murshudov, G. N. (2004). REFMAC5 dictionary: organization of prior chemical knowledge and guidelines for its use. *Acta crystallographica. Section D, Biological crystallography 60*, 2184–95.

Van Duyne, G. D., Standaert, R. F., Karplus, P. A., Schreiber, S. L., and Clardy, J. (1993). Atomic structures of the human immunophilin FKBP-12 complexes with FK506 and rapamycin. *Journal of molecular biology 229*, 105–24.

Van Montfort, R., Slingsby, C., and Vierling, E. (2001). Structure and function of the small heat shock protein/alpha-crystallin family of molecular chaperones. *Advances in protein chemistry 59*, 105–56.

Vaughan, C. K., Mollapour, M., Smith, J. R., Truman, A., Hu, B., Good, V. M., Panaretou, B., Neckers, L., Clarke, P. a., Workman, P., Piper, P. W., Prodromou, C., and Pearl, L. H. (2008). Hsp90-dependent activation of protein kinases is regulated by chaperone-targeted dephosphorylation of Cdc37. *Molecular Cell 31*, 886–95.

Verba, K. A., Wang, R. Y.-R., Arakawa, A., Liu, Y., Shirouzu, M., Yokoyama, S., and Agard, D. A. (2016). Atomic structure of Hsp90-Cdc37-Cdk4 reveals that Hsp90 traps and stabilizes an unfolded kinase. *Science (New York, N.Y.) 352*, 1542–7.

Vranken, W. F., Boucher, W., Stevens, T. J., Fogh, R. H., Pajon, A., Llinas, M., Ulrich, E. L., Markley, J. L., Ionides, J., and Laue, E. D. (2005). The CCPN data model for NMR spectroscopy: Development of a software pipeline. *Proteins: Structure, Function, and Bioinformatics 59*, 687–696.

Walter, S. and Buchner, J. (2002). Molecular chaperones–cellular machines for protein folding. *Angewandte Chemie (International ed. in English) 41*, 1098–113.

Wandinger, S. K., Richter, K., and Buchner, J. (2008). The Hsp90 chaperone machinery. *The Journal of Biological Chemistry 283*, 18473–7.

Wandinger, S. K., Suhre, M. H., Wegele, H., and Buchner, J. (2006). The phosphatase Ppt1 is a dedicated regulator of the molecular chaperone Hsp90. *The EMBO Journal 25*, 367–76.

Wang, X., Venable, J., LaPointe, P., Hutt, D. M., Koulov, A. V., Coppinger, J., Gurkan, C., Kellner, W., Matteson, J., Plutner, H., Riordan, J. R., Kelly, J. W., Yates, J. R., and Balch, W. E. (2006). Hsp90 cochaperone Aha1 downregulation rescues misfolding of CFTR in cystic fibrosis. *Cell 127*, 803–15.

Wayne, N. and Bolon, D. N. (2007). Dimerization of Hsp90 is required for in vivo function. Design and analysis of monomers and dimers. *The Journal of biological chemistry 282*, 35386–95.

Weaver, A. J., Sullivan, W. P., Felts, S. J., Owen, B. A., and Toft, D. O. (2000). Crystal structure and activity of human p23, a heat shock protein 90 co-chaperone. *The Journal of biological chemistry 275*, 23045–52.

Wegele, H., Haslbeck, M., Reinstein, J., and Buchner, J. (2003). Sti1 is a novel activator of the Ssa proteins. *The Journal of Biological Chemistry 278*, 25970–6.

Wegele, H., Wandinger, S. K., Schmid, A. B., Reinstein, J., and Buchner, J. (2006). Substrate transfer from the chaperone Hsp70 to Hsp90. *Journal of Molecular Biology 356*, 802–11.

Wegrzyn, R. D., Hofmann, D., Merz, F., Nikolay, R., Rauch, T., Graf, C., and Deuerling, E. (2006). A conserved motif is prerequisite for the interaction of NAC with ribosomal protein L23 and nascent chains. *The Journal of biological chemistry 281*, 2847–57.

Weikl, T., Abelmann, K., and Buchner, J. (1999). An unstructured C-terminal region of the Hsp90 co-chaperone p23 is important for its chaperone function. *Journal of molecular biology 293*, 685–91.

Weikl, T., Muschler, P., Richter, K., Veit, T., Reinstein, J., and Buchner, J. (2000). C-terminal regions of Hsp90 are important for trapping the nucleotide during the ATPase cycle. *Journal of molecular biology 303*, 583–92.

Welch, W. J. and Feramisco, J. R. (1982). Purification of the major mammalian heat shock proteins. *The Journal of Biological Chemistry 257*, 14949–59.

West, M., Hedges, J. B., Chen, A., and Johnson, A. W. (2005). Defining the order in which Nmd3p and Rpl10p load onto nascent 60S ribosomal subunits. *Molecular and cellular biology 25*, 3802–13.

Wilson, D. N. and Beckmann, R. (2011). The ribosomal tunnel as a functional environment for nascent polypeptide folding and translational stalling. *Current opinion in structural biology 21*, 274–82.

Winkler, J., Tyedmers, J., Bukau, B., and Mogk, A. (2012). Chaperone networks in protein disaggregation and prion propagation. *Journal of structural biology 179*, 152–60.

Woolford, J. L. and Baserga, S. J. (2013). Ribosome biogenesis in the yeast Saccharomyces cerevisiae. *Genetics 195*, 643–81.

Yang, Y., Rao, R., Shen, J., Tang, Y., Fiskus, W., Nechtman, J., Atadja, P., and Bhalla, K. (2008). Role of acetylation and extracellular location of heat shock protein 90alpha in tumor cell invasion. *Cancer research 68*, 4833–42.

Yi, F., Doudevski, I., and Regan, L. (2010). HOP is a monomer: investigation of the oligomeric state of the co-chaperone HOP. *Protein science : a publication of the Protein Society 19*, 19–25.

Young, J. C. and Hartl, F. U. (2000). Polypeptide release by Hsp90 involves ATP hydrolysis and is enhanced by the co-chaperone p23. *The EMBO journal 19*, 5930–40.

Zhao, R., Davey, M., Hsu, Y.-C., Kaplanek, P., Tong, A., Parsons, A. B., Krogan, N., Cagney, G., Mai, D., Greenblatt, J., Boone, C., Emili, A., and Houry, W. a. (2005). Navigating the chaperone network: an integrative map of physical and genetic interactions mediated by the hsp90 chaperone. *Cell 120*, 715–27.

Zhuravleva, A. and Gierasch, L. M. (2011). Allosteric signal transmission in the nucleotide-binding domain of 70-kDa heat shock protein (Hsp70) molecular chaperones. *Proceedings of the National Academy of Sciences of the United States of America 108*, 6987–92.

Zhuravleva, A. and Gierasch, L. M. (2015). Substrate-binding domain conformational dynamics mediate Hsp70 allostery. *Proceedings of the National Academy of Sciences of the United States of America 112*, E2865–73.

Zolkiewski, M. (1999). ClpB cooperates with DnaK, DnaJ, and GrpE in suppressing protein aggregation. A novel multi-chaperone system from Escherichia coli. *The Journal of biological chemistry 274*, 28083–6.

Zuehlke, A. D. and Johnson, J. L. (2012). Chaperoning the chaperone: a role for the co-chaperone Cpr7 in modulating Hsp90 function in Saccharomyces cerevisiae. *Genetics 191*, 805–14.

Zuiderweg, E. R. P., Bertelsen, E. B., Rousaki, A., Mayer, M. P., Gestwicki, J. E., and Ahmad, A. (2013). Allostery in the Hsp70 chaperone proteins. *Topics in current chemistry 328*, 99–153.

List of Figures

List of Tables

Acknowledgements

This thesis was prepared at the Technische Universität München, Lehrstuhl für Biotechnologie under the supervision of Prof. Dr. Johannes Buchner.
First of all, I would like to thank Prof. Dr. Johannes Buchner for giving me the opportunity to prepare my PhD thesis in his group, which provides excellent scientific equipment and knowledge. In addition, I would like to thank him for the great working atmosphere and the continuous support during the past four years. Moreover, I am grateful for his support for the attendance of two Hsp90 conferences in 2012 and 2014, and a EMBO conference in 2015.
Next, I would like to thank Astrid König, Eva Huber and Michael Groll for their excellent help with crystallization experiments and Daniel Rutz for help with aUC. Additionally, I would like to thank Tobias Madl and his group for their support with SAXS measurements and Lee Freiburger and Michael Sattler for their help with NMR spectroscopy. I am also grateful to Tim Hassemer and Ulrich Hartl for the ability to use their facility to perform ribosome fractionation as well as to Jochen Rech and Stefan Jentsch for their support with SGA screening.
Moreover, I would like to thank my practical and master students Marcel Genge, Maximilian Biebl and Christopher Dodt for their technical support and hard work. I am also thankful to the members of my TAC, Serena Schwenkert and Stefan Jentsch, for the fruitful discussions.
In addition, I would like to thank all technicians and secretaries in the group for their support in science and bureaucracy. I am also deeply grateful to the IMPRS-LS coordination office, for their support and the organization of the excellent coursework. Moreover, I would like to thank all my colleagues at the Chair for Biotechnology for great four years.
I am extraordinarily thankful to Daniel Rutz, Mathias Rosam, Katrin Back and Frank Echtenkamp for a lot of fun not only at work, but also during the time in Munich in

general.
I would also like to thank my family and all my friends for their support.

Last but not least, I would like to thank my wife Anna - for everything in life that really matters.

Declaration

Hereby I declare that this thesis was composed independently, without use of other resources or references than the stated ones. This work has not been presented to any examination board yet.

Hiermit erkläre ich, dass die vorliegende Arbeit selbständig verfasst wurde. Dabei wurden keine anderen als die hier angegebenen Hilfsmittel oder Quellen verwendet. Die Arbeit wurde noch keiner Prüfungskommission vorgelegt.

Florian Helmut Schopf
München, August 2016